
ETD Archive

2014

A PSA Process for an Oxygen Concentrator

Aaron A. Moran
Cleveland State University

Follow this and additional works at: <https://engagedscholarship.csuohio.edu/etdarchive>

 Part of the [Biomedical Engineering and Bioengineering Commons](#)

How does access to this work benefit you? Let us know!

Recommended Citation

Moran, Aaron A., "A PSA Process for an Oxygen Concentrator" (2014). *ETD Archive*. 749.
<https://engagedscholarship.csuohio.edu/etdarchive/749>

This Thesis is brought to you for free and open access by EngagedScholarship@CSU. It has been accepted for inclusion in ETD Archive by an authorized administrator of EngagedScholarship@CSU. For more information, please contact library.es@csuohio.edu.

A PSA PROCESS FOR AN OXYGEN CONCENTRATOR

AARON A. MORAN

Bachelor of Science in Chemical Engineering

Miami University

May 2012

Submitted in partial fulfillment of requirements for the degree

MASTER OF SCIENCE in Chemical Engineering

at the

CLEVELAND STATE UNIVERSITY

June 2014

APPROVAL

We hereby approve this thesis

For

AARON A. MORAN

Candidate for the Master of Science in Chemical Engineering degree

For the Department of

Chemical and Biomedical Engineering at the Washkewicz College of Engineering

And

**CLEVELAND STATE UNIVERSITY's
College of Graduate Studies by**

Dr. Orhan Talu

Department of Chemical & Biomedical Engineering

June 16, 2014

Dr. Dhananjai B. Shah

Department of Chemical & Biomedical Engineering

June 16, 2014

Dr. Sridhar Ungarala

Department of Chemical & Biomedical Engineering

June 16, 2014

June 16, 2014

Date of Defense

ACKNOWLEDGEMENTS

First and foremost, I would like to offer my sincerest gratitude to Dr. Talu for his guidance, encouragement, and support throughout my time learning under him. It has been a pleasure to work under him and his insight into PSA has been invaluable. Without him I would not have learned nearly as much as I did throughout the process of writing this thesis.

Next, I would like to thank my committee, Dr. Shah and Dr. Ungarala for their input and critique of my thesis. They provided beneficial contributions to the final draft of my thesis and were valuable resources during the writing of my thesis.

Additionally, I wish to thank Jim Barker for his help with the electrical side of the setup of the PSA process used in this thesis. He was extremely helpful in providing the necessary improvements to the apparatus in order to allow me to conduct the experiments I wished to perform.

Lastly, I must express my sincerest gratitude to my parents for their support and encouragement throughout this process. Without them, I would not be in the position I am today.

A PSA PROCESS FOR AN OXYGEN CONCENTRATOR

AARON A. MORAN

ABSTRACT

Oxygen is used in a variety of chemical processes and for medical purposes throughout the world. Pressure swing adsorption (PSA) has become a viable alternative to cryogenic distillation for the separation of oxygen from air with the development of advanced adsorbents like zeolites. PSA processes are inherently complex because it is a dynamic process. Efficient operation of a PSA process is necessary in order to utilize the capacity of the adsorbent as much as possible and reduce the power requirements of the process.

In this thesis, a novel zeolite adsorbent was utilized in a PSA process for oxygen generation with the goal of designing cycles for high recovery and a low bed size factor (BSF). A secondary goal was to determine the kinetic limit of the novel zeolite to determine how fast of an adsorption rate the zeolite has and if it is a candidate for rapid PSA processes.

This thesis demonstrates cycles that efficiently utilize the new adsorbent at different operating conditions. This provides a range of operating conditions from which to determine how to best utilize the zeolite to develop larger PSA processes. Also, it was found that this novel zeolite is in fact an enhanced zeolite with a fast adsorption rate capable of supporting rapid PSA processes. Unfortunately due to system constraints, the kinetic limit was not found.

TABLE OF CONTENTS

	Page
ABSTRACT.....	iv
LIST OF TABLES.....	ix
LIST OF FIGURES.....	x
NOMENCLATURE.....	xii
 CHAPTER	
I. INTRODUCTION.....	1
1.1 Purpose.....	1
1.2 Scope of Work.....	2
II. BACKGROUND.....	4
2.1 Zeolites.....	4
2.1.1 History.....	5
2.1.2 Composition and Structure.....	6
2.1.3 Applications.....	11
2.2 Adsorption.....	14
2.2.1 Adsorption Fundamentals.....	15
2.2.2 Adsorption Thermodynamics.....	16
2.2.3 Adsorption Kinetics.....	18

2.2.4	Adsorption Column Dynamics.....	20
2.3	Air Separation through Pressure Swing Adsorption.....	24
2.3.1	PSA Principles.....	24
2.3.2	History and growth of PSA.....	26
2.3.3	Improvements to PSA Cycles.....	32
2.3.4	Air Separation Applications.....	35
2.3.5	PSA Literature Review.....	36
III.	THEORY.....	38
3.1	Intermolecular forces.....	38
3.1.1	Electrostatic Forces.....	39
3.1.2	Induction and Dispersion Forces.....	40
3.1.3	N ₂ and O ₂ Interaction with Zeolites.....	41
3.1.4	Exchangeable Cations.....	43
3.1.5	LiX Zeolite Limitations and Improvements.....	45
3.2	Adsorption Thermodynamics and Equilibrium Models.....	46
3.2.1	Henry's Law.....	46
3.2.2	The Langmuir Isotherm.....	47
3.2.3	Multi-Component Adsorption.....	49
3.3	Adsorption Kinetics.....	52
3.3.1	Diffusivity.....	53
3.3.2	Enhanced Zeolites.....	55
3.4	PSA Analysis.....	57
3.4.1	Material Balances.....	57

3.4.2	Design Parameters.....	62
3.4.3	Performance Parameters.....	65
IV.	EXPERIMENTAL.....	68
4.1	Type of Zeolite.....	68
4.2	Isotherm Generation.....	69
4.3	Column Packing.....	71
4.4	PSA System.....	72
4.4.1	PSA Flow Diagrams.....	73
4.4.2	PSA Instrumentation, Process Control, and Data Collection.....	76
4.4.3	System Design.....	79
4.5	Experimental Procedure.....	81
4.5.1	Preliminary Experiments.....	82
4.5.2	PSA Experiments.....	83
4.6	Experimental Design.....	86
4.6.1	Variance of Pressure Ratio and Cycle Time.....	86
4.6.2	Variance of Adsorption Pressure.....	88
V.	RESULTS AND DISCUSSION.....	90
5.1	Isotherms.....	90
5.2	Experimental Results.....	93
5.2.1	Calculations and Error Analysis.....	93
5.2.2	Changing of Equalization Step Time.....	94

5.2.3	Changing of Pressure Ratio.....	96
5.2.4	Changing of Feed Rate (Cycle Time).....	98
5.2.5	Changing of Adsorption Pressure.....	103
VI.	CONCLUSIONS.....	108
6.1	Thesis Summary and Contributions.....	108
6.2	Future Work.....	109
	REFERENCES.....	111
	APPENDIX.....	115
	Appendix A: Nitrogen Isotherm Data.....	116
	Appendix B: Column Packing.....	117
	Appendix C: Flow Calibrations and Pressure Drop Data.....	118
	Appendix D: Experimental Data and Calculations.....	121

LIST OF TABLES

Table	Page
3.1 Quadrupole Moment and Polarizabilities of Nitrogen and Oxygen Molecules.....	42
4.1 DSL Calculated Coefficients.....	71
4.2 PSA Schematic Symbol Description.....	74
4.3 Experimental Set #1: Equalization step time variance.....	87
4.4 Experimental Set #2: Pressure ratio variance (20 sec.).....	87
4.5 Experimental Set #3: Pressure ratio variance (15 sec.).....	88
4.6 Experimental Set #4: Pressure ratio variance (10 sec.).....	88
4.7 Experimental Set #5: Pressure ratio variance (Low adsorption pressure).....	89
4.8 Experimental Set #6: Adsorption pressure variance.....	89
5.1 Performance of cycles from Experimental Set #1.....	95
5.2 Performance of cycles from Experimental Set #2.....	97
5.3 Performance of cycles from Experimental Set #3.....	99
5.4 Performance of cycles from Experimental Set #4.....	100
5.5 Performance of cycles from Experimental Set #5.....	103
5.6 Adsorption pressure comparison.....	106

LIST OF FIGURES

Figure		Page
2.1	Examples of zeolite basic secondary units.....	7
2.2	Sodalite unit with Si, Al atoms.....	8
2.3	Structure of Type A and Type X or Y zeolites.....	8
2.4	Potential energy diagram for adsorption.....	16
2.5	The five types of isotherms.....	17
2.6	Depiction of pores and mass transfer resistances in adsorption.....	19
2.7	Shapes of isotherms in determining the sharpness of concentration wavefronts.....	21
2.8	Self-sharpening wavefront and dispersive wavefront.....	22
2.9	Mass transfer zone inside a column.....	22
2.10	Column breakthrough curve.....	23
2.11	Schematic diagram of two-column Air Liquide PSA system.....	28
2.12	Basic two-column pressure swing adsorption system.....	29
2.13	Column pressure during Skarstrom cycle.....	30
3.1	Calculated potential energy curves of nitrogen and oxygen.....	43
3.2	Potential energy curves of Na^+N_2 and Li^+N_2	44

3.3	Example isotherms to illustrate swing capacity.....	66
4.1	Cahn®-1000 Microelectronic Balance (low pressure).....	69
4.2	PSA system feed side schematic.....	75
4.3	PSA product side schematic.....	75
4.4	PSA middle exit manifold schematic.....	76
5.1	Nitrogen isotherms for zeolite used in this thesis.....	91
5.2	Oxygen isotherms for zeolite used in this thesis.....	92
5.3	Binary adsorption isotherms at 23.6 C and nitrogen concentration similar to air...	92
5.4	BSF and Recovery vs. Pressure ratio for the Experimental Set #2.....	98
5.5	BSF and Recovery vs. Pressure ratio for Experimental Sets #2-4.....	101
5.6	Approach of kinetic limit at different pressure ratios.....	102
5.7	BSF and Recovery vs. Pressure ratio at different adsorption pressures.....	104
5.8	BSF and Recovery vs. Adsorption pressure.....	107

NOMENCLATURE

B = Boltzmann's constant

b = Adsorption equilibrium constant

b_i^0 = Pre-exponential constant (DSL model) for gas i for first site

c_0 = Inlet adsorbate concentration

c_e = Equilibrium adsorbate concentration

D_p = Effective macropore diffusivity

d = Equilibrium constant for second site (DSL model)

d_i^0 = Pre-exponential constant (DSL model) for gas i for second site

E = Potential energy

E_a = Energy of activation for adsorption

E_d = Energy of activation for desorption

e = Electric charge

F = Instantaneous flow rate

\bar{F} = Average flow rate

f = Force

G = Gibbs free energy

H = Enthalpy

K = Henry's Law constant

K_0 = Henry's Law constant at a reference state

k_a = adsorption rate constant

k_b = Desorption rate constant

k_i = Mass transfer coefficient of component i

m = Mass of adsorbate molecule

N_i = Total number of moles of component i
 N_T = Total number of moles of adsorbate
 n = number of components
 M = Quadrupole Moment
 P = pressure
 P_s = Saturated vapor pressure
 p = partial pressure
 Q = Heat of Adsorption
 $Q_i^{(b)}$ = Heat of Adsorption of gas i for first site (DSL model)
 $Q_i^{(d)}$ = Heat of Adsorption of gas i for second site (DSL model)
 q = Amount adsorbed
 q^* = Equilibrium value of adsorbed phase concentration
 \bar{q} = Adsorbed phase average concentration
 q_i = Amount adsorbed of component i
 $q_0^* = q^*$ at C_0
 q_s = Adsorption saturation capacity
 R = Ideal gas constant
 r = Distance between charges
 r_p = Adsorbent particle radius
 S = Entropy
 s = selectivity
 T = Temperature
 t = Time
 t_c = Cycle time
 t^i = Time of step i

t_b = Breakthrough time

t_s = Stoichiometric time

v = Rate constant for desorption

w = Magnitude of charge

x_s = mole fraction in the adsorbed phase

y = mole fraction in the fluid phase

y^j = mole fraction in the fluid phase of step j

z = Ionic valences

α = Polarizability

θ = Fractional surface coverage

ε_p = Void fraction inside adsorbent particle

ε_b = Interparticle column void fraction

σ = Condensation coefficient

ϵ = Error of Material Balance

ε_0 = Dielectric Permittivity

Γ = Potential energy

CHAPTER I

INTRODUCTION

1.1 Purpose

Oxygen is one of the keys to the abundance of life on Earth and is plentiful in the gas form in our atmosphere at a concentration of approximately 21%. However, the need for oxygen in a purer form has increased tremendously with the rise of new manufacturing processes and medical applications. Industrial uses for purified oxygen include the production of steel, chemicals, petrochemicals, glass, ceramics, paper, and the recovery of non-ferrous metal [19]. Medical applications mainly involve surgical procedures, ambulatory use, and COPD (Chronic Obstructive Pulmonary Disease) patients who require a purer form of oxygen to breath than what is in air. Oxygen has grown from the fourth largest distributed chemical in the mid 1990's to the second largest in 2006 behind only nitrogen [1, 2].

Adsorption involves molecular interactions between an adsorbate molecule and the surface of a solid. Production of oxygen through air separation is possible by passing air over an adsorbent that is selective for nitrogen molecules over oxygen molecules to produce pure oxygen at the exit. Once the adsorbent in a column is saturated with nitrogen molecules, it needs to be cleaned so that it can be reused. This makes the process of adsorption dynamic, which is unique compared to most other chemical processes that operate at steady state

Pressure swing adsorption (PSA) and vacuum-swing adsorption (VSA) are two processes that perform air separation to achieve oxygen at 90-94% purity (the difference is mostly argon). Use of zeolites in these processes aid in energy efficiency, process efficiency, processing rates, product quality, and the environmental impact of the oxygen purification process [19]. This thesis will examine a novel LiX zeolite and its impact on the efficiency of a PSA/VSA process.

1.2 Scope of Work

There are many ways to approach the optimization of a PSA process. A PSA process can be optimized around a number of different design factors. The goal of this thesis is to treat the system used to develop PSA cycles as a “Pilot” type system. In essence, it is a scaled down version of a larger process that is used for quickly testing how a process operates on a small scale before attempting to operate on a larger scale. One drawback to operating a PSA process on a small scale is that any “dead volume” (volume in a column not filled with adsorbent) is magnified. This can have a significant effect on the performance of the cycle on the smaller scale. Thus, this is a problem that requires careful attention in order to reduce its effects as much as possible.

This thesis focuses on optimizing the recovery of oxygen and the bed size factor (productivity) of the process. The vacuum pump is purposely oversized because the power to the pump is not of concern for this thesis and a pump is not required for pressurizing feed gas because it is supplied by high pressure bottled air. This allows for flexibility in designing cycles around different pressure ratios, adsorption pressures, and desorption pressures. Thus, the recovery and BSF can be evaluated over a wide range of operating conditions to determine where these design factors are optimized with few limitations due to the pump(s) used in the process.

CHAPTER II

BACKGROUND

This section introduces the ideas and concepts needed to understand the methods and results of this thesis. In general, adsorption is a separation process that involves the attraction of molecules to the surface of an adsorbent based on its size or molecular interactions with a solid. A number of texts are useful for further learning in the areas of adsorbents, adsorption, and adsorption processes [5, 13, 27, 36]. This thesis will focus on a specific adsorbent, LiX zeolite, and a specific adsorption process, pressure swing adsorption, for the application of oxygen production from air.

2.1 Zeolites

Zeolites are one of many adsorbents used for separation and purification processes. Adsorbents are microporous materials that permit mobility of adsorbate molecules (molecules that adsorb to an adsorbent surface) within the adsorbent and

provide a high surface area to enhance interactions of guest molecules with the solid surface. Adsorbents vary in structure and composition enabling them to interact differently with various types of molecules. Selection of the right type of adsorbent is critical to any adsorption process in order to achieve the desired separation.

2.1.1 Zeolite History

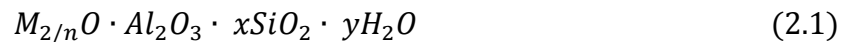
A Swedish man named Baron Cronstedt first depicted zeolites in literature in the 1750's [1, 7]. He proposed the name “zeolite” after heating a natural zeolite and witnessing it bubble and dance as steam released from the pores of the zeolite [3]. Natural occurring zeolites usually contain impurities and an irregular chemical composition that limit their impact scientifically and industrially [22]. Consequently, zeolites went largely unstudied for close to 200 years as they were viewed as rare minerals without a purification method. In 1905 in Germany, a synthetic zeolite with a larger capacity compared to natural zeolites was manufactured, which allowed for the first commercial use of zeolites as a way to soften water. Two years later also in Germany, natural zeolites were used to create the first “self-acting” laundry detergent [3].

Organized research into zeolites did not begin, however, until the late 1930's when Richard Barrer developed the first classification of zeolites dependent on the size of the pores that limit which molecules can adsorb. His synthesis of the zeolite mordenite along with the first zeolite without a natural equivalent, prompted researchers at Union Carbide to develop methods of synthesis for the first synthetic zeolites (i.e. zeolites A, X, and Y) for industrial use [2, 3, 19]. Union Carbide was able to use readily available raw materials along with a lower synthesis pressure and temperature compared to former

methods to create these zeolites. The key features of these synthetic zeolites were a larger pore size to accommodate larger molecules, an enhanced pore volume to increase the capacity, and a higher purity of the crystalline phase compared to natural zeolites [19]. The ability to imagine and create a zeolite with a structure and function tailored to a specific process allowed the industrial potential of zeolites to expand [3]. This has produced zeolites today that are crucial to many industrial processes as adsorbents and catalysts.

2.1.2 Zeolite Composition and Structure

Of the approximately 40 naturally occurring zeolites, only chabazite, faujasite, and mordenite are primarily used in industry. Commercially, the most important synthetically created zeolites are Type A, Type X or Y, synthetic mordenite, and all of their ion-exchanged variations [5]. The composition of a zeolite consists of microporous crystalline aluminosilicates with a chemical formula of the form seen in equation 2.1:



where M is a metal cation of valence n , x is 2.0 or more, and y is the moles of water in the pores. Cavities (or cages) within the zeolite structure are linked to other cavities by pores that allow adsorbate molecules to permeate into the structure. Zeolites differ from other adsorbents because their uniform crystalline structure provides a well defined pore size for molecules to travel through while also allowing them to act as effective molecular sieves. IUPAC convention classifies pores by their size as follows [13]:

- 1) Micropores: Less than 2 nm
- 2) Mesopores: Between 2-50 nm
- 3) Macropores: Greater than 50 nm

Micropores, unlike the larger mesopores and macropores, have the ability to trap guest molecules using their solid surface force field. The larger pores serve to assist with diffusion by allowing molecules to travel to the micropores easily. The porosity of a zeolite solid provides a much larger total surface area compared to its external surface, which produces a solid with a high adsorption capacity.

Molecular characteristics specific to a zeolite (i.e. pore size, shape, and properties like polarity) control how adsorption and desorption (opposite of adsorption) occur within a zeolite. The main building blocks of zeolites consist of SiO_2 and Al_3O_2 units that connect tetrahedrally through the oxygen atoms in the units. Several of these units form larger secondary units that serve as the building blocks for the zeolite structure. These secondary units, shown in figure 2.1, illustrate silicon and aluminum atoms at the apices with lines representing oxygen bridges between them that show the diameter of an

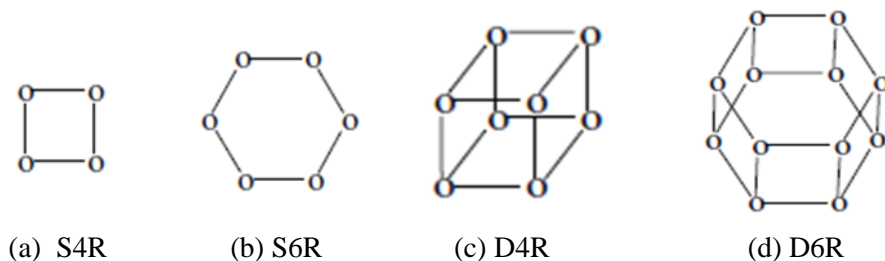


Figure 2.1. Examples of zeolite basic secondary units [2].

oxygen atom. More secondary units exist, but the units in figure 2.1 represent the units used to build the more common zeolite types A, X, and Y. These secondary units are

linked in 3-D space to create a porous crystalline structure. For example, shown in figure 2.2 is a sodalite unit formed from S4R and S6R units (Fig. 2.1.a and Fig.2.2.b respectively). Eight sodalite units form the eight-membered oxygen ring of type A zeolites and are connected by D4R units (Fig. 2.1.c) with the final crystal shown in figure 2.3. Ten sodalite units organized in a different fashion in 3-D space form the twelve-membered oxygen ring of type X and Y zeolites and are connected by D6R units (Fig.

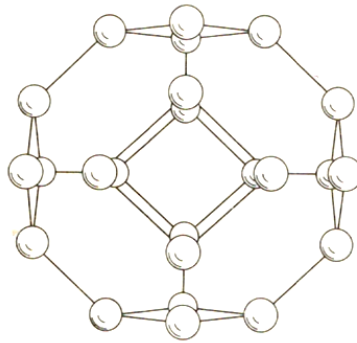


Figure 2.2. Sodalite unit with Si, Al atoms [27].

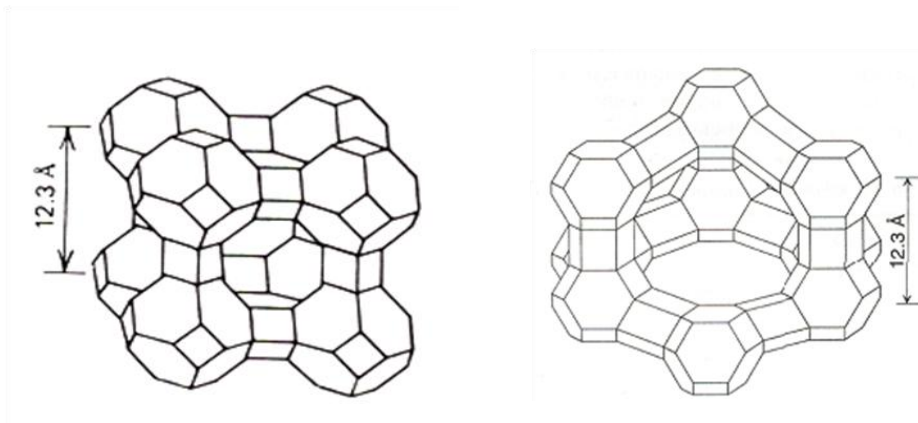


Figure 2.3. Structure of Type A (left) and Type X or Y zeolites (right) [5].

2.2.d), also seen in figure 2.3. These oxygen rings are responsible for providing entry for adsorbate molecules into the cavity of the zeolite. They determine the pore size within a zeolite and what size molecule can enter the structure. Since zeolites are 3-dimensional

structures, it is difficult to accurately represent them on a 2-D surface. Figure 2.3 is one of the better illustrations in texts and literature [36]. By comparison, a single methane molecule is approximately 4.3 Å while a benzene ring is 2.8 x 6.1 Å.

The silicon and aluminum atoms within these structures are interchangeable (although it can be difficult), allowing for a range of Si/Al ratios between one and infinity [36]. If the amount of aluminum added causes the ratio to go below one, the structure collapses. Adding an aluminum atom to the zeolite induces a net negative charge on the structure that requires an exchangeable cation to preserve the electroneutrality of the structure. The cations are electrostatically bonded near an Al atom and are therefore not part of the zeolite structure, this allows them to be exchanged with other cations.

Adjusting a zeolites Si/Al ratio and type of exchangeable cation allows for modification of a zeolite for a specific purpose. A higher Si/Al ratio increases the hydrophobic nature of a zeolite, which is useful in the removal of organics from water and in catalytic applications for reactions where water is undesirable. The Si/Al ratio is what differentiates Type X and Y zeolites as Type X zeolites have a ratio between 1 and 1.5, while Type Y zeolites have a ratio between 1.5 and 3. A lower Si/Al ratio gives a higher cation exchange capacity and increases the zeolites ability to adsorb polar molecules such as water. Examples of commonly used exchangeable cations include the ions Na^+ , K^+ , and Ca^{2+} . The type and size of the exchangeable cation determines the pore size and properties of the zeolite. The number of cations per unit cell controls the location of the exchangeable cations in the zeolite. Within the sodalite structure there are Type I, Type II, and Type III active exchangeable ion location sites that are able to hold a different number of cations. Type I are the most readily accessible sites and fill up first while

Type III are the most difficult to access and fill up last. As an example, a Type 4A zeolite utilizes the exchangeable cation Na^+ and all twenty three available sites within a unit cell. For a Type A zeolite, the Type II sites are located on the eight membered ring that serves as the opening into the central cavity. Na^+ cations located on the ring will restrict the free diameter of the ring to 3.8 \AA (commonly referred to as a 4A zeolite). Forming a 3A zeolite requires substitution of a Na^+ with a K^+ cation, which further reduces the free diameter because the K^+ cation is larger than Na^+ cation. A Ca^{2+} or Mg^{2+} cation substitution creates a relatively unobstructed ring because one bivalent cation replaces two univalent cations. This results in a shift of the cation location from the main cavity window to the main cavity. Zeolite Types X and Y have similar exchangeable ion locations to Type A with varying degrees of accessibility. Much like Type A zeolites, utilization of different exchangeable ions allows for adjustment of the size of the twelve-membered ring that controls the window size into the central cavity.

The selectivity, s , of a zeolite (or any adsorbent) is the degree to which a zeolite can adsorb one type of molecule over another. It is numerically described by equation 2.2:

$$s = \frac{x_i/y_i}{x_j/y_j} \quad (2.2)$$

where x_i and y_i represent the mole fractions of component i in the adsorbed and fluid phases respectively. Selectivity depends on the type of zeolite used and the molecules undergoing separation. Three types of separation are possible with zeolites. First, equilibrium separation occurs if there exists a difference in molecular interactions between the zeolite surface and the adsorbate molecules. Equilibrium separation usually

hinges on the polarity of the zeolite surface and the adsorbate molecules. Another possibility, kinetic separation, exists if there is a difference in the transport rate (i.e. diffusion) of the adsorbate into the internal cavity of the zeolite. This requires the adsorbent micropore size to be similar to that of the adsorbate molecules undergoing separation. Finally, molecular sieving occurs if the size of a zeolite pore is too small for one molecule but not another in the fluid mixture.

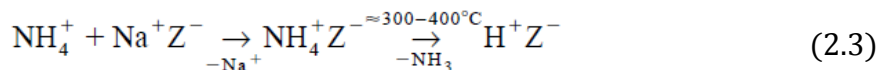
2.1.3 Zeolite Applications

The benefit of zeolites to industry has grown enormously over the last sixty years. Primary industrial applications include petroleum refining, petrochemical processing, detergent production, and separation and purification processes. Consumer applications include portable oxygen concentrators, automotive air conditioning, stationary refrigerant drying, insulated glass windows, and air brake dryers for trucks and trains. In addition, zeolites have numerous environmentally friendly applications with regards to laundry detergent, radioactive waste management, and air and water pollution control [19]. It is easy to see with all these applications why the zeolite industry is growing so rapidly and will continue to expand with increased research.

The applications of zeolites fall into three main categories: Reaction catalyzation, ion exchange, and separation and purification processes. Perhaps the largest industrial application is catalysis, which first became important in 1962 with the addition of zeolites as catalysts in a petroleum process called fluid catalytic cracking. Zeolites developed during this time were significantly more reactive in comparison to their predecessors, which lead to a decrease in processing costs and a substantial increase in the amount of

gasoline produced [22]. Zeolites also became a significant part of numerous other petroleum processes, further advancing the processing of hydrocarbons [19]. Zeolite catalysis is not the main zeolite application of this study and thus an exhaustive review of this application is not given. However, the basic chemistry behind this application lies with two characteristics of zeolites, surface acidity and shape selectivity.

Zeolite catalysis is possible because of the active sites found on the zeolite structure that promote the reactions they help catalyze. Zeolites can have both Brønsted and Lewis acid sites. However, it is the Brønsted sites that are usually responsible for the catalytic activity. An example of how these sites form is seen in equation 2.3. This reaction is an ion exchange with an ammonium salt and then a thermal decomposition of the ammonium ions inside the zeolite [22].



This reaction creates only one Brønsted acid site. Methods with increased complexity allow for the creation of two or three Brønsted acid sites within the zeolite. Hydrogen exchanged zeolites are essentially “solid” acids where the acidic strength depends on the amount of aluminum in the zeolite structure. This is because silicon’s electronegativity is higher than aluminum, which means the strongest Brønsted acid sites reside on AlO_4 -tetrahedra with SiO_4 -tetrahedra immediately next to it.

The other application for catalytic zeolites involves taking advantage of its shape selective ability. Shape selectivity may occur three different ways within a zeolite. The first is reactant shape selectivity where reactants of different reactions vary in size. A

smaller reactant will travel into the zeolite faster than a larger reactant, leading to one reaction occurring more often than the other. Product shape selectivity is another case where a difference in product size determines which reaction occurs more often. Finally, transition state shape selectivity occurs when the size of transition states or intermediates restricts the completion of one reaction compared to another [22].

Use of zeolites as ion exchangers has several important applications. One of the most significant applications lies in the removal of Ca^{2+} and Mg^{2+} in domestic water. Another major application involves removal of Ca^{2+} , Mg^{2+} , and NH_4^+ from industrial wastewater [2]. The ability of zeolites to exchange cations with a solution is a result of the mobile electrostatically bonded cations located inside the pores. For the application of ion exchange in laundry detergent, water softens through an ion exchange of the Ca^{2+} and Mg^{2+} ions found in water with a zeolite with Na^+ cations. Zeolite A with Na^+ ions is highly selective for calcium and is softer than Ca^{2+} and Mg^{2+} , which is why zeolite A is commonly found in detergents [19]. Ion exchange is also a key step in the synthesis of zeolites for use as catalysts. For this application, ion exchange mechanisms introduce Brønsted acid sites on the zeolite to create specific catalysts required for a desired reaction [22].

The final application of zeolites involves use in separation and purification processes. Examples include: 1) Removal of CO_2 , chlorides, and mercury from different process streams in petroleum refining; 2) Drying of hydrocarbon liquids, hydrogen, and cracked gas in petrochemical processes; 3) Drying and desulfurizing natural gas; 4) Removal of water, N_2 , and CO_2 from air for cryogenic distillation or PSA processes; 5) Hydrogen purification; and 6) Xylene isomer separation, etc.

Zeolites can be utilized in different ways to affect separation and purification processes. One method, kinetic separation, takes advantage of a zeolite's pore size compared to the molecules traveling through them. The other way is to utilize a zeolite's polarity through equilibrium separation. The latter is the method used in this thesis for air separation where the utilization of a zeolite that preferentially adsorbs nitrogen allows for production of nearly pure oxygen. Oxygen, nitrogen, and argon, the three main components in air, all have molecules with similar size and polarizability leading to similar van der Waals forces. However, nitrogen preferentially adsorbs due to a stronger quadrupole moment compared to the other two molecules. 5A and 13X zeolites are commonly used to accomplish this separation in a PSA process.

The importance of zeolites in industry is enormous and with endless potential zeolite structures, research towards improved zeolites will no doubt continue in the future [40]. Future applications could include strong base and oxidation catalysis, chiral synthesis, membrane reactors, sorption heat pumps, and desiccant cooling and dehumidification [19]. Endeavors around the world are currently at work to use zeolites for new applications that include electrochemistry, photochemistry, and membrane science and technology [22].

2.2 Adsorption

Adsorption by definition is the accumulation of fluid molecules at a surface. This phenomenon occurs because of an attraction between adsorbate molecules (either a gas or liquid) and an adsorbent surface (porous solid) [5]. The thermodynamics of adsorption are the key to understanding and controlling how the process occurs. There are two main

methods adsorption occurs, physical adsorption and chemisorption. Physical adsorption is the more common of the two because it is easily reversible and can form more than one layer. Chemisorption involves the formation of bonds between the adsorbate and adsorbent surface. However, it can only form one molecular layer on the surface of a solid and it is not easily reversible, which limits its industrial impact for separation and purification processes. Chemisorption is not the focus of this study, so it is not discussed any further and all references in this thesis to adsorption from this point forward refer to physical adsorption only.

2.2.1 Adsorption Fundamentals

The attraction between an adsorbent and adsorbate molecules is a result of molecular interactions, which are a combination of permanent dipoles, induced dipoles, and London dispersion forces. Permanent dipoles occur in polar molecules as a result of an uneven distribution of charge in the electron cloud. Polar molecules can also induce an uneven charge distribution (i.e. polarity) in nonpolar molecules if they are close enough to interact. Nonpolar molecules do not have permanent dipoles when their charge is averaged over time. However, at any instantaneous moment they will have a dipole that has the potential of inducing a dipole on another nonpolar molecule, creating London Dispersion forces. Repulsion forces occur when molecules are too close to each other and their electron clouds start overlapping with each other. When adsorption occurs, there is equilibrium between these repulsion forces and the forces of attraction. Illustrated in figure 2.4 is a potential energy diagram for adsorption that shows potential energy (sum of all the interactions that exist between the adsorbate and adsorbent) as a function of the distance of the adsorbate molecule from the adsorbent surface. The high

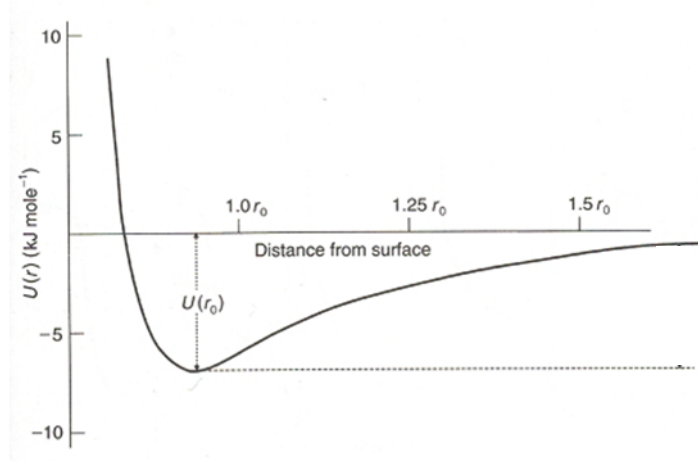


Figure 2.4. Potential energy diagram for adsorption [5].

positive repulsive potential energy near the adsorbent surface is where the electron cloud overlap would occur. The depth of the potential well, $U(r_0)$, is related to how attractive the adsorbate is to the surface. The larger the potential energy difference, the greater the adsorbate would be attracted to the surface if it was a distance, r_0 , from it. At zero Kelvin where there is no kinetic energy, a molecule would settle at the bottom of the well. At all other finite temperatures, the molecule will oscillate around the minimum potential energy.

2.2.2 Adsorption Thermodynamics

Adsorption equilibrium determines how much of a fluid molecule will be trapped in an adsorbent at a defined pressure, temperature, and composition. Adsorption causes a gas molecule to lose at least one of its translational degrees of freedom because it restricts the gas molecule to move along the surface of the adsorbent. This causes a decrease in entropy (ΔS) and since adsorption is a spontaneous process, Gibbs free energy (ΔG) is reduced as well. Thus from the thermodynamic expression seen in equation 2.4, ΔH

(enthalpy) also must decrease, which generates a release in heat making adsorption an exothermic process.

$$\Delta G = \Delta H - T\Delta S \quad (2.4)$$

The equation for the isosteric heat of adsorption is seen in equation 2.5:

$$\Delta Q = \frac{\partial \ln P}{\partial T} RT^2 \quad (2.5)$$

where R is the ideal gas constant and P is pressure. Isotherms are a typical method of representing equilibrium for single component adsorption. Isotherms are measured at a constant temperature while the pressure is varied and the amount of adsorbate is measured. Isotherms can take different shapes as shown in figure 2.5. The main difference between the types of isotherms is whether or not the adsorption capacity

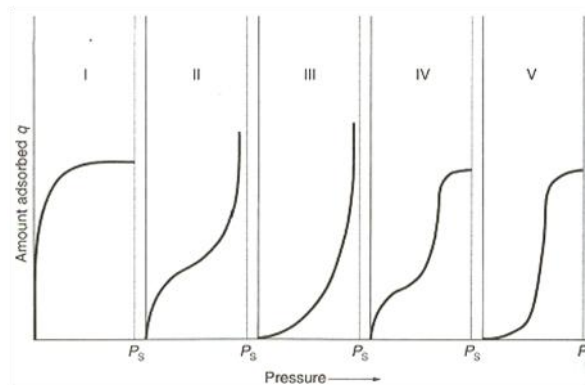


Figure 2.5. The five types of isotherms [5].

increases as it reaches the adsorbate saturated vapor pressure (P_s) and by differences in the intrinsic affinity of a solid for an adsorbate. Type I isotherms are most relevant to this study and represent adsorbents that have pores similar in size to the adsorbate molecules and that fill up and approach a saturation limit. The other types of isotherms have larger pores compared to the adsorbate and thus do not experience this saturation limit except in

the case of the type IV and V isotherms near P_s . Type III isotherms represent systems where an adsorbate interacts more strongly with other adsorbates rather than the adsorbent. Type II isotherms can have multiple adsorbed layers because of their larger pore size, thus they do not exhibit a saturation limit. This is the other type of isotherm also sometimes used in PSA process.

2.2.3 *Adsorption Kinetics*

Diffusional resistances normally regulate the approach to equilibrium described in the previous section. There are three resistances to mass transfer during adsorption. The first is the resistance that occurs around the adsorbent particles as film resistance if the fluid is a mixture. The other two occur within the particles in the macro/mesopores between the crystals in an adsorbent particle and in the micropores within the crystals themselves. These resistances are in series, but typically only one is rate controlling. Zeolites are also often synthesized with a porous binder material that holds the crystals together, especially for separation processes where a sudden change in pressure occurs. An example of a zeolite particle structure is represented in figure 2.6 on the next page.

Macropore diffusion occurs in adsorbent pores that are significantly larger than the diameter of the diffusing sorbate. With zeolites, these are the pores between the microporous crystals. For macropore diffusion, several different types of diffusion are possible. When the pore size is much greater than the mean free path of the sorbate molecules, diffusion occurs by bulk gas diffusion. At low pressures and with smaller pores, collisions between the diffusing molecule and pore wall become important

resulting in Knudsen diffusion. Poiseuille flow (pressure flow) becomes relevant with larger pore and particle sizes and higher pressures, like during the pressurization step of a PSA process. A final possible method of macropore diffusion occurs only under high adsorbate concentrations and when the adsorbed phase is mobile. Under these conditions it is possible for the adsorbed molecules to diffuse on the surface of the pore as well [13]. When multiple different diffusion mechanisms happen simultaneously in macropores, the diffusivities are additive to create an overall effective diffusivity.

Micropore diffusion is the diffusion of adsorbate molecules in comparable

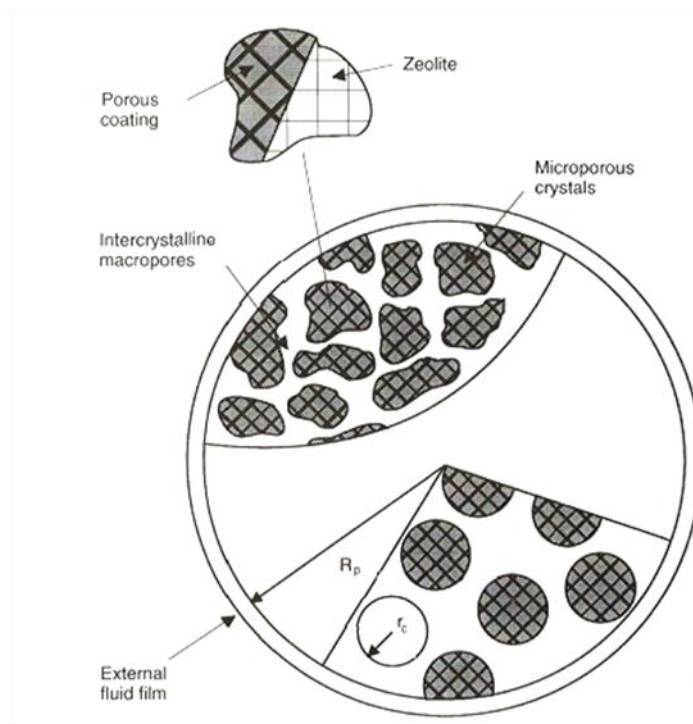


Figure 2.6. Depiction of pores and mass transfer resistances in adsorption [5].

size adsorbent pores. For zeolites, this occurs within its crystals where the pore size is limited by the oxygen windows into the cavity of the zeolite. If a binder is present,

micropore diffusion will occur through the binder as well. The “adsorbed phase” in this type of diffusion refers to the adsorbed molecules on the pore wall along with the molecules trapped in the middle of the pore [13]. Micropore diffusion is an activated process because unlike macropore diffusion, it is not possible for the adsorbate molecules to escape the forces of the pore wall. Micropore diffusion is affected by many factors. Temperature influences micropore diffusion because diffusion in a potential field is an activated process. The channel size and geometry of a crystal affects how quickly adsorbate molecules can diffuse through transition states. The type and distribution of the exchangeable cation affects the micropore size, which affects the adsorbate diffusivity into the micropores along with how strongly it attracts adsorbate molecules. Finally, crystal lattice defects can impact the intracrystalline diffusivity as well.

2.2.4 Adsorption Column Dynamics

PSA processes utilize a column packed with an adsorbent where feed mixture is introduced in one end of the column and product exits the other end. The feed gas concentration changes with time within the column causing a concentration wave to form in the column as the adsorbate moves from the fluid phase into the adsorbed phase. This occurs in a “mass transfer zone (MTZ)” that travels through the column and eventually reaches the opposite end of the column. This results in what is called a breakthrough curve, which occurs when the outlet concentration of the adsorbate begins to increase, eventually reaching the inlet adsorbate concentration. The shape of this breakthrough curve is heavily dependent on the shape of the adsorption isotherm that exists between the adsorbent and adsorbate and whether the equilibrium is favorable or unfavorable for adsorption. For adsorption, figure 2.7 illustrates how to determine the favorability of an

adsorption isotherm. If favorable, during adsorption the concentration wave within the column will be compressive or self-sharpening as seen in figure 2-8. This is a result of

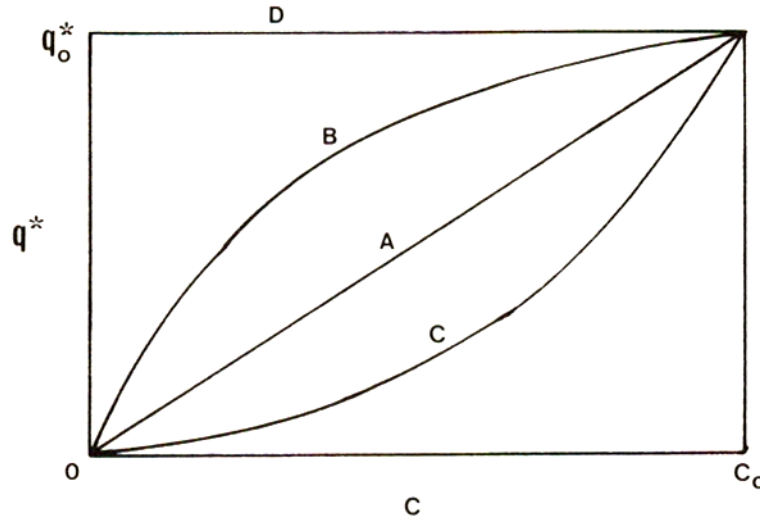


Figure 2.7. Shapes of isotherms in determining the sharpness of concentration wavefronts: (A) linear; (B) favorable; (C); unfavorable; (D) irreversible. q^* = equilibrium amount adsorbed and C = concentration of adsorbate in gas phase [36].

the high adsorbate concentration front traveling faster than the low adsorbate concentration front. The limit of this wave is a shock wave or discontinuity. An unfavorable isotherm will lead to a dispersive wavefront, the opposite of a compressive front [36]. The sharper the wave front in the column, the smaller the MTZ within the column and the higher the efficiency will be. This is illustrated in figure 2.9 which shows the MTZ from $z = L_e$ to $z = L$ where c_0 is the inlet adsorbate concentration and c_e is the equilibrium adsorbate concentration. Desorption also results in a dispersive wavefront similar to what is seen in figure 2.8.

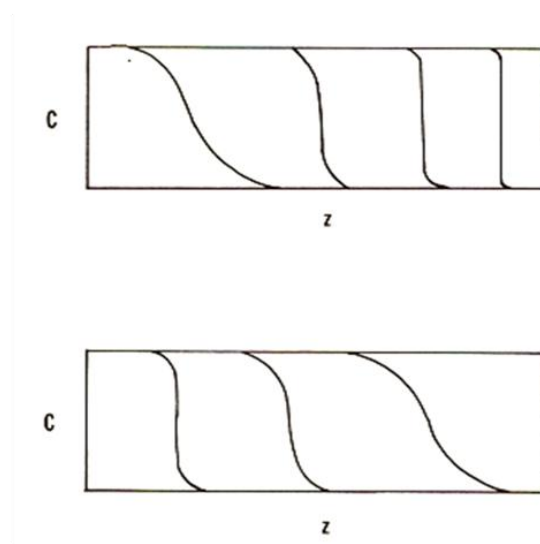


Figure 2.8. Self-sharpening wavefront (top) and dispersive wavefront (bottom). c is adsorbate concentration and z is column length [13].

Mass and heat transfer resistances that exist in the column further extend the length of the MTZ depending on the degree to which these resistances affect mass transfer. Because adsorption is an exothermic process, temperature increase will affect the equilibrium and thus impact the MTZ. Also, the shape and size of the

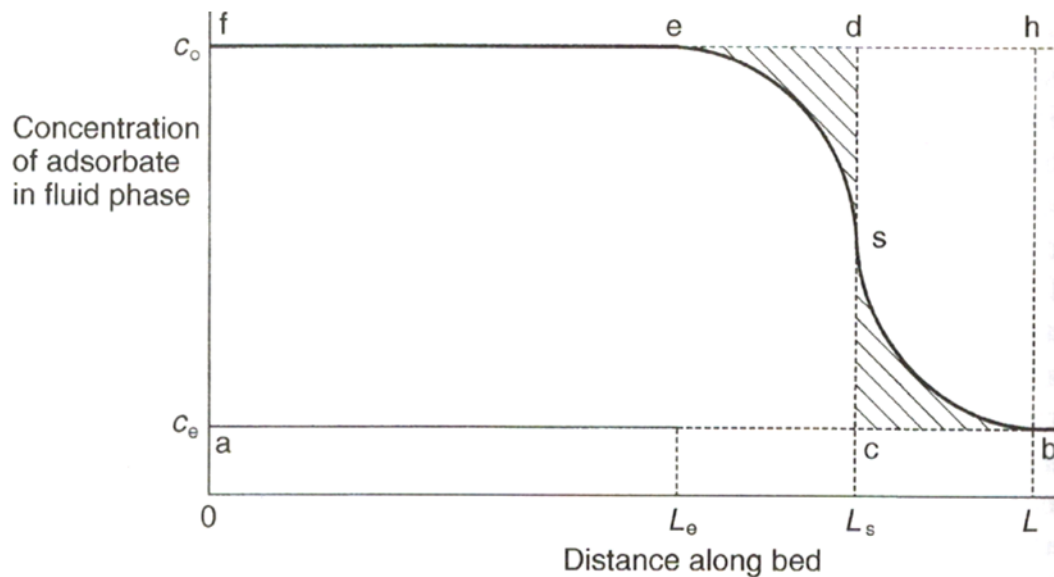


Figure 2.9. Mass transfer zone inside a column [5].

adsorbent/adsorbate create mass transfer resistance that will affect adsorption if significant transfer limitations to the adsorption sites exist within the adsorbent. Increasing the flow velocity within the column is another possible way to affect the concentration wave as it will have a dispersive effect on the concentration wave within the column.

Figure 2.10 illustrates an example of a breakthrough curve shape where t_b represents the time when breakthrough occurs. Observing the outlet of a column over

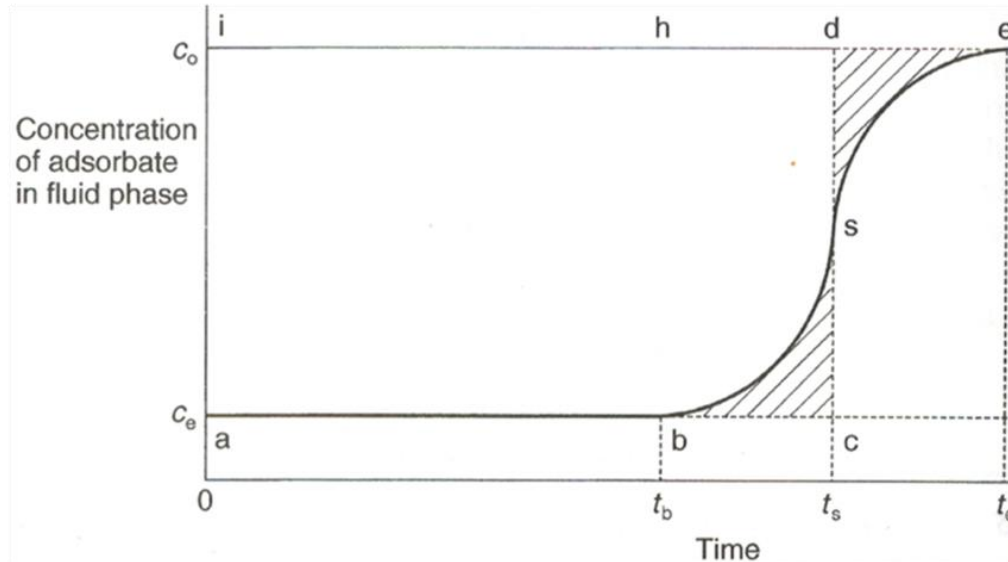


Figure 2.10. Column breakthrough curve [5].

time creates what is called a breakthrough curve. It is in essence a mirror image of the MTZ in the column. The shaded region between point b and point c represent the unused portion of the column, which determines the efficiency of a process. If mass and heat transfer resistances are small and the adsorbent has a favorable adsorption isotherm, the breakthrough curve will be steeper since the MTZ is sharper, reducing the amount of unused column in the MTZ and increasing the efficiency.

2.3 Air Separation by Pressure Swing Adsorption

Pressure swing adsorption (PSA) is a process designed for efficient gas separation and purification by utilizing a molecules ability to adsorb to the surface of an adsorbent. Depending on the adsorbent/adsorbate interaction, this is accomplished through either kinetic or equilibrium separation. This study will focus on equilibrium separation for O₂ production only. Air separation utilizing equilibrium separation is feasible because of the previously mentioned higher quadrupole moment of nitrogen compared to oxygen. This allows zeolites to selectively attract nitrogen over oxygen and provide nearly pure oxygen. Thus, knowledge of the adsorption equilibrium of oxygen and nitrogen on the adsorbent is critical to PSA processes because it provides the thermodynamic restrictions for the capacity of the adsorbent at a specified gas composition, temperature, and pressure [6].

2.3.1 Pressure Swing Adsorption Principles

The basic premise of a pressure swing adsorption process involves one or more columns packed with an adsorbent (zeolite, carbon molecular sieve, etc.) which preferentially adsorbs one type of gas molecule compared to other(s) in a gas mixture that passes through the column(s). This normally occurs at some pressure above atmospheric pressure until the gas nearly saturates the column with the more strongly adsorbed gas molecule (heavy component). The “raffinate” product is the gas molecule type that adsorbs less (light component) and comes out the product end of the column. In order to reuse the column later in the process, the heavy component needs to be removed from the column through desorption or regeneration. Desorption of the column is critical to the

efficiency of the process and is a step where improvements are made to increase the extent of regeneration in order to maximize the removal of the heavy component and increase the efficiency of the process. As previously mentioned, adsorption equilibrium is determined by the gas composition, temperature, and pressure. A change in any of these properties regenerates the adsorbent in the column. Since desorption is the opposite of adsorption, the process is endothermic in nature. Desorption in a PSA process occurs through changes in the pressure and composition of the column because they provide the quickest method of regeneration. Desorption occurs at either atmospheric or vacuum pressure causing the pressure to swing from high pressure during adsorption to a low pressure during desorption, hence the name “Pressure Swing”.

What makes a PSA system unique compared to other processes is that while most other separation processes operate under steady state, a PSA process is dynamic as conditions within the column are constantly changing. The process operates within cycles in which a column repeatedly experiences a series of pressurization, adsorption, and regeneration steps. PSA processes ideally operate under cyclic steady state (CSS) which occurs when the conditions in the column at the end of each step is the same from cycle to cycle. At CSS, the performance of a cycle remains the same over time.

To evaluate the performance of a PSA system, three design parameters are examined: product purity, product recovery, and BSF. The selectivity of the adsorbent for a chemical species primarily determines the possible purity. Product recovery is a measure of how much desired component is in the high pressure product stream compared to the feed stream. BSF measures how productively the adsorbent mass is utilized. Purity and recovery are an indirect way of measuring the separation efficiency

and help determine if a process design is capable of producing the desired results [6]. There is a trade-off between recovery and purity; i.e. high purity usually results in lower recovery. Maximum potential recovery is established by the affinity of the solid for the heavy component over the light component through equilibrium. Recovery determines the energy efficiency of the process since it determines how much high pressure feed is utilized per product rate. The kinetics of the column primarily determine the size, cycle time, and amount of adsorbent, which all have an impact on the BSF of the column. All of these performance parameters are mutually dependent on each other and changing one will have an impact on the others.

2.3.2 History and growth of Pressure Swing Adsorption

Pressure swing adsorption is a technology that has developed primarily within the last 50 years. It has become a valuable part of processes such as air drying, hydrogen purification, n-paraffin removal, xylene isomer separations, and air separation [36]. There are several important factors about PSA processes that make it more feasible over other separation techniques. First, the availability of an extra thermodynamic degree of freedom to define the adsorption process due to the existence of the solid allows for a greater flexibility in process design compared to other separation processes like distillation, extraction, and absorption. Second, there are a large number of adsorbent types including zeolites, activated carbons, silica gels etc., with different properties capable of separation through adsorption in a variety of ways. Finally, optimizing a process for a specific adsorbent or end product allows for creativity, engineering, and continuous growth in PSA technology [37]. For example, there are numerous ways to design and operate an air separation process using PSA to achieve essentially equivalent

results. Improvement of PSA processes can occur through either developing new adsorbents (material science) or developing more efficient steps in the cycle to regenerate the adsorbent (engineering) [6]. Discussion on the development of adsorbents, specifically zeolites, occurred earlier. The emergence of more efficient cycles takes place later in this discussion.

The original intent for research and development of the PSA process in the 1950's and 1960's was for the application of air separation. Production of ultrapure oxygen through cryogenic distillation is economically feasible only in large scale applications because of the extremely low temperatures (96 K) involved in the process. However, for smaller scale operations or when a high purity is not required, PSA processes have proven to be more economical than cryogenic distillation. The low adsorption selectivity of early solids rendered air separation before the 1950's more challenging compared to air drying, hydrogen purification, and n-paraffin removal [36]. However, with the development of synthetic zeolites (i.e. 5A, 13X), separation of air through adsorption was thrust into the forefront of adsorption research [36]. This led to the development of two different types of PSA cycles in the late 1950's that served as the basis for later designs of PSA systems. The first patent was for the Skarstrom cycle assigned to Esso Research and Engineering Company [11]. The other was for the Guerin-Domine cycle assigned to L'Air Liquide [32]. The main difference between the cycles lies in the regeneration step of the cycle. The Skarstrom cycle accomplished regeneration through a blowdown and low pressure purge using light product while the Guerin-Domine cycle opted to use vacuum desorption for regeneration of the column [13].

The Guerin-Domine cycle has a flexible design that allows for operation of one to six columns, different cycle designs, and a variety of ways to connect the columns [13, 36]. Figure 2-11 illustrates an example of this cycle with two columns. Compressed air enters column 1 in the first step while column 2 evacuates. Column 1 then depressurizes through column 2, which adsorbs some of the oxygen while allowing the rest to leave the column as raffinate product. Column 1 next evacuates and then the column events are switched which completes the cycle and allows for collection of nearly pure nitrogen and oxygen [5]. Use of vacuum in the process allows for good separation of air with a two column cycle producing 98% (argon-free basis) oxygen purity at 51 % recovery and 96.3% nitrogen purity at 58% recovery [13]. As will be seen later, this method has a

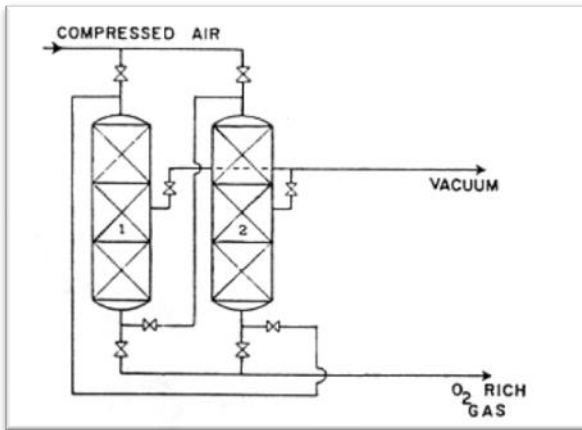


Figure 2.11. Schematic diagram of two-column Air Liquide PSA system [13].

better performance compared to the Skarstrom cycle in large part because of the use of vacuum desorption which the original Skarstrom cycle does not use. Because of the low adsorption selectivity between oxygen and nitrogen, vacuum desorption along with elution of oxygen through a clean column allows for the higher purity and recovery [36]. This however comes at the cost of a mechanical energy requirement to create the vacuum

within the columns along with the disadvantage of having an extract product below atmospheric pressure [13]. Around the same time, Skarstrom filed for a patent for a cycle with some similarities, but also noticeable differences [11]. Figure 2-12 illustrates an example of a traditional two column Skarstrom cycle. A cycle consists of both columns

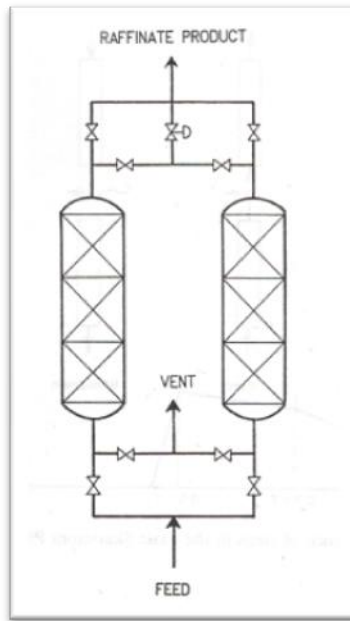


Figure 2.12. Basic two-column pressure swing adsorption system [13].

experiencing the following steps: 1) Pressurization, 2) Production, 3) Countercurrent (opposite of feed flow) blowdown, 4) Countercurrent purge. The pressurization and production steps are similar in that they both involve the input of feed gas and thus will be referenced in the future as a combined “feed” step. The cycle works such that one column undergoes the feed step while the other is blowing down and purging. The purge step involves passing a fraction of the purified light product through the column at low pressure after the blowdown step. Figure 2-13 illustrates the pressure seen in the column during each step. Skarstrom cycles usually operate their feed (production) steps at a pressure above atmospheric pressure while the blowdown occurs at atmospheric pressure

and the purge at a pressure slightly above atmospheric. Regeneration in a Skarstrom cycle occurs mainly by lowering the partial pressure of nitrogen in the column. The blowdown step accomplishes this by dropping the overall pressure to atmospheric pressure. The stream from the pressure reduction (blowdown) part of this process is primarily composed of the heavy component concentration or “extract”. The purge step

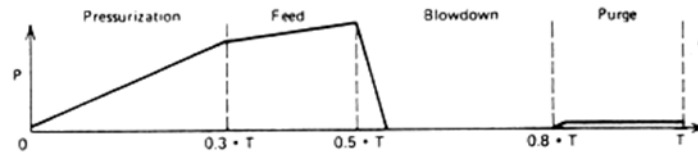


Figure 2.13. Column pressure during Skarstrom cycle [13].

further lowers the nitrogen partial pressure by countercurrently flowing part of the purified oxygen product through the column. The purge step is perhaps the most important step as it is responsible for pushing back the heavy component concentration front (MTZ) towards the feed side of the column, preventing negative effects on the product purity in the next cycle. Product purity rises when the amount of product used for the purge increases, but only to a certain point as the purity increase eventually becomes minimal. Raising the purge amount also has an obvious negative impact on the possible recovery since it reduces the amount of product. At a higher column operating pressure, the portion of the product gas required for the purge step reduces because of the increase in volume going from higher to lower pressure. However, the higher pressure creates a greater energy requirement and after a certain pressure, the extent of extra adsorption that occurs does not outweigh the energy costs of the higher column pressure. Also, higher column pressure increases the amount of raffinate product that is lost during the blowdown step, which eventually limits the recovery at high pressures [13]. A part of

the engineering design that goes into a PSA system deals with finding the optimum pressure ratio (ratio of adsorption pressure to desorption pressure) and critical purge. Critical purge occurs when there is just enough purge gas taken from the product to achieve a specified product purity. This can be useful information to find for a PSA process in order to determine the operating conditions of the process. Finding the optimal purge amount that provides the necessary purity and highest possible recovery is a major challenge when engineering PSA systems. Another significant challenge is to find the optimal purge amount for a specific purity while reducing BSF (or reducing the amount of adsorbent solid needed).

Skarstrom's invention had two key ideas valuable to future improvements. The first aimed at countering the changes in temperature in the columns due to the occurrence of both exothermic and endothermic processes. Heat of adsorption proved to have a negative effect on separation efficiency for longer cycles and higher feed rates to the column. Skarstrom suggested keeping the swing in temperature in the column minimal with shorter cycles and a smaller feed volume to the columns. This would allow the transfer of the sensible heat of the solid between different steps in the cycle. The other idea was the volume of the purge and feed with respect to their pressures should at least be equivalent to completely purge the column [36]. The Skarstrom process is effective for air drying, but air separation only produced 90% oxygen at a recovery of 10% with a 13X zeolite adsorbent [13]. The advantage the Skarstrom cycle had over the Guerin-Domine cycle is a higher pressure product and less of an energy requirement per product. Clearly however, enhancements to the cycle were necessary in order for it to become economical to use for air separation.

2.3.3 *Improvements to PSA cycles*

Several key improvements to the original Skarstrom cycle have allowed it to become a viable option for smaller scale air separation operations. The cycle has two main areas where improvements are possible. One area is improving the regeneration steps for the column, namely the purge and blowdown steps. The exit streams from these steps are considered waste streams and mostly contain unwanted strongly adsorbed molecules. However, a significant amount of raffinate product still remains, reducing recovery. Another area for improvement involves maximizing the capacity of the column by limiting the amount of the heavily adsorbed molecules in the column prior to the feed step. The key improvements include using a portion of the product for pressurization of the column, pressure equalization between the columns, operation of the blowdown step at vacuum pressure, and lowering the cycle time. These improvements aim to either increase recovery, lower energy requirements, or limit the size of the system.

The first improvement requires the addition of another step to the Skarstrom cycle in which some of the product gas is used to pressurize a column after the purge step, but before the feed gas is introduced. Product pressurization will increase the product purity because product gas used to pressurize the column helps keep the product end clean of the heavy component by pushing back the heavy component front further towards the column feed side. A nearly full pressurization with product gas would require a large tank, which is why full product pressurization is not always desirable. However, a partial pressurization is still advantageous for an improvement in recovery while maintaining a high purity. The product gas used for partial pressurization reduces the purge gas requirement and will mostly be recovered during the feed step.

The next improvement is the addition of a pressure equalization step that was first suggested in a patent filed in 1964 by Marsh [41]. The idea behind pressure equalization is to conserve what is normally waste gas during the blowdown step and use it to partially pressurize another column before the feed step. Instead of an immediate blowdown step after the end of the feed step, two columns are connected and the pressure equalizes to some extent between the two columns causing one column to partially blowdown and the other column to partially pressurize. This saves energy because the column now needs less feed gas to pressurize to the desired adsorption pressure. If the raffinate product is the goal of the process, then ideally the product side of the columns are connected for equalization so that any leftover raffinate product still in the column travels to the other column. This conserves separative work during the following feed step thus increasing recovery [6]. For large capacity operations, using pressure equalization with PSA processes that involve more than two columns further improves the recovery and allows for a continuous product stream flow without requiring an extra storage tank [6, 13].

Another possible improvement to the Skarstrom cycle is blowing down the column to vacuum instead of atmospheric pressure. The process is called vacuum swing adsorption (VSA) if the adsorption pressure is atmospheric. If the adsorption pressure is above atmospheric, then it is considered a hybrid PSA-VSA process. Under vacuum, a lower blowdown pressure requires less purge flow to regenerate the adsorbent. The extra energy requirement to attain vacuum can be offset to some extent by a lower adsorption pressure requirement in the column which allows VSA and PSA-VSA processes to be a viable solution in some applications. Vacuum operation in air separation usually lies in the Henry's law region of the isotherm where the pressure ratio determines the possible

purity and recovery [13]. Under vacuum, the adsorbent selectivity is always higher which leads to an improved recovery of the raffinate product and a potential of up to 30% energy savings [5].

The previous improvements had the aim of improving the purity and recovery of the raffinate product. There is one other PSA performance evaluator not discussed yet and that is BSF. Once again, BSF is the measure of the amount of adsorbent in pounds per product mass flow rate in tons per day. By definition, there are three ways to decrease the BSF of a PSA process. First, employing an adsorbent with an increased capacity allows for either increased production of raffinate or a reduction in the amount of sorbent needed in the column, both of which will decrease the BSF [6]. The next possible way of improving BSF is lowering the cycle time. Typical industrial PSA processes have a cycle time around 10 minutes. When the cycle time is lowered to 30 seconds or below, it is called Rapid PSA. Lowering the cycle time requires an increase in feed rate for a given amount of adsorbent, which causes numerous potential problems associated with high gas velocity in the column including improper gas distribution, fluidization of the sorbent, increase in pressure drop in the column, and higher gas dispersion. More importantly, higher gas velocity reduces contact time with solid. Given a finite rate of adsorption, the result is a stretched MTZ which causes premature breakthrough, thus reducing purity. These problems all can lead to lower separation efficiency and a decrease in product purity and recovery due to the increase in size of the mass transfer zone as the feed rate increases [37]. However, as long as the productivity increase is greater compared to the decrease in swing capacity, it is possible to reduce the

column size, which is ideal for certain applications like portable medical oxygen concentrators and reducing the size of hydrogen PSA processes [6].

2.3.4 Air Separation Applications

The largest application of air separation is the production of 90-94% pure oxygen gas for use in industrial processes and medical applications. The advancements discussed earlier produced improved PSA/VSA units in the mid-1980's and 1990's that used five times less adsorbent and two times less power. A simple two-column VSA system was able to produce over 100 tons of oxygen per day, which provided an alternative to cryogenic air separation. Compared to cryogenic systems with similar production, the VSA system had a higher capital cost, but allowed for a significant energy savings [19].

A significant application for air separation through RPSA is portable oxygen concentrators (POC) for medical use. These oxygen concentrators utilize a RPSA cycle to significantly reduce the weight of a POC to less than 4.5 kilograms and can provide up to 6 liters per minute of oxygen. Originally the design of POC's was for use in ambulances and short term travel. They have grown however for use over longer periods of time. Numerous companies have entered this market including Inogen One, Invacare, AirSep, and Respironics. The design of all POC units is similar because they all have the same engineering and design fundamentals. The difference in performance comes from trade-offs made in the design process to provide different specifications and characteristics that lower energy requirements and target the specific needs of different patients [35].

Because of the complex and dynamic nature of a PSA process, in addition to the process dynamics of all the supporting equipment such as valves, tanks, etc, modeling of the process remains difficult making the design and optimization of the process principally experimental in nature. Modeling the process requires numerous partial differential equations describing the number of different process steps, initial conditions, and boundary conditions for each step. Solving these equations is both time consuming and difficult to do with the accuracy and reliability [37]. Further adding to the problem is the difficulty in understanding multi-component gas-solid interactions that are needed for solving the equations in the model. Predicting these interactions from limited experimental data is difficult because of the range of conditions (pressure, temperature, and composition) that occur within PSA system throughout the process. Currently the best solution is developing simplified models for predicting a PSA process and then improving the process through a pilot plant [37]. Improving the knowledge of multi-component adsorption will remain the focus of research for years to come because of the challenges it provides. While air separation is a fairly established PSA process, utilizing the technology for other applications is another challenge for researchers. Current work is directed at improving PSA process for CO₂ capture from flue gases, olefin-paraffin separation, and CH₄-CO₂ separation [6].

2.3.5 *PSA Literature Review*

Literature for PSA processes is normally in three different categories. One focuses on the simulation side of the process, another on the experimental side of PSA processes, and the last normally is a combination of both in which experimental results are compared with simulation results. PSA literature reviewed for this thesis relate to

experimental/simulation results for cycles utilizing either a similar 13X zeolite for air separation or a PSA cycle with an equalization step.

An important case study conducted by Kayser and Knaebel examines the effects of isotherm nonlinearity in an equilibrium-based model for a PSA cycle designed for air separation with a 13X zeolite [18]. The model demonstrates a reduction in recovery of oxygen as either the desorption pressure or adsorption pressure moves out of the linear portion of the isotherm. Rege and Yang performed simulations to examine the limits of air separation using a LiX zeolite and compare it to a NaX zeolite [38]. They found that LiX zeolites gave higher recovery than NaX zeolites and that LiX zeolites are capable of performing at a pressure ratio of 2 with high product purity, recovery, and low BSF. Mendes et al. performed simulations and experiments utilizing a 5A zeolite for air separation to show how the pressure rising rate during the adsorption step affected the performance of the cycle [4]. They concluded that at higher pressure rising rates, dispersion in PSA column also rose leading to a decrease in product purity and recovery. Shin et al. compared a complete pressure equalization step against an incomplete pressure equalization step for the process of air separation using a 13X zeolite [16]. They found that a complete pressure equalization step allowed for a maximum recovery, but an incomplete pressure equalization step allowed for a minimum BSF. Chai et al. examined the effects of reducing the size of a medical oxygen concentrator on the performance of a PSA process [39]. They found that the BSF cannot be indefinitely reduced because of mass and heat transfer resistances along with the increasing affect of pressure drop during the desorption step.

CHAPTER III

THEORY

This section introduces the theory and concepts behind adsorption of a gas on a surface through a brief discussion of intermolecular forces. Then using these concepts, the interaction of oxygen and nitrogen molecules with zeolites is explained with consideration for how different exchangeable cations affect selectivity. Finally, isotherm models are reviewed along with how the calculations of PSA performance parameters were conducted.

3.1 Intermolecular Forces

A brief discussion of intermolecular forces occurred in the previous section with regards to van der Waal's forces and the potential energy curve of adsorption. However, a more rigorous description of these forces is required to fully understand what provides zeolites their selectivity, especially in the case of air separation. These forces also offer an explanation as to why different exchangeable ions produce

zeolites with different selectivity's. There are normally several different kinds of molecular interaction forces between molecules or ions. The level of interaction between molecules or ions due to a specific type of force depends on the types of molecules involved. In a PSA process when an equilibrium separation is occurring, the interaction of oxygen and nitrogen molecules with a zeolite is dependent on electrostatic, induction, and dispersion forces. The type of molecules involved determines which of these forces has a greater impact on the level of interaction. These forces are reviewed to the extent necessary to understand air separation. Additional resources are available that specifically discuss intermolecular forces in greater detail [21, 26].

3.1.1 *Electrostatic Forces*

An electrostatic force is a broad term that encompasses several types of intermolecular forces. Coulomb's law illustrates the simplest type where two ions approximated as point charges will have a force, f , between them as illustrated in equation 3.1:

$$f = \frac{w_i w_j}{4\pi\epsilon_0 r^2} \quad (3.1)$$

Where w is the magnitude of the point charges, r is the distance between the point charges, and ϵ_0 is the dielectric permittivity. An integration of equation 3.1 gives the potential energy, Γ , between the two ions seen in equation 3.2:

$$\Gamma_{ij} = \frac{z_i z_j e^2}{4\pi\epsilon_0 r} \quad (3.2)$$

where z_i and z_j are ionic valences of the two point charges and $e = 1.60218 \times 10^{-19} \text{ C}^1$ is the electron charge. Full understanding of these equations is not necessary for this study; however it is important to notice that the potential energy between the ions is inversely related to the distance between the ions. When the ions are not approximated as point charges, their charges are shielded due to the electron clouds of the ions, which causes the potential energy to vary inversely with the distance (between the ions) to higher powers.

Electrostatic forces are not solely between ions, interactions between molecules with dipole and quadrupole moments are included in these forces. Polar molecules exhibit dipole moments because their asymmetrical molecular shape creates an unbalanced distribution of electrons around the molecule resulting in a separation of effective charge between any two locations in the molecule. Non-polar molecules have a symmetrical molecular geometry that does not produce an effective charge distribution resulting in a dipole moment. Molecules can also exhibit higher order charge distribution. For example, a quadrupole signifies an effective charge difference at four points in the molecule and an octupole signifies an effective charge difference at eight points in the molecule. For the application of air separation, oxygen and nitrogen molecules are both non-polar molecules that exhibit quadrupoles (see Table 3.1).

3.1.2 Induction and Dispersion Forces

Intermolecular interactions also take the form of induction forces when electrons of a molecule become disturbed in an electrical field. The molecule (polar or non-polar)

¹ The factor $1/4\pi\epsilon_0$ is used only for SI units. Note also that equation 3.1 and 3.2 are for vacuum conditions and a modified version for non-vacuum can be seen in Prausnitz [21].

essentially gains an instantaneous charge distribution from the electrical field of a polar (or quadrupolar) molecule or ion in the immediate vicinity; hence the name “induced” electrostatic interaction. This causes the molecule to experience an attractive force with the polar (or quadrupolar) molecule or ion. The ease of which electrons are dislocated in a molecule is called the polarizability, α , of the molecule. Accordingly, induced electrostatic interactions are a strong function of polarizability. Induction forces are also capable of inducing quadrupole moments (and higher order charge distributions) in both nonpolar and polar molecules.

Finally, intermolecular interactions occur as a result of the instantaneous coupling of electron clouds. This type of interaction, called a dispersion force, exists for all molecules in nature, even if the molecules are non-polar since the effective charge distribution for a non-polar molecule is only zero when averaged over time. At any given instant, the molecule (polar or nonpolar) will have a momentary dipole moment capable of inducing an effective charge distribution on a neighboring molecule. Thus the electrons in the interacting molecules essentially move in tandem resulting in a net attractive (negative) potential energy. The ionization potential and polarizability of the molecules involved will determine the level of interaction. Dispersion forces, together with dipole-dipole (and higher order charge distributions) and induction forces are called van der Waals forces.

3.1.3 N₂ and O₂ Interaction with Zeolites

A simple way to view the interaction of oxygen and nitrogen molecules with zeolites is to treat the exchangeable cations of zeolites as point charges [17]. With this

model, the important intermolecular forces are due to the interaction of the quadrupole moments of these molecules with the point charge, the induced dipole moments of these molecules from the point charge, and the always present dispersion energy. When the point charge and one of the molecules are arranged linearly (most energetically stable orientation), the interaction due to the quadrupole moment depends on $1/r^3$, while the interaction energy due to the induced dipole depends on $1/r^4$. This shows that the quadrupole interaction energy is effective further away from the point charge compared to the interaction energy due to the induced dipoles. Table 3.1 shows there is a significant difference in quadrupole moments between nitrogen and oxygen molecules while the polarizabilities are very similar. The similar polarizabilities indicate that N_2 and O_2 molecules have similar induction and dispersion forces with the point charge. Thus for this simplified model with regards to intermolecular forces, the ability of a zeolite to attract nitrogen molecules over oxygen molecules is mainly because of a difference in the quadrupole moments of the molecules. Figure 3.1 shows the potential energy curves for the point charge model with nitrogen and oxygen molecules, which illustrates the difference in potential energy between the two molecules as they approach the point charge (y-axis in figure 3.1). Beyond this simple demonstration, additional factors can also play roles in the zeolite selectivity for nitrogen molecules including the relative position of the cations on the zeolite, the orientation of the nitrogen and oxygen molecules relative to the exchangeable cation, and the structure of the zeolite itself [17].

Table 3.1. Quadrupole Moment and Polarizabilities of Nitrogen and Oxygen Molecules [21, 26].

Molecule	$M \times 10^{40} \text{ (C-m}^2\text{)}$	$\alpha \times 10^{25} \text{ (cm}^3\text{)}$
O_2	-1.3	16.0
N_2	-5.0	17.7

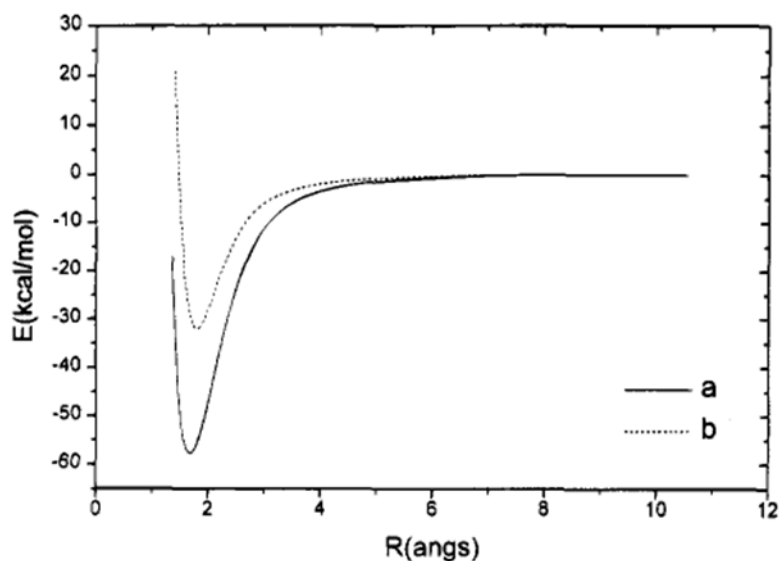


Figure 3.1. Calculated potential energy curves of N₂ (a) and O₂ (b) in the linear arrangement as a function of distance, R , between the point charge and midpoint of the diatomic molecules [17].

3.1.4 Exchangeable Cations

The type of exchangeable cations in a zeolite has a significant impact on its selectivity for nitrogen and oxygen molecules. A study conducted by Papai et al. specifically looked at using exchangeable cations Li⁺ and Na⁺ in zeolites [17]. Their conclusion was that substituting a Li⁺ cation for a Na⁺ cation increases the binding energy for nitrogen molecules more than it does for oxygen molecules, which in turn increases the selectivity for nitrogen molecules. This is visually represented in figure 3.2 in which the potential energy curve of a nitrogen molecule and a Li⁺ cation is compared with the potential energy curve of a nitrogen molecule and a Na⁺ ion. The potential energy difference is explained by the Li⁺ cation's lack of core electrons when compared to a Na⁺ cation. These core electrons of the Na⁺ cation give it a lower charge density than a Li⁺

cation which has a smaller ionic radius. The higher charge density of the Li^+ cation enhances the interaction with nitrogen molecules, while its smaller ionic radius also allows nitrogen molecules to get closer to the center of the ion where the attraction due to the short range interaction forces is stronger. This interaction with a smaller cation both increases the potential (i.e. depth of potential well) and decreases the separation between the ion and nitrogen molecule (i.e. collision diameter). This is illustrated in figure 3.2 by

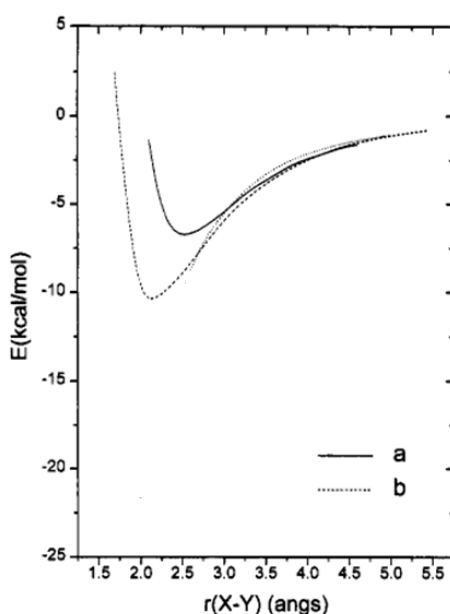


Figure 3.2. Potential energy curves of Na^+N_2 (a) and Li^+N_2 (b) [17].

how much closer the location of the minimum potential for the Li^+N_2 curve is to the cation (y-axis in the figure 3.2) compared to the minimum potential of the Na^+N_2 ion curve.

Several patents highlight the effects of using Li^+ as the exchangeable cation for air separation [8, 10, 14]. Use of Li^+ ions in zeolites has been studied as early as 1964 by Mckee [14]. Chao further explored the extent of Li^+ cation exchange necessary for

effective nitrogen adsorption [8]. His invention showed that the greater the Li^+ ion exchange, preferably around 90%, the better the zeolite capacity and selectivity for nitrogen. He also noted that a Si/Al ratio near 1.0 significantly increased the adsorption capacity and selectivity as well.

3.1.5 LiX Zeolite Limitations and Improvements

LiX zeolites have improved adsorption capabilities in comparison to NaX and CaX zeolites as mentioned earlier in this section. However, ion exchange using a Li^+ ion does have some limitations. Highly Li^+ cation exchanged zeolites are expensive to produce because ion exchange with Li^+ ions is less thermodynamically favorable compared to ion exchange with Na^+ and Ca^+ ions. This has limited their impact in PSA processes because of the high cost of production of these zeolites.

Current research is aimed towards reducing the higher cost of producing highly exchanged Li^+ zeolites through improved ion exchange methods [33, 44]. Coe et al. proposed creating a zeolite with a mixed Li^+/Ca^+ exchange to achieve a separation similar to highly exchanged Li^+ zeolites, but at a lower cost due to the more thermodynamically favorable exchange of calcium compared to lithium. Use of Ca^+ ions also prevented the decline in performance with a rise in temperature that was seen with mixed Li^+/Na^+ zeolites [10]. Chao et al. have also shown that adding alkaline earth metals like calcium can improve the thermal stability and prevent zeolite degradation at higher activation temperatures while remaining close to the high adsorption capacity of pure Li^+ ion zeolites [9]

3.2 Adsorption Thermodynamics and Equilibrium Models

The introduction to this thesis discussed how equilibrium between an adsorbent and adsorbate occurred. The ability to model this phenomenon is extremely important not only for PSA processes, but other applications as well. Collection of isotherm data is tedious and time consuming, so the development of an accurate model to describe how adsorption occurs is important. There are numerous different models for both single component and multi-component adsorption. Several of the models related to this study are described in this section starting with the most basic and then increasing in complexity. Equilibrium modeling has been well studied and written about in numerous texts, specifically ones written by Crittenden & Thomas, Ruthven et al., Suzuki, and Yang [5, 13, 27, 36]. This section draws from these texts and provides a brief summary of equilibrium models used for this study.

3.2.1 *Henry's Law*

Equilibrium between a solid adsorbent and adsorbate molecules is determined from thermodynamics. The adsorbed layer(s) is considered to be a separate phase thermodynamically speaking. At low adsorbate concentrations, the equilibrium relationship closely resembles a linear function, which is defined as Henry's Law seen in equation 3.3:

$$q = Kp_i \quad (3.3)$$

where q is the amount adsorbed, K is the "Henry's Law" constant (adsorption equilibrium constant), and p_i is the partial pressure of adsorbate in the gas phase. A typical vant Hoff

relationship for the temperature dependence of the adsorption equilibrium constant is represented by equation 3.4:

$$K = K_0 e^{-\Delta Q/RT} \quad (3.4)$$

where ΔQ is the heat of adsorption, R is the ideal gas constant, K_0 is related to the adsorption entropy change, and T is the temperature. Henry's law does not have a saturation capacity and adsorption increases to infinity as pressure rises. This however is not possible in microporous adsorbents with a finite pore volume. However, at low pressures as density approaches zero, all adsorption systems must thermodynamically approach Henry's law with a finite slope at the origin.

3.2.2 *The Langmuir Isotherm*

The simplest and most commonly used adsorption model for microporous solids that includes a saturation capacity with a finite number of sites (each site can only accommodate one molecule) is the Langmuir isotherm. The Langmuir model makes the assumption of a monolayer surface coverage of the adsorbate on the adsorbent surface [24]. The surface is assumed to be energetically uniform and the adsorbed molecules are assumed to be isolated with no interaction forces between them. The Langmuir model has wide use for describing the dynamic equilibrium for physical adsorption systems at lower surface concentrations. Many systems show at least relative consistency with the Langmuir model. Furthermore, the Langmuir model reduces to Henry's Law at low concentrations, which is a requirement for thermodynamic consistency in any physical adsorption system. This allows the Langmuir isotherm to at least serve as a starting point

for the design of PSA systems [13]. A summary of the key assumptions of the Langmuir isotherm are as follows:

- 1) The heat of adsorption, ΔH , is constant and independent of coverage (due to assumption of isolated adsorbed molecules with no lateral interactions)
- 2) Only one adsorbate molecule is located at a site
- 3) Localized adsorption (adsorbed molecules remain adsorbed until desorption occurs)
- 4) The solid possesses finite number of adsorption sites

Langmuir contended that the rate of adsorbate gas molecules colliding with the adsorbent surface is proportional to the partial pressure of the gas and the probability of adsorption occurring is proportional to the fraction of empty sites. Additionally, he asserted that the rate of desorption is directly proportional to the fraction of occupied sites. Finally, he contended that at dynamic equilibrium, the rates of adsorption and desorption are equal [5]. For a single adsorbate system, the rate equation looks like equation 3.5:

$$k_a p_i (1 - \theta) = k_d \theta \quad (3.5)$$

where p_i is the adsorbate gas pressure, θ is the fractional surface coverage, and k_a and k_d are the rate constants for adsorption and desorption respectively. θ is the ratio q/q_s where q_s is the adsorption saturation capacity of the adsorbent assuming only monolayer coverage. When k_a and k_d are combined together (since they cannot be experimentally determined individually), the Langmuir isotherm equation is typically represented by equation 3.6:

$$\theta = \frac{bp}{1 + bp} \quad (3.6)$$

where b is the ratio k_a/k_d (adsorption equilibrium constant). Equation 3.6 correctly approximates the asymptotic behavior that appears as sites fill up during adsorption. The equation simplifies to Henry's Law at low concentrations and nears a saturation limit at high concentrations. From the application of the kinetic theory of ideal gases, b can be found from equation 3.7:

$$b = \frac{\sigma}{v} (2\pi mBT)^{-1/2} \exp\left(\frac{\Delta Q}{RT}\right) \quad (3.7)$$

where v is rate constant for desorption, σ is the condensation coefficient (fraction of molecules that are adsorbed with an activation energy greater than the energy of activation for adsorption, E_a , m is the mass of the adsorbate molecule, B is the Boltzmann constant, and ΔQ is the heat of adsorption (the difference between the activation energies E_d and E_a necessary for desorption and adsorption). The equilibrium constant b is directly related to the Henry's constant ($K=bq_s$). Both b and K decrease with an increase in temperature because of the exothermic nature of adsorption. This gives isotherms at lower temperatures more curvature compared to isotherms at higher temperatures.

3.2.3 *Multi-Component Adsorption*

The Langmuir equation can be extended to gaseous mixtures by assuming that equilibrium develops between the partial pressure of one of the gaseous components and

the adsorbate surface. For a component i , the resulting partial isotherm can be approximated by the equation 3.9:

$$\frac{q_i}{q_{si}} = \frac{b_i p_i}{1 + \sum_1^n b_j p_j} \quad (3.9)$$

where q_{si} is the saturation capacity of component i in a monolayer of mixed adsorbates. Equation 3.9 helps represent the competition for adsorption sites between the different molecule types in the mixture. For thermodynamic consistency of equation 3.9, the saturation capacity for each component q_{si} must be the same, which is very seldom observed experimentally. This restricts the model to adsorbate molecules that are similar in size (like oxygen and nitrogen molecules) and at moderate to low surface concentrations. This means that just like the single component Langmuir isotherm model, the multi-component model is merely an approximation and only accurately represents a few mixed gas systems. Nevertheless, mixed Langmuir is still heavily used in process simulations due to its simplicity and the relatively low adsorbent loadings that PSA processes normally operate under.

For a mixture, the equilibrium selectivity of a gaseous mixture becomes the ratio of the equilibrium constants, which is seen in equation 3.10 for a binary mixture. From this equation, it can be seen that the equilibrium selectivity is independent of composition, which is why the ideal Langmuir model is commonly called the “constant separation factor” model [13].

$$s_{ij} = \left(\frac{x_i}{y_i}\right) \left(\frac{1 - y_i}{1 - x_i}\right) = \frac{b_i}{b_j} \quad (3.10)$$

Since the equilibrium constants are directly related to the Henry's Law constants, comparing the Henry's Law constant of two different adsorbents can provide insight into the equilibrium selective capabilities of those adsorbents.

An extension of Langmuir is the "Dual Site Langmuir (DSL)" model which takes into account an additional adsorption site that the Langmuir model does not [33]. With two adsorption "sites", the DSL model has greater mathematical flexibility and thus can represent almost any pure component data. In addition to the electrostatic interactions with the exchangeable cations, the model accounts for the much smaller attraction of nitrogen and oxygen molecules to the zeolite structure due to dispersion forces. In essence, when the DSL model is used with zeolites, it is rationalized that there is one site representing the electrostatic and induced electrostatic interactions with the exchangeable cations and another site representing the dispersion interactions with the zeolite structure. The DSL model for a pure component gas can be seen in equation 3.11:

$$q = \frac{q_s^b bP}{1 + bP} + \frac{q_s^d dP}{1 + dP} \quad (3.11)$$

where q_s^b and b can be regarded as the saturation capacity and equilibrium constant respectively for the exchangeable ion sites while q_s^d and d are the same parameters due to the dispersion interaction effect. It is assumed that b is greater than d because the exchangeable ions have a greater affinity for the adsorbate molecules than the neutral zeolite structure. If the saturation capacity of each of the gas molecules is assumed to be equal for each site, the DSL multicomponent model takes the form seen in equation 3.12:

$$q_i = \frac{q_s^b b_i P y_i}{1 + \sum_j b_j P y_j} + \frac{q_s^d d_i P y_i}{1 + \sum_j d_j P y_j} \quad (3.12)$$

The equilibrium constants assume Arrhenius temperature dependencies as seen in equations 3.13 and 3.14:

$$b_i = b_i^0 e^{Q_i^{(b)}/RT} \quad (3.13)$$

$$d_i = d_i^0 e^{Q_i^{(d)}/RT} \quad (3.14)$$

where b_i^0 and d_i^0 are the two pre-exponential constants for gas i and $Q_i^{(b)}$ and $Q_i^{(d)}$ are the heats of adsorption of gas i on the two sites. It is important to re-emphasize that in order for the Langmuir models to be thermodynamically consistent, the saturation capacities of the different gases involved must be identical for a given adsorbent. Mathias et al. have shown the DSL model to be accurate for both pure component gases and nitrogen/oxygen mixtures using zeolite 5A since they have similar saturation capacities [33]. This allows the DSL model to closely predict adsorption equilibrium for the application of air separation and makes it a useful model for this thesis.

3.3 Adsorption Kinetics

Adsorption equilibrium and thermodynamics determine the ultimate separation efficiency of a process, which would take infinite time to achieve. Yet processes operate within a finite time frame. Adsorption kinetics and dynamics determine how equilibrium is achieved at any location in a column at a given time. This section reviews the essential fundamentals of adsorption kinetics and dynamics to the extent necessary for this thesis. It also briefly reviews how the kinetics of zeolites can be improved to produce enhanced zeolites for PSA processes. An abundance of literature exists that provides far greater

detail on column dynamics and kinetics, specifically ones written by, Ruthven, Ruthven et al., Suzuki, and Yang [12, 13, 27, 36].

3.3.1 Diffusivity

Adsorption rate within a zeolite is dependent on how fast diffusion occurs within the zeolite pores. The rate of diffusion is determined by rate properties that include an adsorbent particle's intrinsic characteristics like the structure, size, and shape of the macropores. The adsorption rate in a zeolite is approximately related to the inverse of the square of the particle radius and is directly proportional to the macropore diffusivity and porosity. This relationship is evident from a mass transfer model for adsorption rate called the Linear Driving Force (LDF) model. In this model, the adsorption rate is found from equation 3.15:

$$\frac{\partial q_i}{\partial t} = k_i(q_i^* - \bar{q}_i) \quad (3.15)$$

where q_i^* is the equilibrium value of the adsorbed phase concentration at a fluid phase concentration, c , and \bar{q}_i is the adsorbed phase average concentration over an adsorbent particle. In this model, the mass transfer coefficient, k_i (a combination of the adsorbent intrinsic and particle properties), for a spherical particle is represented by equation 3.16:

$$k_i = \frac{15\varepsilon_p(1 - \varepsilon_b)D_{pi}}{r_{pi}^2} \quad (3.16)$$

where D_p is the effective macropore pore diffusivity, ε_p is the void fraction inside the particle, ε_b is the interparticle column void fraction, and r_p is the particle radius. D_p is in essence a “lump-sum” parameter that accounts for all three mass transfer resistances

described in section 2.3.3, namely film resistance, macropore diffusion, and micropore (activated) diffusion. Breakthrough experiments can be used to experimentally determine the mass transfer coefficient. For many significant applications, specifically air separation using type-X zeolites, the mass transfer coefficient is primarily influenced by macropore diffusion and not by other potential diffusion mechanisms like bulk diffusion, micropore diffusion, and surface diffusion.

There are three primary ways to increase the adsorption rate through manipulation of the intrinsic properties of a zeolite: 1) increasing the effective macropore diffusivity, 2) increasing the intraparticle void fraction, and 3) decreasing the particle size. Individually altering the last two properties leads to a reduction in the selectivity of the zeolite and efficiency of a PSA process. By attempting to increase the macropore diffusivity by only increasing the intraparticle void fraction (larger macropores), the porosity rises and the amount of active adsorbent content in the zeolite decreases. This requires more adsorbent to achieve the same nitrogen adsorbate capacity per column volume. Higher porosity also creates lower density particles with a lower crush strength. While this is not of high importance for small scale PSA units, large industrial size columns require zeolites that do not crush under its own weight. Furthermore, a higher void fraction allows for a higher percentage of the particle volume to be for non-selective gas retention, which hinders the separation ability of the zeolite and reduces recovery. Decreasing particle size benefits dynamics by decreasing diffusion path length. But, decreasing particle size has the consequence of a higher pressure drop across the adsorbent column, higher risk for particle fluidization within the column, and an increased difficulty with particle retention, all of which have a negative impact on a PSA process performance.

Among the trade-off options available is increasing the mass transfer coefficient through the proper simultaneous manipulation of the effective macropore diffusivity, intraparticle void fraction, and particle size, which results in an increase in recovery and decrease in BSF [29]. This is where most current research efforts are devoted and is discussed further in the next section. Another method recently investigated involves developing a zeolite with improved micropore diffusivity by the use of caustic digestion during zeolite synthesis [7].

3.3.2 *Enhanced Zeolites*

PSA processes benefit greatly from the development of enhanced zeolites with improved kinetic characteristics as they allow for improvement in process performance, specifically column size and adsorbent utilization. Much of the advancement is aimed at increasing the diffusion of adsorbent molecules within the zeolite and stems from research into new zeolite synthesis techniques (as mentioned in the previous section) and improved binder material used in zeolite particle manufacturing. If these improvements are properly utilized, they lead to a more efficient and productive process because of an increase in adsorption rate. This allows for a shorter column and a higher column working capacity due to the reduction in size of the MTZ.

Zeolites with enhanced intrinsic properties have been used successfully to improve PSA processes through various designs. Ackley et al. have utilized these enhanced zeolites with faster cycles and shallower columns to improve separation efficiency. This is achieved through improvements in the adsorbent BSF and utilization which reduces the power needed to achieve a desired separation [28]. They have also

applied these principles to show that enhancing the intrinsic properties of a zeolite allows for the effective operation of PSA processes at lower pressure ratios while maintaining or increasing adsorbent productivity. This is a result of the higher diffusivity within the zeolite reducing the negative impact on recovery caused by lower pressure ratios [30].

Development of particles with improved binder material used in the manufacturing of zeolite particles has also been shown to increase adsorption rate. Binder material allows individual zeolite crystals to bind together to create specific shaped zeolite particles, while also limiting the pressure drop in an adsorption column. Binder material is normally comprised of clays like kaolin, palygorskite-type minerals like attapulgite, and smectite-type clay minerals like montmorillonite or bentonite. Until recently, the type of binder material used was not thought to play a significant role in mass transfer within a zeolite. However, recent inventions of improved binders have shown that mass transfer is indeed faster with enhanced binders. Zheng et al. have produced zeolites with a high adsorption rate and high crush strength using a colloidal binder solution that creates a well-dispersed and consistent allocation of the binder in the zeolite [23]. Sampson et al. have created a zeolite with highly dispersed attapulgite fibers with reduced amounts of non-attapulgitic matter (no binding ability) in the final binder material [34]. This binder was used by Weston et al. to develop a zeolite with faster adsorption rate and higher mechanical strength compared to previous attapulgite fiber binding zeolites [25].

3.4 PSA Analysis

The performance of PSA systems is evaluated using several types of criteria to determine if they are successfully accomplishing the desired results. Because of the nature of PSA, improving the process performance usually requires the designer to examine several different tradeoffs in an attempt to optimize the process, since improving one aspect of the process normally means decreasing another. This means there is usually no one single solution to optimizing a PSA process and the engineer must design the process based on finances and functionality. The normal process parameters used to evaluate PSA systems include the recovery and the Bed Size Factor (BSF).

Analysis of PSA processes is somewhat complicated since the process is inherently non steady-state. In effect, the process contacts the column with different gases in a sequence of (batch) steps with the aim of achieving the same conditions in the column at the end of a cycle. Hence each step is a batch transient process while the cycle repeatedly achieves the same conditions, hence the word cyclic-steady-state (CSS).

3.4.1 *Material Balances*

Material balances are conducted on the process to examine what is entering, exiting, and retained during the process. Material balances are important for PSA processes to validate the process and to provide insight into interplay between process parameters. A general balance for any system with no chemical reaction is seen in equation 3.17.

$$\text{Input} - \text{Output} = \text{Accumulation} \quad (3.17)$$

In order to calculate material balances, the flow rate into and out of the process is measured along with the composition of the entrance and exit streams.

The instantaneous molar flow rate at different points in the process is useful for plotting a flow rate versus time chart. This visual representation of the data is useful for interpreting what is occurring within the system in real time and for determining when a process reaches CSS. A material balance using these flow rates at any instant is shown by equation 3.18:

$$F_{in} - F_{out} = \frac{dN_T}{dt} \quad (3.18)$$

where F is the instantaneous flow rate, t is time, and N_T is the total number of moles of adsorbate (both in the adsorbed and gas phase) in the column. Determining the individual component material balances at any instant is done with equations 3.19 and 3.20:

$$F_{in}y_{O_2} - F_{out}y_{O_2} = \frac{dN_{O_2}}{dt} \quad (3.19)$$

$$F_{in}y_{N_2} - F_{out}y_{N_2} = \frac{dN_{N_2}}{dt} \quad (3.20)$$

where y_i is the mole fraction of component i in the corresponding stream.

While instantaneous flow is useful for plotting real time data, for a process that involves constantly changing flow rates, it is not useful for determining what is occurring over the course of time. Since PSA processes are dynamic, there is not always a steady

flow in and out of the process. When there is an absence of steady flow, a time averaged flow rate is calculated to conduct material balances. This is described by equation 3.21:

$$\bar{F} = \frac{\int_0^t F dt}{t} \quad (3.21)$$

where \bar{F} is the average flow rate, and t is the time interval over which the average is taken. Averaging the flow rate over time provides a more meaningful value for calculating the flows of the different steps in the process and the process's overall performance. The overall material balance using averaged flow rates becomes what is shown in equation 3.22.

$$\bar{F}_{in} - \bar{F}_{out} = \frac{\Delta N_T}{t} \quad (3.22)$$

For individual component balances, the balances become equations 3.23 and 3.24.

$$\bar{F}_{in} y_{O_2} - \bar{F}_{out} y_{O_2} = \frac{\Delta N_{O_2}}{t} \quad (3.23)$$

$$\bar{F}_{in} y_{N_2} - \bar{F}_{out} y_{N_2} = \frac{\Delta N_{N_2}}{t} \quad (3.24)$$

To calculate the recovery and BSF of a PSA process, it is useful to calculate the amount of gas into and out of the process on a per cycle basis. It is additionally beneficial to calculate the amount of gas used for each step in the cycle. This requires not only a measurement of the flow rate at the entrance and exit of the process, but also a flow rate measurement internal to the process on the product side, before the purge and product pressurization streams enter the columns. In order to get the amount of gas per cycle, the flow needs to be averaged over the cycle time or a multiple of cycle time.

Using a multiple of cycle time averages the flow over multiple cycles, which to a certain extent provides a better flow average for calculating the amount of gas per step in the cycle. With the average flow per cycle calculated, the amount of gas for each step is solved for by simply multiplying a step's average flow per cycle(s) by the cycle time to get the amount of gas per cycle for that step, like it is seen in equation 3.25:

$$\Delta N^{step} = \frac{\int_0^t F^{step} dt}{t} * t_c \quad (3.25)$$

where ΔN^{step} is the amount of gas used/produced during that step in the cycle and t_c is the cycle time. Calculating the amount of gas per step in a cycle is a convenient way to conduct a material balance to validate the calculated recovery and BSF. For a material balance on a PSA process, the input is the amount of gas in the feed stream, while the exit streams consist of the product stream, exit stream of the purge step, and the exit stream from blowdown step. For this thesis, the streams from the exit of the purge and blowdown steps are measured with the same flow meter, so this stream is collectively referred to as the waste stream. Thus the overall material balance for the cycle can be calculated from equation 3.26:

$$\Delta N^F - \Delta N^P - \Delta N^W = \epsilon \quad (3.26)$$

Where ϵ is the material balance error, N^F is the amount of feed gas used, N^P is the amount of product gas produced, and N^W is the amount of waste gas generated, all on a per cycle basis. The individual component balances can then be solved by equations 3.27 and 3.28:

$$N^F y_{O_2}^F - N^P y_{O_2}^P - N^W y_{O_2}^W = \epsilon_{O_2} \quad (3.27)$$

$$N^F y_{N_2}^F - N^P y_{N_2}^P - N^W y_{N_2}^W = \epsilon_{N_2} \quad (3.28)$$

where y_i^F , y_i^P , and y_i^W are the mole fractions of either nitrogen or oxygen in the feed, product and waste streams respectively. At CSS, values of ϵ must be zero; however for experimental work this almost never occurs due to uncertainty in measurement and data collection. However, it is important to minimize the amount of error and close material balances as closely as possible to validate process calculations like BSF and recovery.

For internal streams such as the purge flow, product pressurization flow, and equalization flow, separate flow measurements are necessary. For the experimental setup of this thesis, the purge and product pressurization streams flow through the same needle valve for control and are measured by the same flow meter. This means in order to differentiate between the purge and pressurization streams for the average flow from this flow meter, the amount of gas during the cycle time needs to be multiplied by the ratio of cycle time spent on one step to the time spent on both steps. In equation form, it looks like equations 3.29 and 3.30:

$$N^U = N^C * \left(\frac{t^U}{t^U + t^R} \right) \quad (3.29)$$

$$N^R = N^C * \left(\frac{t^R}{t^U + t^R} \right) \quad (3.30)$$

where N^U , N^R , and N^C are the amount of gas used per cycle of the purge stream, pressurization stream, and combined stream, and t^U and t^R are the purge and pressurization step times respectively.

3.4.2 Design Parameters

When designing a cycle for a PSA process, there are several parameters that are decided on that determine how the process will operate. These parameters are set based on the purity of product desired and allowable power consumption for the process. They include product purity, the purge to feed ratio, pressure ratio, and feed stream velocity (cycle time).

Product purity is the amount of oxygen in the product stream divided by the sum of all the components in the product stream. Product purity is determined by column length and the adsorption rate. It is represented by equation 3.31:

$$\% \text{ Oxygen Purity} = \frac{N_{O_2}}{\sum_{i=1}^n N_i} * 100 \quad (3.31)$$

where N is number of moles and n is the number of components in the product. For a PSA process, it is useful to express oxygen concentration as a concentration averaged over both the flow and time because the concentration exiting the process varies with both time and flow rate. This requires dividing a time average of the flow of oxygen by a time average of the total flow. This is represented by equation 3.32:

$$\text{Average \% Oxygen Purity} = \frac{\int_0^t F y_{O_2} dt}{\int_0^t F dt} * 100 \quad (3.32)$$

The purge/feed ratio is a highly important parameter in PSA as it controls product purity and the amount of product the process generates. The purge/feed ratio is represented by equation 3.33:

$$\frac{\text{Moles } O_2 \text{ (Purge Step)}}{\text{Moles } O_2 \text{ (Feed Step)}} = \frac{N^U y_{O_2}^U}{N^F y_{O_2}^F} \quad (3.33)$$

A higher P/F ratio means a greater amount of the product gas produced is used in the regeneration of the columns and will further push back the MTZ towards the feed end of the columns. For adsorbents with slow adsorption rates, this will increase the purity of the product stream to a certain extent. After a certain P/F ratio is reached, the purity of the product will not increase even if the P/F ratio is increased. For high rate adsorbents similar to the one used in this thesis, the P/F ratio has a very limited impact on purity as it is difficult to operate cycles at a purity less than a completely pure product due to the rapid drop in purity when the critical P/F ratio is reached. The critical P/F ratio is the ratio that gives the desired product purity, but a decrease in the P/F ratio causes an undesired product purity. In order to ensure that the product purity is maintained at the desired level, it is not advisable to operate a process at the critical P/F ratio, but rather at a ratio slightly higher than the critical ratio. Column length can also play a role in the product purity as increasing the column length allows a longer contact time for the adsorbent with the solid, which shrinks the MTZ and increases the purity. However, after a certain length the increase in purity becomes minimal and the pressure drop across the column becomes too large for efficient operation.

The pressure ratio is the other design parameter that is set based on the power allowances for the process. The pressure ratio is defined by equation 3.34 below.

$$\text{Pressure ratio} = \frac{P_{High}}{P_{Low}} \quad (3.34)$$

For a PSA process, the blowdown/purge step occurs at atmospheric pressure and a pump is required to pressurize the columns to the desired adsorption pressure during the feed/production steps. For a VSA and combined PSA/VSA processes, the blowdown/purge step occurs at a set vacuum pressure and the adsorption pressure is at either atmospheric pressure for VSA cycles or some pressure above atmospheric for PSA/VSA cycles. For these cycles, a pump is necessary to pull vacuum on the columns during the blowdown and purge steps. Depending on the cycle type, the higher the adsorption pressure or the lower the vacuum pressure, the more power used to operate the process. Normally a pressure ratio is selected that allows for minimal power consumption while delivering the desired amount of recovery.

The last design parameter is the feed velocity which is directly related to the cycle time, which for this thesis is fixed during the process. The cycle time is determined by the step times. The step times have some flexibility to be changed, however, it is a requirement for the combined time of the purge, product pressurization, and blowdown steps to equal the combined time of the feed pressurization and production steps. Decreasing the cycle time leads to an increase in the amount of product produced over time, however, at some point, the decrease in cycle time will lead to a sharp decrease in recovery and increase in BSF. This decrease in recovery is caused by either reaching the adsorption rate limit or the increase in pressure drop caused by the higher velocity of the gas in the columns. The cycle time at which this occurs is dependent on the diameter of the bed, the type of adsorbent used, and the type of cycle used for the process.

3.4.3 Performance Parameters

The performance of a PSA system is mainly evaluated through two different performance parameters mentioned earlier in the introduction, the recovery and the bed size factor (BSF). Recovery is the amount of desired component fed into the system that is available as product. In essence, it is related to the energy efficiency of a process. For air separation, it can be calculated based on the product stream or the waste stream. If it is based on the product stream, it is calculated from equation 3.35 using the amount of gas per cycle of the product and feed streams.

$$\% Recovery = \frac{\text{moles } O_2 \text{ (product)}}{\text{moles } O_2 \text{ (Feed)}} * 100 = \frac{N^P y_{O_2}^P}{N^F y_{O_2}^F} * 100 \quad (3.35)$$

If it is calculated based on the waste stream, it is calculated from equation 3.36 using the amount of gas per cycle of the feed and waste streams and an oxygen material balance.

$$\% Recovery = \frac{N^F y_{O_2}^F - N^W y_{O_2}^W}{N^F y_{O_2}^F} * 100 \quad (3.36)$$

For a cycle at CSS, recovery is inversely related to purity. An increase in product purity decreases the recovery, mainly because a higher purity requires more purge gas, which leaves less gas available for recovery as product. Recovery is dependent on separation efficiency just like purity. Thus, it is possible to increase recovery with better selective zeolites or the addition of added steps to a PSA process like product pressurization and pressure equalization that increase the efficiency of regeneration.

The other performance parameter is BSF which is seen in equation 3.37:

$$BSF = \frac{\text{adsorbent mass}(lbs)}{\text{oxygen production}(\frac{Tons}{day})} \quad (3.37)$$

BSF is related to the length of the column, feed flow rate, and cycle time and corresponds to the size of system and thus the capital costs of the process. The adsorption rate also plays a significant role in the BSF as a faster adsorption rate allows for smaller columns, shorter cycle times, and higher product flow rates.

Another parameter useful in evaluating a PSA process is the swing capacity of the material used. The swing capacity is the amount of adsorbate that adsorbs/desorbs per cycle. This capacity is found from the amount of gas in the column between the end of

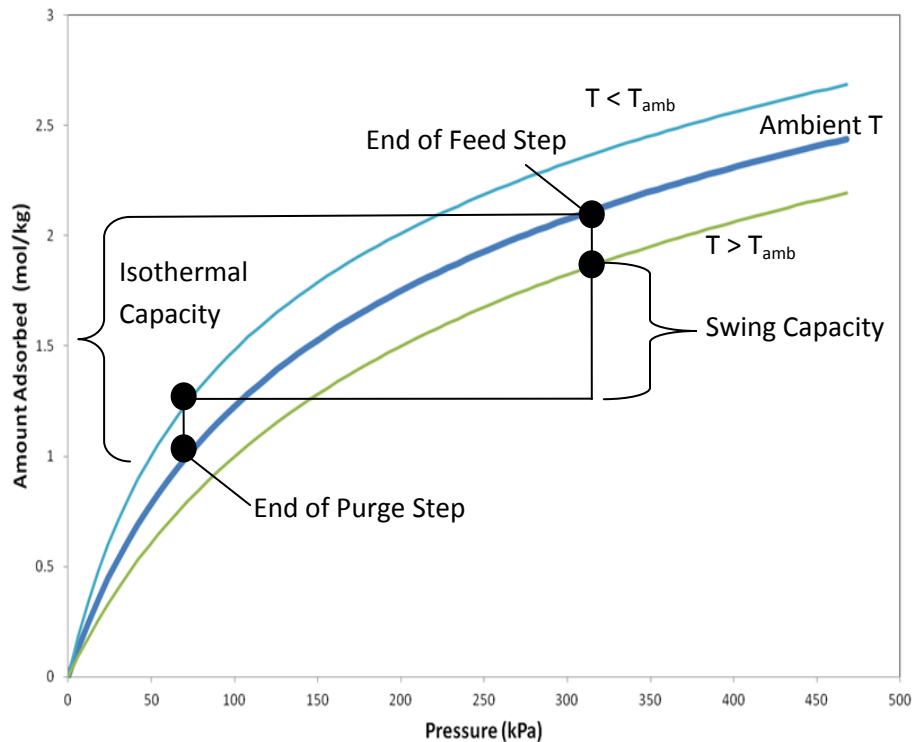


Figure 3.3. Example isotherms to illustrate swing capacity.

the purge step and the end of the feed step, which corresponds to the “cleanest” and “dirtiest” conditions of the solid adsorbent. This is equal to the feed amount calculated per step in a cycle as previously described in the material balances section. From this amount, the moles of nitrogen can be calculated and then divided by the mass of the adsorbent in the columns. Figure 3.3 visually demonstrates what the swing capacity represents on an isotherm plot. At the end of the feed step, the column temperature has risen (since adsorption is exothermic), which changes the isotherm that determines adsorption equilibrium. Conversely, at the end of the purge step, temperature in the column has decreased (since desorption is endothermic), which again changes the isotherm that determines adsorption equilibrium. As can be seen from figure 3.3, the swing capacity is the difference in adsorption at the end of the feed and purge steps between the two isotherms that are higher and lower than the ambient temperature isotherm. While this illustrates what is actually occurring during a PSA process in the columns, it is very difficult to measure the temperature of the zeolites in the columns to see this transpiring. That is why an average temperature isotherm is generated to estimate the swing capacity and why process optimization is needed to utilize the columns as efficiently as possible.

CHAPTER IV

EXPERIMENTAL

This section introduces the type of zeolite, instruments, and devices utilized to conduct the experiments for this thesis. Data collection methods for preliminary experiments as well as PSA experiments are also discussed in detail. Finally, the conditions and details for the experiments conducted are outlined.

4.1 Type of Zeolite

The zeolite used in this thesis is a LiX zeolite with a Si/Al ratio near 1.0, a high Li⁺ ion exchange, and manufactured to increase the adsorption rate, specifically through the use of zeolite particle that was about 0.5 mm in size.

4.2 Isotherm Generation

As previously mentioned in the theory section, an isotherm is critical to the development of a PSA process because it is the starting point from which the design begins. Generating an isotherm for the zeolite used in these experiments was a three step process. The first two steps involved using the Cahn®-1000 Microelectronic Balance (low pressure) seen in figure 4.1 below. The last step involved correlating an isotherm model to the data collected to facilitate calculations.

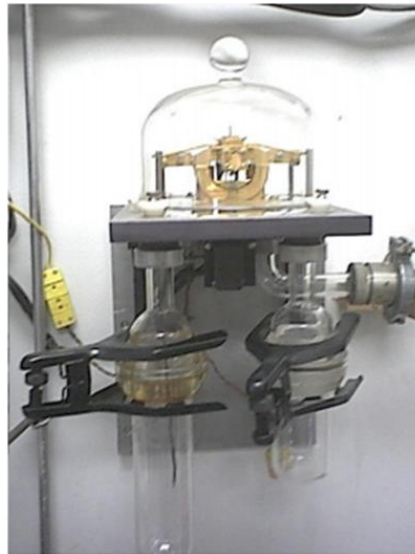


Figure 4.1. Cahn®-1000 Microelectronic Balance (low pressure).

The Cahn balance provided a way for gravimetrically generating an isotherm. Generating an isotherm using this method was done by measuring the weight change of an adsorbent sample at different pressures under a constant temperature. A small sample of the zeolite used in this thesis was placed in the balance sample bucket and then activated. Activation for zeolites involves heating the zeolite under vacuum to eliminate water molecules (and any other adsorbed molecules) from the zeolite. Water molecules

have a strong dipole moment that causes the exchangeable ions to strongly attract them and reduce the selectivity of the zeolite for nitrogen. The activation was done under 10^{-4} torr vacuum pressure by increasing the temperature by 50°C every thirty minutes until the temperature reached 317°C . After reaching this temperature, a measurement of the mass of the zeolite was immediately taken. The zeolite sample was then allowed to cool to room temperature and the mass was taken again to ensure nothing further had adsorbed to the zeolite. The zeolite sample was then exposed to a range of nitrogen pressures from 0-760 torr at an average temperature of 23.6°C , which was near the average temperature expected to be seen in the column during a PSA cycle for this thesis. The zeolite was exposed to a specific pressure after which the mass of the sample plus adsorbed nitrogen was measured. The system was then flushed with helium and brought back to the low vacuum pressure and the process was repeated for a different nitrogen pressure. The amount of nitrogen adsorbed was calculated in a manner similar to method described by Talu [31]. A summary of the results from these measurements can be found in the appendix.

The last step in the isotherm generation process was to use the DSL model mentioned in the theory section to create an isotherm for the full range of pressures experienced during PSA experiments. A previous graduate student supplied three isotherms for a zeolite similar to the one used for this thesis, but with a slightly different binder content. These isotherms were used to generate the coefficients needed for the DSL model predictions at 25°C . These coefficients are seen in table 4.1 below. The isotherm data collected with the Cahn balance for the zeolite used in this thesis was very similar to this DSL model. Thus the coefficients from the model were used to generate a

binary adsorption isotherm at 23.6 °C by discounting the DSL coefficients slightly until the model fit the measured isotherm data. It was found that using 7% discounted coefficients, an isotherm for the full range of pressures needed for this thesis could be generated for 23.6 °C .

Table 4.1. DSL Calculated Coefficients

Coefficient	Nitrogen	Oxygen
b^0 (mol/kg-kpa)	0.124	0.158
d^0 (mol/kg-kpa)	0.513	3.386
Q^b (1000 K)	3.365	2.373
Q^d (100 K)	2.263	1.221
q_s^b (mol/kg)	1.88325	1.32618
q_s^d (mol/kg)	2.23386	5.74461

Note: Coefficients found through regression performed with amount adsorbed (mol/kg) and pressure (kpa).

4.3 Column Packing

Any PSA system requires a careful packing of the columns used in the process to ensure that the amount of zeolite in the column is known as accurately as possible in order to determine the adsorption capacity of the columns. Future calculations involving process design and evaluation are highly dependent on these values, which is why great care was taken to be as accurate as possible. Column packing involves several steps so the adsorption capacity of the columns could be calculated after activation.

The activation process began with leaving enough zeolite to fill two columns on a balance over the course of several days to allow ambient water vapor to adsorb on the zeolite. The zeolite was determined to be fully saturated with water once the mass of the water plus zeolite stopped increasing. Then a small sample was taken from the balance and activated in the Cahn balance to determine the ratio of water adsorbed per milligram

of zeolite. This ratio is used after the columns are activated to determine the mass of the zeolite in the columns without water adsorbed. The next step involved filling two columns (Dimensions found in Appendix A) with zeolite from the balance and measuring how much of the zeolite with water adsorbed was added to the columns. Activation of the columns was performed in a furnace under vacuum and low helium flow. The activation itself is similar to the Cahn balance in that the temperature was increased 1 °C every minute until the temperature reached 120 °C. The oven then held this temperature for an hour before again increasing 1 °C every minute until the temperature reached 345 °C, at which the temperature was held for at least seven hours. The column in the furnace was then pressurized with helium to atmospheric pressure and allowed to cool to room temperature before installation into the PSA system.

4.4 PSA System










The PSA apparatus used to conduct the experiments in this thesis is a highly complex system with a number of different types of valves and flow controllers so the user can produce and control a cyclic process necessary for PSA. The overall system itself is made of 1/8 inch stainless steel tubing and fittings that connect various types of valves and flow controllers. It is purposely highly instrumentated so that the physical changes occurring at different points in the process can be measured, which provides insight on how to tune and improve the process. The system is capable of collecting data for pressure, temperature, flow rate, and gas composition. The data is collected during the process by a data acquisition system so that it can be systematically displayed on a

computer screen. The experiments conducted with the system fall into two categories, preliminary experiments and PSA experiments.

4.4.1 PSA Flow Diagrams

The system is divided into three sections relative to the columns. One section is on the feed side of the columns where feed gas enters and waste gas exits. Another section is on the product end where product gas exits the column and purge and/or product gas enter the column. The last section, the exit manifold, lies next to the columns and in between the feed end and the product end. It contains a manifold of valves that control how the gas exits the system. The following schematic diagrams show the details of the experimental PSA process used in this thesis. Table 4.2 gives a key for the symbols found in the figures. Figure 4.2 shows a schematic of the feed section, Figure 4.3 shows a schematic of the product end, and Figure 4.4 shows a schematic of the exit manifold section of the system.

Table 4.2. PSA Schematic Symbol Description

Acronym	Symbol	Meaning
PV#		Pneumatic Valve
COLUMN#		Adsorption Column
BPC#, NEEDLVAL		Back Pressure Controller, Needle Valve
SV#-#		Switch Valve: First number is physical valve on system, second number is the port number on the valve
FC#, FLOWTRANS		Flow Controller/Transducer
HV#		Hand Valve
MS#, P#, PTRANS D		Mass Spectrometer sample port, Pressure transducer port, Pressure Transducer
PUMP		Vacuum Pump
O2TANK		Oxygen Product Tank

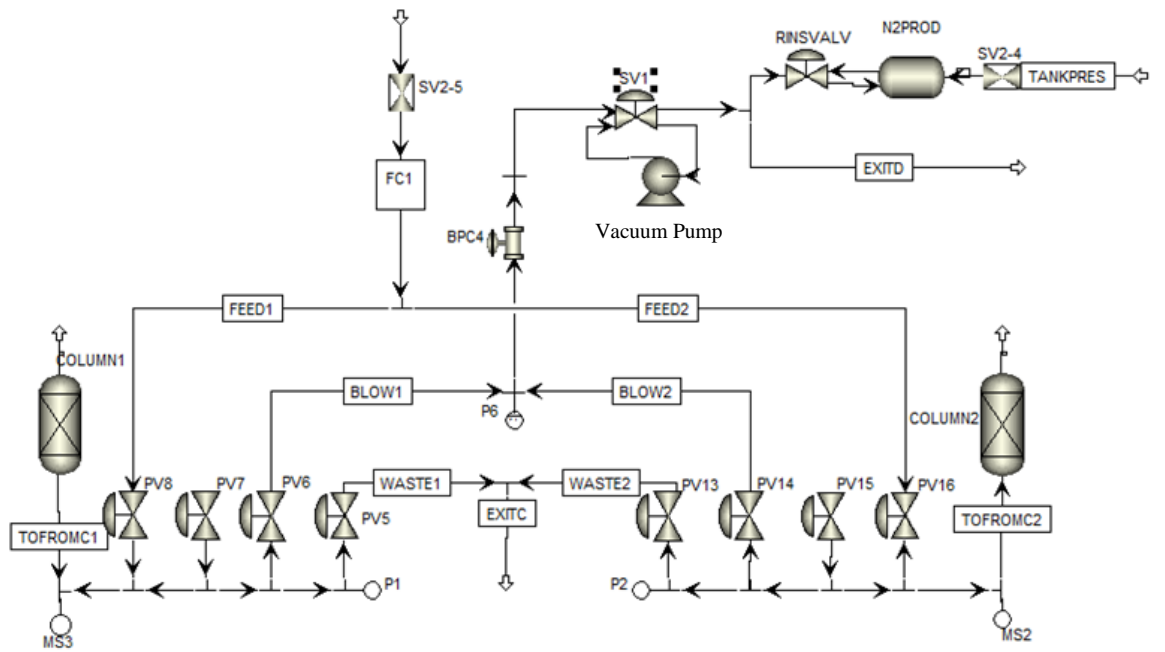


Figure 4.2. PSA system feed side schematic.

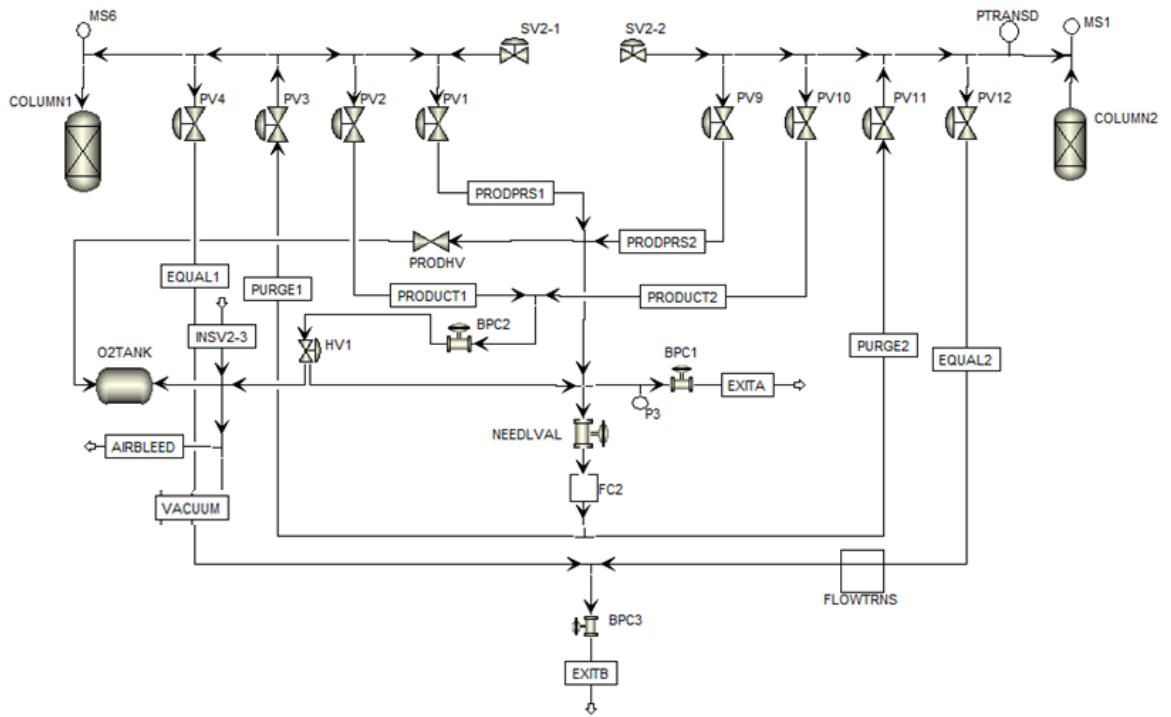


Figure 4.3. PSA Product Side Schematic.

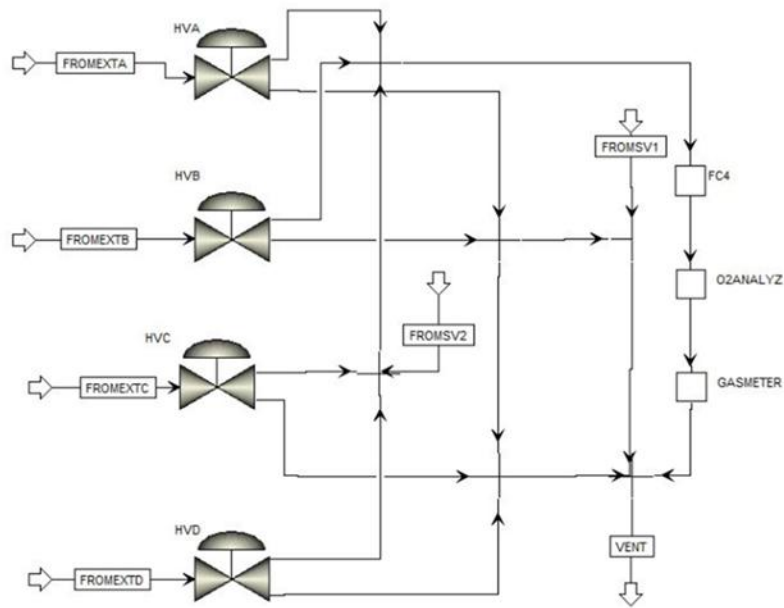


Figure 4.4. PSA middle exit manifold schematic.

4.4.2 PSA Instrumentation, Process Control, and Data Collection

There are three types of valves used in the system, hand valves, pneumatic valves, and switch valves. The hand and switch valves allow for the flow to be directed in the system manually. The pneumatic valves are switched on/off by solenoid coils that are either controlled manually or by an EZPLC programmable logic controller (PLC). The PLC provides automated control of the pneumatic valves through a programmed repeated sequence of events in which the valves open and close at different times to create a cyclic PSA process. It is located on a controller switch board that contains sixteen manual switches that put the valves in manual, PLC, or off mode. The position of the switches on the controller switch board determine the mode. The up position delegates control to the controller, the down position switches the valve on, and the middle position turns the valve off.

Two different pressure transducers placed at two separate points in the process collect pressure data. The first is an Omega Dyne transducer (PTRANS D on Figure 4.3) that has a very limited amount of dead volume and is used primarily to determine the column pressure. The other pressure transducer is a MKS Baratron Type 722A absolute pressure transducer that is connected to a switch valve (not pictured on the figures). The switch valve has seven ports and is connected to six different points in the process (P1-P6 on figures 4.2 and 4.3) with one port left open to measure the atmospheric pressure. This switch valve provides flexibility when checking pressures throughout the system and allows for quick checks of the pressure at different points in the apparatus. This pressure transducer does however have a significant amount dead volume and is normally only used on the product end of the process as to not impose extra dead volume to the columns. Pressure is controlled by back pressure controllers (BPC) placed at various points in the process.

The flow rate of gases in the system are controlled and measured by three MKS Mass Flow Controllers/Mass Flow Meters that are located at three separate points in the process. One flow meter/controller is on the feed line (FC1 on figure 4.2), another on the purge/product pressurization line (FC2 on figure 4.3), and a third on the exit manifold (FC4 on figure 4.4). There is an additional Omega FDMA-1600A Gas Flow Meter (FLOWTRNS on figure 4.3) that is used to measure mass flow rate, pressure, and temperature for the equalization flow exclusively. Generally, only FC1 is used to control flow rate while the other flow meters/controllers are left open (set to 2000 cc/min) and are used primarily to measure the flow rate through them. For the case of FC4, it is only used to measure exit gas and thus flow rate control is not needed. For FC2, since it is on

the purge/product pressurization line, it experiences a significant amount of sudden changes in flow and the flow controller does not have a rapid enough response time to properly control the flow. For this reason, FC2 was kept open during experiments and a needle valve (NEEDLVAL on figure 4-5) was placed before FC2 to control the purge/product pressurization flow into the columns.

Composition of the exit flow is measured by an AMI (Advanced Micro Instruments) Oxygen Analyzer (O2ANALYZ on figure 4.4) located on the product end of the process within the exit manifold. There are also ports (MS1, MS2, MS3, MS6) at both ends of each column for capturing a small amount of gas to analyze in a mass spectrometer. These ports were only used if the mass spectrometer was used for fine tuning of a process.

The most meaningful temperature data in a PSA process comes from the zeolite surface, but this is extremely difficult to measure accurately. That is why temperature in this process was measured just at the surface of the columns. Three thermocouples are located on the surface ends of each of the columns. Column 1 has one thermocouple at the product end of the column and column 2 has a thermocouple at both ends of the column. The temperature is read from the thermocouples by a digital readout that is attached to a switch dial, which allows for rotation between the different thermocouple locations.

Collection of the data from the pressure transducers, flow controllers, oxygen analyzer, and thermocouples was done with a National Instruments 7025E data acquisition system. The data was then displayed on a computer using Lab Windows

software. The software was also used to record the data sent to the computer into a Microsoft Excel file for further analysis.

4.4.3 *System Design*

Gas into the system was supplied to either the feed side or product side of the system through a switch valve (SV2-5 on figure 4.3 or SV2-3 on figure 4.3). Four types of gases are connected to a separate switch valve (not shown on figures) which controls the type of feed gas supplied to the system. The gas options are nitrogen, oxygen, helium, and dry air, which were all stored in compressed gas cylinders. A vacuum pump was connected to the product end to allow for vacuum pressure in the columns during the purge/blowdown step. It was connected to a switch valve (SV1) that takes the pump offline if it was not used in the process. An industrial back pressure controller (BPC6) with pressure control above and below atmospheric pressure is located upstream of the pump and is responsible for controlling the purge/blowdown pressure. A product tank is connected on the product end of the system if product collection is needed for cycles involving product pressurization and/or equalization steps. Two hand valves (HV1 and HV2) control whether flow enters or bypasses the tank during the process. The pneumatic valves (PV1-16) that control the flow into and out of the adsorption columns are housed together in 4 valve blocks on both sides of each column.

On the feed side of the system (Figure 4.2) during a PSA process, feed gas enters during the feed/production step through SV2-5. It then flows through the line labeled Feed 1 and Feed 2 to PV8 and PV16 which lead to the adsorption columns. During the blowdown and purge steps, flow travels from the column through PV6 and PV14 into the

lines labeled Blow1 and Blow 2, which lead to the vacuum pump and to exit D. PV7 and PV15 were not used for the experiments and thus the lines leading to them were not displayed in order to simplify the diagram. Pressure on the feed side of the process is measured primarily at P6, which provides the pressure during the blowdown and purge steps. P1 and P2 are not advised to be used for an extended period of time because of the dead volume induced on the columns as was discussed earlier.

The product side of the system (Figure 4.3) is more complex. During normal operation, product flowed through a combination of PV1 and PV9 if the product tank was bypassed during process operation, or PV2 and PV10 if the product tank was online during process operation. If the tank was online, HV2 was also opened, otherwise it remained closed. The product tank could be pressurized with oxygen prior to the start of the process through SV2-3. Also on the oxygen tank line is a connection to a vacuum pump that was used to zero the pressure transducers. PV3 and PV11 are important valves that allowed for purge flow into the columns as well as product pressurization flow for processes utilizing product pressurization. As previously mentioned, the needle valve located before FC2 controlled the flow to PV3 and PV11 while FC2 was only used to measure the flow rate to the columns. PV4 and PV12 were only used for processes with a pressure equalization step. BPC3 is located on this line connecting these valves, but remained closed during the entirety of the experiments. Pressure on the product side was measured in two places, immediately before column 2 with PTransd, or at P3. Column pressure was controlled through either BPC1 or BPC2 depending on whether or not the tank was online for the process.

The middle manifold section of the system is represented in figure 4-6 and controlled how gas exited the system. Exits in the exit manifold correspond with the exits locations located in figure 4-4 and 4-5. Gas entered the manifold either through exit A (product flow) from the product side or exit D (waste flow) from the feed side. Gas can enter through exit B and C, but for this thesis, only the flows through exit A and exit D were used. The manifold consists of four hand valves that direct the flow out of the system either through FC4 and the oxygen analyzer, or directly to the atmosphere. The function of this manifold was for the calculation of a material balance for the process. It provided measurement of the flow rate and oxygen concentration out of the system before the gases were vented to the exhaust. The manifold had the flexibility to either allow one of the streams to be analyzed separately while the other was directed straight to the exhaust, or allow both product and waste streams to be analyzed together. This allowed a measurement of just the product (or waste) flow rate and purity, or the flow rate and composition of all the gas streams exiting the process.

4.5 Experimental Procedure

The experimental process of this thesis was broken down into two phases. The first phase consisted of preliminary experiments on the PSA system to check the pressure drop in the system, calibrate the necessary instruments, and confirm the activation of the zeolite in the columns. The second phase consisted of operating different PSA cycles in order to compare and optimize the process for the type of zeolite used in this thesis.

4.5.1 Preliminary Experiments

Since pressure is such an important component of a PSA process, pressure drop in different sections of the PSA apparatus was examined to determine if there was any section with significant pressure drop that would affect the cycle performance. The basic procedure was to find the pressure drop in a section of the system in between two of the ports (P1-P6) that were connected to the six port switch valve with the pressure transducer attached. This was done at flow rates (500-1950 std.cc/min) and pressures (vacuum -4 atm,) in the range of what was expected to be seen during PSA cycles for this thesis. While the pressure drop was found to be negligible, a summary of the pressure drops in some of the more relevant sections of the system can be found in appendix A.

Before any other testing could begin, several calibrations and instrument zeroing was completed. The pressure transducers were zeroed by using the vacuum pump connected near the oxygen storage tank. The flow meters used were calibrated against an industrial gas meter to generate flow factors for the rest of the experiments. The oxygen analyzer was also calibrated by flowing nitrogen, oxygen, and dry air through the analyzer to properly adjust the % oxygen it was measuring.

The final preliminary test conducted was confirmation of the activation of the zeolite in the columns. In order to do this, the PSA system was utilized to run quick breakthrough experiments. This consisted of equilibrating one of the columns with oxygen gas at a set pressure and then flowing nitrogen at a low flow rate through the column until breakthrough fully occurred. The amount of nitrogen adsorbed was then compared to the DSL model to determine the extent of the zeolite activation. If the

zeolite was not adsorbing as much as expected, the column was reactivated until it was determined the zeolite was fully activated.

4.5.2 *PSA Experiments*

For this lab scale PSA test system, a certain method was devised for the startup, operation, and shutdown of the process. Before the startup procedure, it was necessary to login to the LabWindows/CVI software that controls the data collection of the PSA process and hit the “start acquiring” button on the “Run Details Panel”. On the same panel, details pertaining to the data collection and recording file generation were specified for the cycle about to be started. Different colored sections on the “Run Details Panel” controlled different aspects of the data collection or recording. There was a section on the panel (blue box) for adjusting the sampling and data display rates. Another section (green box) specified the details pertaining to the recording file length and recording speed. There was also a section (red box) for changing the integration time for flow averaging calculations. Finally, there was a section (pink and black box) that pertained to the scaling and length of the strip charts on which the data collected was displayed. This section was also where the lag time was set for the lag trace. This lag trace was displayed as a time delayed trace (according to the lag time) on the strip charts that plot the real time data. This trace was useful for determining if a cycle was at CSS or if the cycle was changing over time.

Once all the details were entered for data collection and display purposes, the startup procedure began. If it was the first cycle run for the day, it was necessary to zero the MKS flow meters as their zero point tended to float overnight. It was then necessary

to purge the columns of nitrogen before starting a cycle so that the columns start in the same state with regards to the amount of oxygen/nitrogen in them. This was done by first changing the switch valve that controls the type of feed gas to position 2 (oxygen). Next, flow was directed through both columns and the oxygen analyzer in the exit manifold using the necessary pneumatic valves and hand valves. The columns were completely purged once there was a steady flow through FC4 and the oxygen concentration through the oxygen analyzer was constant. The oxygen analyzer maintained good calibration for an oxygen concentration close to air, however at pure oxygen concentration levels, the maximum floated between 98% and 102% depending on the atmospheric pressure. Because of this, the maximum oxygen concentration was noted before each run to most accurately assess purity of the product flow later during a cycle. After the columns were oxygen equilibrated, the pressures, flows, and valve timing were set. Feed flow was set to the desired flow by the flow controller digital readout that controls the MKS flow meters or the LabWindows software. This was done on the first channel which controls FC1. Channel 2 and 4 set the flow rate for FC2 and FC4 and should be set to 2000 cc/min (fully open) as discussed earlier. The needle valve before flow controller 2 was opened at least partially to start the process to allow purge/product pressurization to occur at the start of the cycle. It was later further adjusted during the operation of the cycle to tune the cycle. To set the adsorption pressure in the column, a feed flow rate similar to what was expected during the cycle operation was established through one of the columns using oxygen gas. Then using either using BPC 1 or BPC2, the pressure was adjusted either using the pressure transducer digital readouts or LabWindows software.

To set the valve sequence that corresponds to the cycle type desired, the PLC that controls the pneumatic valves was programmed using the PLC Editor software. This was done by simply utilizing a drum type sequence within the software. The drum sequence easily allowed for the programming of a repeating sequence that opened and closed the pneumatic valves at set times in the PSA cycle.

The main type of cycle used was a combined PSA/VSA cycle with feed pressurization cycle and an equalization step. The feed pressurization cycle with equalization consisted of six steps in the following sequence: 1) Feed Pressurization 2) Production 3) Equalization 4) Blowdown 5) Purge 6) Equalization. For this six step process, the equalization step was done on the product end of the process in order to conserve any leftover oxygen at the end of the production step.

To begin cyclic operation in the system, the feed gas was switched to port 6 (dry air) on the feed switch valve. The PLC was started to begin the cycle and the pump was powered on. Once the cycle was started, it needed to be tuned in order to make sure the desired pressures were occurring in the columns and that the required product gas purity was reached. If the desired blowdown pressure was not achieved during the cycle, BPC4 was adjusted until the desired pressure was attained. Adjusting the adsorption pressure to the desired pressure was not as simple. Flow rates were first adjusted to attempt to reach the desired adsorption pressure. This meant adjusting the feed flow rate and the purge/product pressurization flow rate. Sometimes it was additionally necessary to adjust BPC1 to achieve the desired column adsorption pressure. Once the adsorption pressure was at or near the desired pressure, the next tuning procedure depended on the type of cycle. For a six step equalization cycle, a purity of 98% was found by varying the P/F

ratio. Once the cycle reached CSS at the desired pressures and product purity, all the pressures and flows (including the waste stream) were collected and recorded. To stop the cycle, the PLC was stopped, the feed flow was turned off, and the pump was shutdown.

4.6 Experimental Design

The types of cycles performed for this thesis reflect the two main goals of this work. The first main goal was to determine how the provided zeolite performed under a variety of operating conditions. These different operating conditions included different pressure ratios, feed velocities, step times, cycle types, and adsorption pressures. The other goal was to determine experimentally what the kinetic limit of the zeolite was by increasing cycle speed (minimize BSF). Several experiments were run as sets to investigate how different factors affected the performance of the process. It should be noted that all cycles were run without a product storage tank.

4.6.1 Variance of Pressure Ratio and Cycle Time

The goal of this set of experiments was to examine the dependence of recovery and BSF on the pressure ratio. The first type of cycle involved feed (air) pressurization and an equalization step. Since the optimal length of the equalization step varies depending on the pressure ratio, a set of experiments (Table 4-3) were conducted at a constant pressure ratio to determine the most advantageous equalization time. Using these results, the equalization time for other pressure ratios could be better estimated.

The next set of experiments involved changing the pressure ratio with 20 second cycles. These experiments are summed up in table 4-4. In order to examine the effects of lowering cycle time on recovery and BS, the cycle times were reduced by 5 seconds while keeping the total gas flows per cycle for the different steps as similar as possible. The goal was to make sure that any changes in recovery and BSF were only due to the cycle time reduction. A summary of the 15 second cycles are seen in table 4-5. Table 4-6 is for 10 second cycles. It should be noted that these experiments were all run with bottled Ultra Air which contains no argon and has a slightly higher nitrogen content to that of ambient air.

Table 4.3. Set #1: Equalization step time variance (20 sec. feed pressurization with equalization cycles and an average adsorption pressure of 1441 torr. Sc stands for standard cubic centimer)

Feed(s)	Blow(s)	Purge(s)	Equil.(s)	Cycle(s)	Feed (scc/cycle)	P/F ratio	P. ratio
9.8	7.8	2	0.2	20	349	0.24	4.3
9.7	7.7	2	0.3	20	327	0.26	4.3
9.6	7.6	2	0.4	20	310	0.27	4.3
9.5	7.5	2	0.5	20	301	0.28	4.3

Table 4.4. Set #2: Pressure ratio variance. (20 sec. feed pressurization with equalization cycles and an average adsorption pressure of 1439 torr)

Feed(s)	Blow(s)	Purge(s)	Equil.(s)	Cycle(s)	Feed (scc/cycle)	P/F ratio	P. ratio
9.7	7.7	2	0.3	20	241	0.54	2.5
9.6	7.6	2	0.4	20	280	0.40	3.5
9.5	7.5	2	0.5	20	301	0.28	4.3
9.4	7.4	2	0.6	20	334	0.21	5.4
9.3	7.3	2	0.7	20	346	0.14	6.3
9.3	7.3	2	0.7	20	379	0.09	7.7
9.3	7.3	2	0.7	20	403	0.04	9.4

Table 4.5. Set #3: Pressure ratio variance. (15 sec. feed pressurization with equalization cycles and an average adsorption pressure of 1438 torr)

Feed(s)	Blow(s)	Purge(s)	Equil.(s)	Cycle(s)	Feed (scc/cycle)	P/F ratio	P. ratio
7.2	5.2	2	0.3	15	220	0.38	2.5
7.1	5.1	2	0.4	15	288	0.37	3.5
7	5	2	0.5	15	308	0.27	4.4
6.9	5	1.9	0.6	15	341	0.20	5.4
6.8	5	1.8	0.7	15	358	0.15	6.2
6.8	5	1.8	0.7	15	378	0.10	7.4

Table 4.6. Set #4: Pressure ratio variance. (10 sec. feed pressurization with equalization cycles and an average adsorption pressure of 1435 torr)

Feed(s)	Blow(s)	Purge(s)	Equil.(s)	Cycle(s)	Feed (scc/cycle)	P/F ratio	P. ratio
4.7	3.5	1.2	0.3	10	222	0.29	2.6
4.6	3.5	1.1	0.4	10	283	0.37	3.5
4.5	3.5	1	0.5	10	306	0.28	4.2
4.4	3.4	1	0.6	10	329	0.22	5.3
5.3	4.3	1	0.7	12	340	0.15	6.5
5.3	4.9	0.4	0.7	12	333	0.18	7.2

Note: At a pressure ratio of 6.5 and 7.2, the cycles are 12 seconds because of inlet flow meter limitations

4.6.2 Variance of Adsorption Pressure

The goal of this set of experiments was to examine the effects of adsorption on the performance of PSA cycles. By running this set of experiments at a cycle time of 15 seconds, a comparison could be made to the cycles done in set 3. The bottle of air used for experiments #1-4 was Matheson “Ultra” air which had a nitrogen concentration very similar to ambient air, but with no argon. However, the bottle was emptied after experiment #4 and it was replaced with a bottle of Matheson “Dry” air, which was found

using a mass spectrometer to have a noticeably higher nitrogen concentration compared to ambient air.

Table 4.7. Set #5: Pressure ratio variance with 15 s feed pressurization with equalization cycles and an average adsorption pressure of 1203 torr.

Feed(s)	Blow(s)	Purge(s)	Equil.(s)	Cycle(s)	Feed (scc/min)	P/F ratio	P. ratio
7.2	5.2	2	0.3	15	214	0.37	2.5
7.1	5.1	2	0.4	15	261	0.25	3.5
7	5	2	0.5	15	296	0.27	4.4
6.9	5	1.9	0.6	15	304	0.09	5.5
6.8	5	1.8	0.7	15	322	0.06	6.3
6.8	6	0.8	0.7	15	324	0.07	7.4

Using the “Dry” air, several additional cycles needed to further investigate the effect of increasing the adsorption pressure. These are summarized in table 4.8 below. These cycles were performed for comparison with 15 second cycles at a pressure ratio of 4.4 with “Dry” air from previous experiments. The first cycle in table 4.8 was

Table 4.8. Set #6: Adsorption pressure variance for 15 s feed pressurization with equalization cycles.

Feed(s)	Blow(s)	Purge(s)	Equil.(s)	Ads. P. (torr)	Feed (scc/min)	P/F ratio	P. ratio
7	5	2	0.5	1697	311	0.35	4.3
7	5	2	0.5	2002	340	0.40	4.4

unintentionally set at a pressure ratio of 4.3 instead of 4.4; however, this only has a small effect on the performance of the cycle and does not interfere with the overall purpose of the experiment.

CHAPTER V

RESULTS AND DISCUSSION

This section details the results of the PSA cycles investigated and provides discussion on the performance of the cycles and how they compare to each other. The results are tabulated and also graphed to aid in comparisons between the different cycles. Finally, explanations are offered for the results and how they illustrate what is physically occurring within the process. All cycles were set to perform as optimally as possible in terms of recovery and BSF while keeping the oxygen product purity 97% or above (argon free air).

5.1 Isotherms

The following figures show the isotherms for the zeolite used in the experiments for this thesis. Figure 5.1 and 5.2 show the pure component isotherms for pure nitrogen and oxygen and are the isotherms used to develop the coefficients for the DSL model that was explained in chapter 3, section 2.

Figure 5.3 shows the DSL generated binary adsorption isotherms for the zeolite at 23.6°

C.

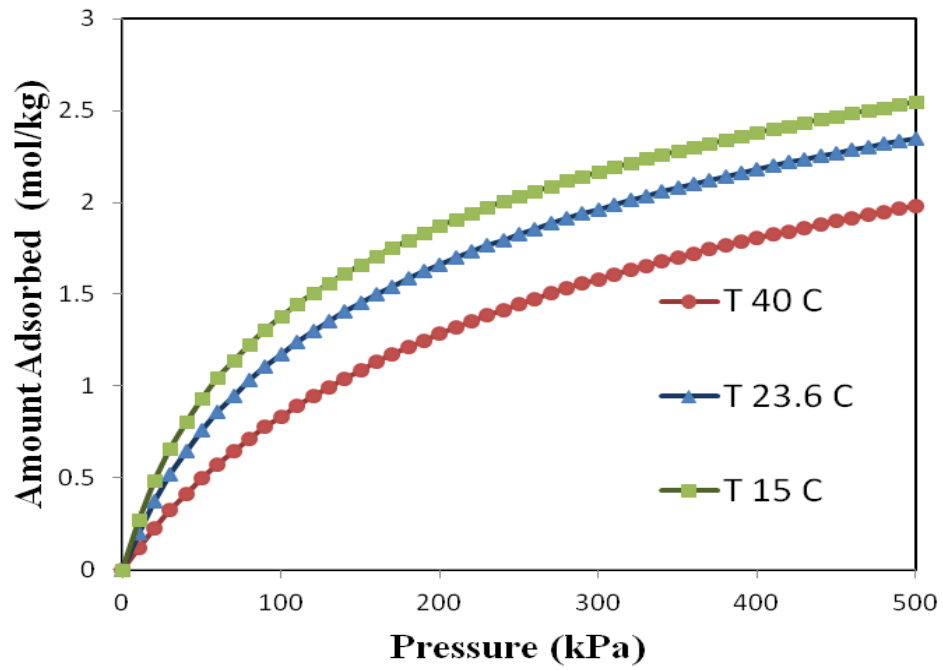


Figure 5.1. Nitrogen isotherms for zeolite used in this thesis.

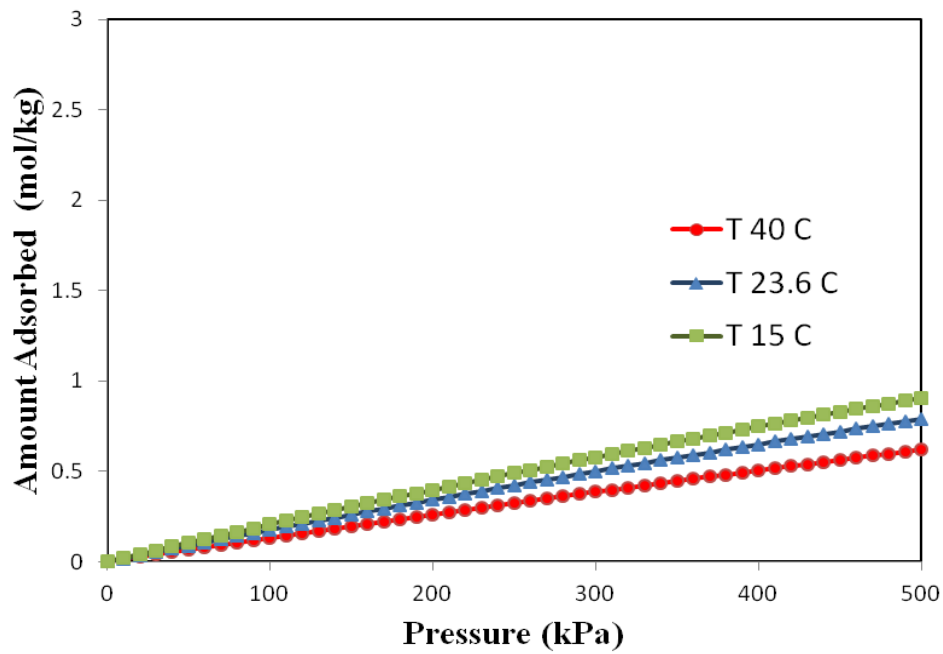


Figure 5.2. Oxygen isotherms for zeolite used in this thesis.

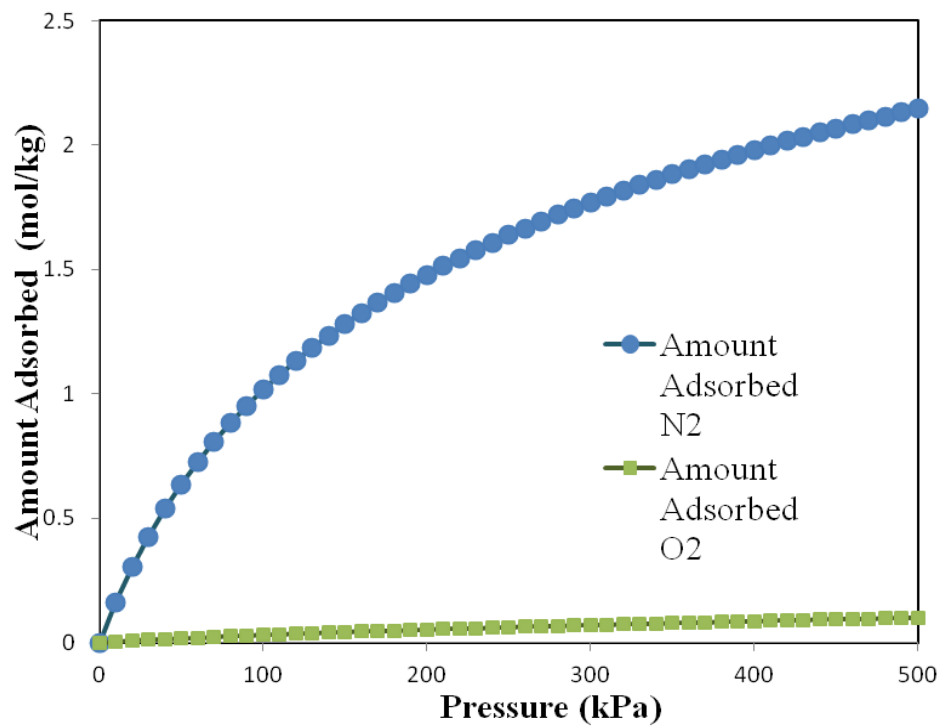


Figure 5.3. Binary adsorption at 23.6 C and nitrogen concentration similar to air.

5.2 Experimental Results

A PSA process can be operated at a number of different conditions with varying degrees of performance. Optimization of the process depends on what the limiting design factor is, whether it is the power needed for the pump, product flow, velocity of the feed gas, or size of the process. In all cases, the product purity is usually prescribed by the specific application. In this work, minimum oxygen product purity was 97% (argon free basis). For the process utilized in this thesis, optimization for pump power is not considered. Only optimization of the product flow (high recovery) and size of the process (low BSF) is examined. This means that all the cycles examined were operated at or close to peak performance in terms of recovery at a fixed pressure ratio and cycle time. BSF was then changed by increasing the feed gas velocity (lowering cycle time) to optimize for the speed of the process, thus increasing zeolite utilization.

5.2.1 *Calculations and Error Analysis*

For the analysis of the cycles found for this thesis, the following explains how calculations were conducted to evaluate a cycle's performance. After cyclic steady state is reached, flow rates were averaged over 2-3 cycles in a manner similar to what was discussed in chapter 3, section 4 and then using these averaged flow rates and the cycle time, the flow rates were found on a per cycle basis. A simple conversion of the volume to moles gave the molar flow on a per cycle basis, which was then used to conduct total and component material balances along with calculating the percent oxygen recovery based on both the product and waste stream. These calculations were done with the equations from chapter 3, section 4. In order to calculate the BSF with equation 3.37, the

amount of moles of oxygen generated per cycle was used with the cycle time and amount of zeolite in the columns.

The reliability (or error) of the performance of the cycles examined in this thesis was considered in two different ways. First, material balances were conducted on a per cycle basis to ensure that all the gas in the feed stream was accounted for in the waste and product streams. The acceptable error in the material balances was set to 5% or less in order for the cycle performance to be considered acceptable. The oxygen material balance was of primary concern because it was the product gas for the process. Thus, as long as the oxygen material balance was 5% or less, the cycle was considered acceptable even if the overall or nitrogen material balance was slightly above the 5% threshold. The other check in the reliability of the performance of the cycles was to compare the oxygen recovery based on the oxygen in the product stream with the oxygen recovery based on the oxygen in the waste stream. If the recoveries were similar, (within 3-4% of each other) and the material balances were closing, then the performance of the cycle was considered reliable.

5.2.2 Changing of Equalization Step Time

As mentioned earlier in chapter 2, section 3, the length of an equalization step for a cycle utilizing equalization has an impact on the recovery. A longer equalization step will up to a certain point improve the recovery. However, too long of an equalization step causes nitrogen to desorb from one column to the other, which has a negative impact on recovery. This means there is an optimal equalization time that will maximize the recovery.

To find the approximate optimal equalization time, experimental set #1 was conducted in order to examine how changing the equalization step at a fixed pressure ratio changed the cycle performance. The performance of the cycles run during this experiment can be seen in table 5.1 below. Details about the cycle parameters can be seen in table 4.4. The equalization step for this experiment was varied from 0.2 seconds to 0.5 seconds and the recovery increased with an increase in equalization time. It was clear from the recovery results that an increase in equalization time past 0.5 seconds would only minimally increase recovery, so the experiment was stopped since the goal was only to optimize the recovery without unnecessarily extending cycle time. It should also be noted that the higher recovery means that the amount of

Table 5.1. Performance of cycles from experimental set #1. (20 s feed pressurization with equalization cycles, an average adsorption pressure of 1441 torr, and same purge flow (18 scc/cycle) and pressure ratio (4.3) for each cycle. Volumes are per cycle where scc stands for standard cubic centimer.)

Eq (s)	Feed (scc)	Waste (scc)	Product (scc)	% MB error	% MB error (O ₂)	% MB error (N ₂)	% Purity	% Rec	% Rec (Waste)	BSF
0.2	349	323	35	2.4	0.36	3.2	98	47	47	222
0.3	327	300	35	2.7	1.4	3.7	98	51	52	220
0.4	310	285	35	3.2	0.059	4.0	98	53	53	222
0.5	301	276	35	3.4	0.33	4.1	98	54	54	224

product per cycle was able to be maintained even with a decrease in the amount of feed gas per cycle as the equalization step time was increased. After optimizing for recovery, the only advantage to operating with a longer equalization step would be to save power to the pump. If this was the main goal, further cycles would need to be examined at higher equalization times to determine the point where nitrogen will start to desorb from one column to the other causing a significant decrease purity, which needs to be compensated

by more purge gas which consequently decreases the recovery. Finding an optimal equalization time for every type of cycle found for this thesis would be highly time consuming. However, because the recoveries do not change much after a certain equalization time, a reasonable equalization time can be approximated from these results without sacrificing much in terms of recovery.

5.2.3 *Changing of Pressure Ratio*

When operating hybrid VSA/PSA cycles like the ones in this thesis, the desorption pressure plays a large role in the performance of the process. Since the desorption pressure occurs under some degree of vacuum, operation of the process enters into the linear portion of the isotherm where the swing capacity increases (due to the straightening of the nitrogen isotherm) and selectivity is enhanced. At a low desorption pressure, less purge gas is required because there is less nitrogen in the columns after the blowdown step occurs, which means more oxygen is available as product gas. Thus, as the regeneration pressure is lowered, the recovery of the process increases and the BSF decreases (if all else is the same).

When operating under vacuum, several design criteria tend to drive how high of vacuum is used to operate the cycle. The main considerations are the amount of oxygen product desired, the power allowance to operate the vacuum pump, and the ability of the pump to provide low vacuum quickly in the columns. Higher product flows per cycle (lower BSF) are achieved at higher pressure ratios (higher vacuum), but at the cost of power to achieve the high vacuum. There are inherently other factors that determine the potential product flow, like the type of adsorbent used and the dimension of the columns

used. For the case of this thesis, the zeolite type and column dimensions were fixed and the power to the pump was not measured. The vacuum pump was oversized for this system and the vacuum level was controlled by an absolute back pressure controller. Thus, the main goal of changing the desorption pressure in this thesis was to determine the possible recoveries over a range of different pressure ratios and desorption pressures with a 97-98% product purity (argon free air). This was first done for a set of cycles in which the pressure ratio was changed while keeping the cycle time the same. The results are summarized in table 5.2 below and figure 5.4 graphically shows what happens to the recovery and BSF as the pressure ratio increases. As expected, as the pressure ratio increased, the recovery increased while the BSF decreased. Also, the necessary purge gas per cycle decreases significantly as the pressure ratio increases. This trend is expected since if it was possible to attain full vacuum, there would not be any need for purging.

Table 5.2. Performance of cycles from experimental set #2. (20 sec. feed pressurization with equalization cycles and an average adsorption pressure of 1439 torr. Volumes are per cycle.)

P ratio	Feed (scc)	Waste (scc)	Purge (scc)	Product (scc)	% MB error	% MB error (O ₂)	% MB error (N ₂)	% Purity	% Rec	% Rec (W)	BSF
2.5	241	228	28	20	3.2	1.8	3.5	97	39	37	385
3.5	280	265	24	28	4.7	1.1	5.6	98	46	45	279
4.3	301	276	18	35	3.2	0.33	4.1	98	54	54	224
5.4	334	300	15	42	2.6	0.74	3.5	98	59	60	185
6.3	346	305	11	46	1.6	2.9	2.8	97	62	65	170
7.7	379	332	8	52	1.3	3.0	2.4	98	65	68	149
9.4	403	349	4	60	1.5	2.5	2.6	98	69	72	131

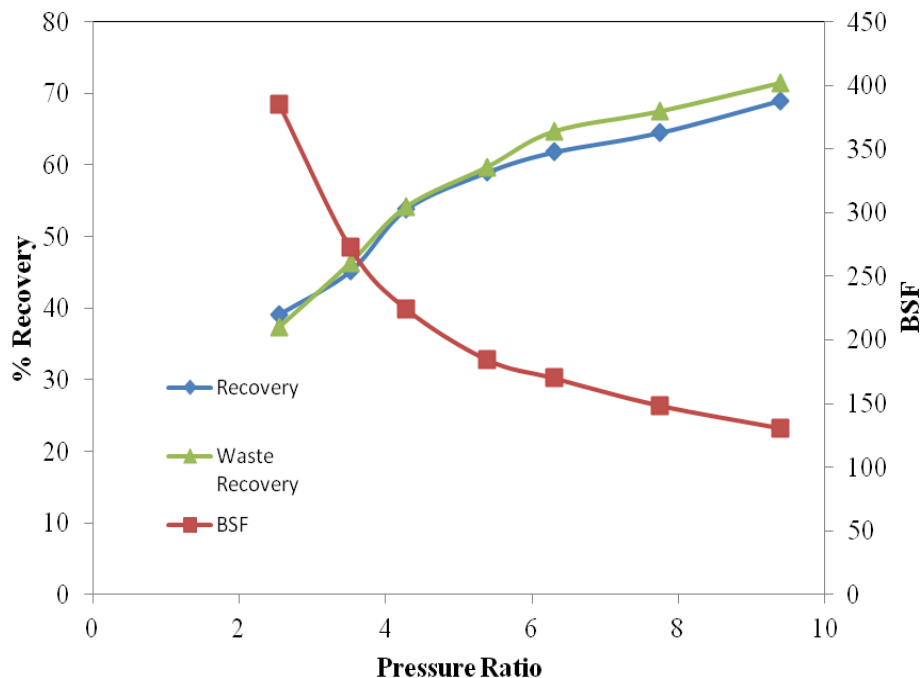


Figure 5.4. BSF and Recovery vs. Pressure ratio for Experimental set #2.

5.2.4 Changing of Feed Rate (Cycle Time)

For any PSA application, the ability to increase the speed of the process by increasing the feed rate provides a way to lower the BSF (without changing the pressure ratio). As previously mentioned, a lower BSF is ideal for a PSA process because it makes it possible to either run the process with less material (lower capital costs) or at a higher product flow rate with the same amount of material. Increasing the velocity of the feed does have some limitations however as mentioned in the section 3 of chapter 3. The main restriction is that mass transfer limitations increase significantly as the velocity of the feed rises. The adsorbate molecules begin approaching the kinetic limit of the solid utilized for the process as they cannot reach the adsorption sites fast enough. Smaller particles are used to alleviate this issue to a certain degree by decreasing the diffusion

path length. But as previously mentioned, smaller particles lead to other problems, including higher pressure drop. Pressure drop, in addition to the kinetic limit, restrict the maximum possible feed velocity for efficient cyclic operation. This was noted by Chai et. al., with regards to rapid PSA cycles [39]. With these limitations in mind, it is clear that there is a feed velocity limit, which means in terms of the BSF, there will be a minimum value that occurs as the feed velocity increases. Once this minimum BSF occurs, it will start to rise with an increase in feed velocity.

In order to examine the effects of increasing the feed velocity and to attempt to find the kinetic limit of the zeolite used for this thesis, experimental sets #3 and #4 were conducted to compare with experimental set #2 and are summarized in tables 5.3 and 5.4.

Table 5.3. Performance of cycles from experimental set #3. (15 s feed pressurization with equalization cycles and an average adsorption pressure of 1438 torr. Volumes are per cycle.)

P ratio	Feed (scc)	Waste (scc)	Purge (scc)	Product (scc)	% MB error	% MB error (O ₂)	% MB error (N ₂)	% Purity	% Rec	% Rec (W)	BSF
2.5	220	209	18	18	3.5	0.64	4.3	98	39	38	322
3.5	288	265	23	28	2.0	2.4	3.1	98	46	48	206
4.4	308	283	18	33	2.8	0.65	3.7	98	50	51	176
5.4	341	303	15	42	1.1	3.1	2.2	98	58	61	139
6.2	358	316	11	47	1.2	3.3	2.4	98	62	65	124
7.4	378	333	8	52	1.6	2.6	2.8	98	64	67	113

Table 5.4. Performance of cycles from experimental set #4. (10 s feed pressurization with equalization cycles and an average adsorption pressure of 1435 torr. Volumes are per cycle.)

P ratio	Feed (scc)	Waste (scc)	Purge (scc)	Product (scc)	% MB error	% MB error (O ₂)	% MB error (N ₂)	% Purity	% Rec	% Rec (W)	BSF
2.6	222	209	14	17	2.1	0.91	2.9	98	36	37	227
3.5	283	257	23	29	1.3	1.3	1.9	98	48	49	134
4.2	306	274	18	35	0.77	2.2	1.6	98	53	55	113
5.3	329	303	15	43	5.2	1.9	6.0	98	61	59	91
6.5	340	309	11	47	4.7	2.2	5.4	98	65	63	99
7.2	333	302	13	45	4.2	1.4	5.0	98	63	62	103

The results indicate that as the BSF is lowered by increasing the feed velocity (reducing cycle time), the recovery is maintained across the different pressure ratios. Since the column size and amount of adsorbent is constant, the lower cycle time causes an increase in the product flow rate, which is why the BSF decreases as the cycle time is reduced. A visual representation is the best way to present these results. Figure 5.5 presents the results from experimental sets #2-4 on the same graph. It can be clearly seen that as the cycle time is reduced (BSF reduced), the recoveries remain consistent at all respective pressure ratios. A few comments on the graph itself, as mentioned in the “Experimental” chapter, the two highest pressure ratios for experimental set #4 (10 second cycles) were actually run at 12 second cycles due to system limitations (not a high enough flow controller for the feed gas). This is primarily the reason that the BSF slightly increases for these cycles. Also at those pressure ratios, because of the high vacuum requirement and the limited amount of time for the blowdown step, the regeneration step was most likely slightly hindered because of pressure drop and/or the pneumatic valves not having a high enough C_v to permit the necessary flow to pull vacuum quickly, which also likely contributed some to the higher BSF. Lastly, in experimental set #3 for a pressure ratio of

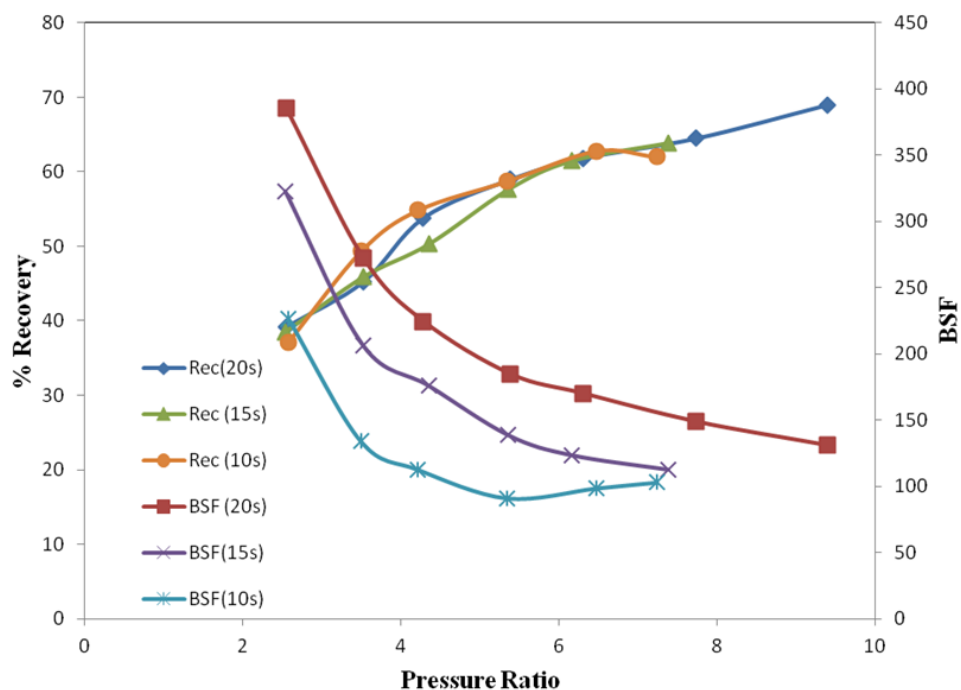


Figure 5.5. BSF and Recovery vs. Pressure ratio for Experimental sets #2-4.

4.4, the recovery is slightly lower compared to the 20 and 10 second cycle. This was the result of it being the only cycle to be run after the air cylinder responsible for supplying the feed gas was changed for a “Dry” air cylinder. As previously mentioned in chapter 4, the “Dry” air had a slightly higher concentration of nitrogen than “Ultra” air. It was found that the higher nitrogen content caused the recovery to be lower than experiments with “Ultra” air by approximately 4-5% and is the reason why the recovery for this cycle was lower than the 10 second and 20 second cycles at the same pressure ratio.

As referred to earlier, it is desirable to determine the kinetic limit of the adsorbent used for a PSA process and to determine whether or not this limit is reached. To do this, the BSF needs to be examined as the velocity of the feed gas increases. In the case of this thesis, it is easier to examine the BSF as a function of cycle time since feed velocity is

directly related to the cycle time. A plot of BSF vs. cycle time will provide insight into what the velocity is where the kinetic limit is found and is seen in figure 5.6. Using this figure, all the shown pressure ratio's show a relatively constant decline in BSF as cycle time decreases. This trend will not continue however, as eventually the BSF will reach a minimum as previously discussed, after which the BSF will start to increase. Clearly this minimum was not found or even approached from experiments #2-4. Unfortunately, due

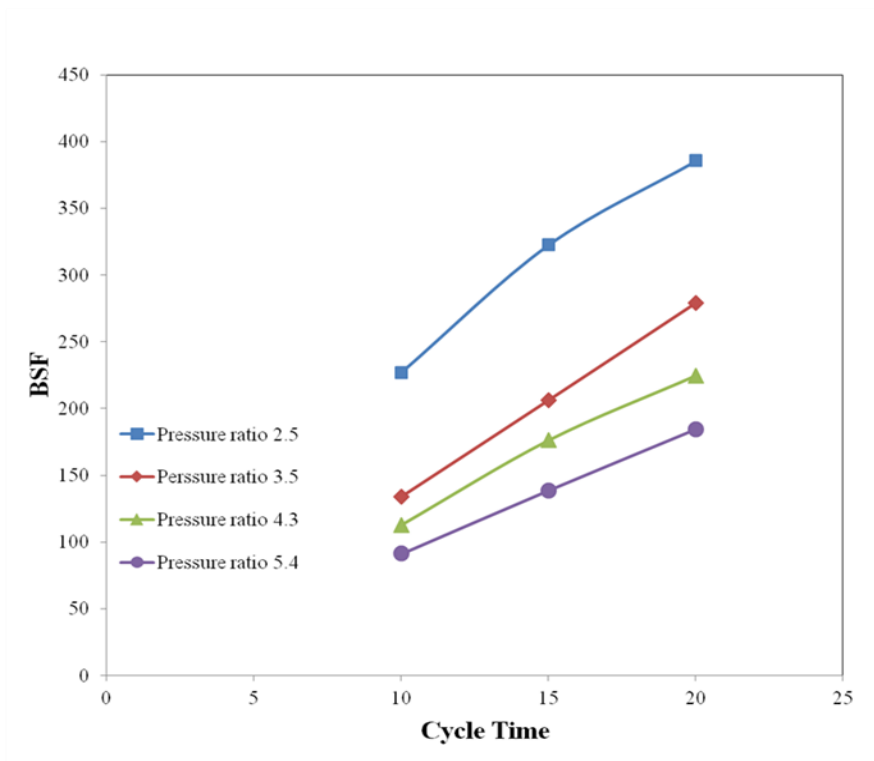


Figure 5.6. Approach of kinetic limit at different pressure ratios.

to the constraints of the experimental system, cycles with lower cycle times were unable to be found. Two main factors prevented this from happening. The first was the system was designed with a 2 sL/min maximum flow for the feed and exit streams. The flow

controllers are unreliable for steady flows over this maximum, which is what would be required to operate cycles with a lower cycle time. Additionally, as previously mentioned, pressure drop (due to 1/8" tubing) and the C_v of the block valves begin to significantly affect the ability of the vacuum pump to effectively bring the columns to the desired vacuum pressure in the amount of time needed for faster cycles.

5.2.5 *Changing of Adsorption Pressure*

Experimental sets #1-4 all dealt with similar adsorption pressures, but it may be desirable to operate at a different adsorption pressure. In order to look at the effects of adsorption pressure, experimental set #5 was performed, which is detailed in table 5.5 below.

Table 5.5 Performance of cycles from Experimental set #5. (15 s feed pressurization with equalization cycles and an average adsorption pressure of 1203 torr. Volumes are per cycle.)

P ratio	Feed (scc)	Waste (scc)	Purge (scc)	Product (scc)	% MB error	% MB error (O ₂)	% MB error (N ₂)	% Purity	% Rec	% Rec (W)	BSF
2.5	214	206	17	17	4.1	1.4	5.6	98	36	38	352
3.5	261	242	14	25	2.0	4.2	3.6	98	44	48	238
4.4	296	272	17	33	3.1	0.36	4.1	98	52	53	176
5.5	304	274	6	39	2.9	0.17	3.6	98	60	60	149
6.3	322	290	4	41	2.9	2.7	4.5	98	60	63	141
7.4	324	286	5	42	1.1	3.2	2.3	98	60	63	140

By operating these cycles at 15 seconds, they could be reasonably compared with experimental set #3. While the velocities in the column will be slightly different due to the different adsorption pressure, by keeping the cycle time the same, only one of the variables in the calculation of the BSF is changed. Experimental sets #3 and #5 are

compared in figure 5.7 below. It bears repeating that experimental set #5 was conducted with “Dry” air which contained a higher concentration of nitrogen than the “Ultra” air used for experimental set #3. So unfortunately these experiments are not great

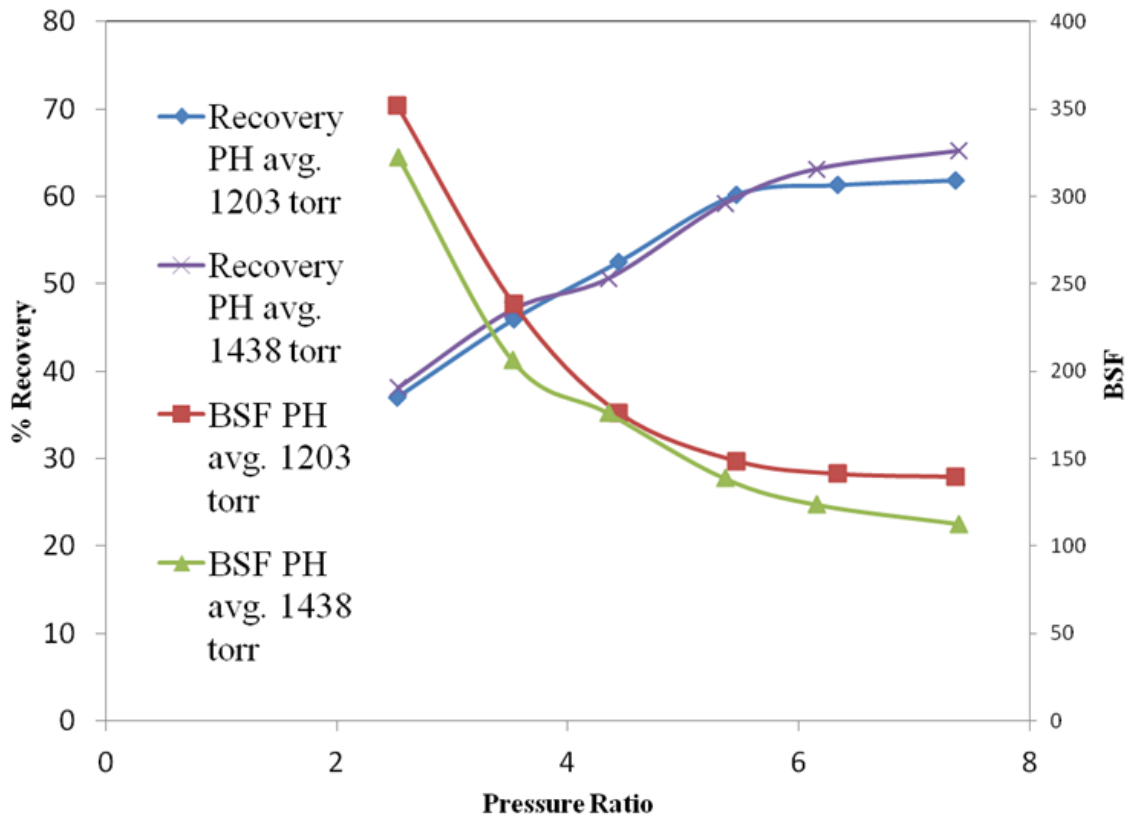


Figure 5.7. BSF and Recovery vs. Pressure ratio at different adsorption pressures. (PH=Adsorption pressure)

comparisons, however, there is still something to be gained from examining their performances. Figure 5.7 shows this comparison graphically, which makes it easy to see that there is not a significant difference in recoveries between these two different adsorption pressures. It should also be reiterated that the cycle found at a pressure ratio of 4.4 for the higher adsorption pressure was done using “Dry” air, which makes it a good comparison for the cycle found at a similar pressure ratio with the lower adsorption

pressure. Comparing these two cycles, the recovery for the lower adsorption pressure cycle was about 2% higher than the higher adsorption pressure cycle, while the BSF's were identical. For the rest of the cycles though, the recoveries are predominantly lower for the cycles operating with a lower adsorption pressure, which lead to a higher BSF. If all the cycles were found using "Ultra" air, it is reasonable to project that the recoveries for the lower adsorption pressure to be slightly higher than those at the higher adsorption pressure, which is theoretically what should occur. Also, the difference in nitrogen concentration between "Ultra" and "Dry" air seems to be mainly responsible for this difference in BSF between the two adsorption pressures. Since the cycles at a pressure ratio of 4.4 did not show a significant change in BSF, it is reasonable to project that if the cycles using a lower adsorption pressures were found using "Ultra" air that they would have similar BSF to the cycles at the higher adsorption pressure.

While the difference in adsorption pressure was not large, it was still noteworthy to find that the recoveries were similar over a range of pressure ratios and more importantly, that the rise in BSF with the lower adsorption pressure is small enough that the difference is most likely due to the difference in nitrogen concentration of the feed air. Since the performances of the two adsorption pressures used in experimental set #5 were so similar, it was of some interest to determine the change in cycle performance with a higher adsorption pressure than what was used than in experimental set #5. Since the cycles at a pressure ratio of 4.4 for the previous two adsorption pressures both were done using "Dry" air, these cycles were used as a comparison with cycles at higher adsorption pressures, but the same pressure ratio (also using "Dry" air). The details of these cycles are found in table 5.6 below and compared graphically with the previous

cycles in figure 5.8. As figure 5.8 shows, a significant decline in performance was found with an increase in adsorption pressure at the same pressure ratio. This is expected as the adsorption pressure rises while maintaining the same pressure ratio because the operation of the cycle starts to enter the curved portion of the nitrogen isotherm (Type 1), which decreases its swing capacity. Furthermore, the desorption pressure is also higher which means more purge gas is required to regenerate the columns, which decreases the amount of oxygen available for the product gas. Additionally, the amount of adsorption that is occurring per cycle increases with a higher adsorption pressure. Since adsorption is exothermic, the temperature in the column will be higher for higher adsorption pressures. This causes the cycle operation to occur on higher temperature isotherms, which negatively impacts recovery. Lastly, there is a significant amount of dead volume on the column itself, which negatively impacts the performance as the adsorption pressure rises.

Table 5.6. Performance of cycles from Experimental set #6. (15 s feed pressurization with equalization cycles at a constant pressure ratio of 4.4. Volumes are per cycle.)

Ads. P. (torr)	Feed (scc)	Waste (scc)	Purge (scc)	Product (scc)	% MB error	% MB error (O ₂)	% MB error (N ₂)	% Purity	% Rec	% Rec (W)	BSF
1200	296	272	17	33	3.2	0.36	4.1	98	52	53	176
1441	308	283	18	33	2.8	0.65	3.7	98	50	51	176
1697	311	294	24	29	3.6	1.0	4.9	98	43	44	203
2002	340	322	29	27	2.5	1.7	3.7	98	36	38	220

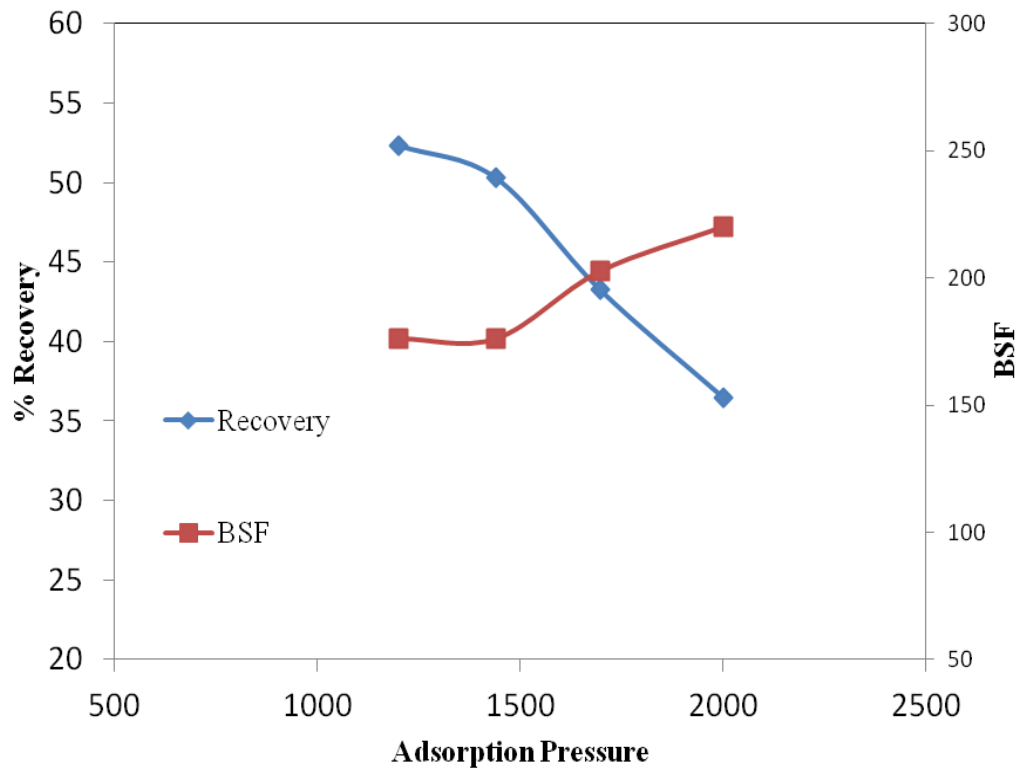


Figure 5.8. BSF and Recovery vs. Adsorption pressure.

Chapter VI

CONCLUSIONS

6.1 Thesis Summary and Contributions

The goal of this thesis was to examine a pressure swing adsorption process utilizing a novel adsorbent for the application of oxygen generation and determine the efficiency of the process. As evidenced by the results and discussion chapter, there are numerous ways to operate a PSA process depending on what the process is designed for. This leads to the secondary goals of this thesis, which was to optimize for high recovery of oxygen and for the development of a fast, productive process. It was specifically of interest to investigate the kinetic limit of the adsorbent used.

The results from chapter 5 have several important takeaways. First, based on the ability of the adsorbent used in this process to maintain its efficiency when the feed gas velocity was increased to create 10 second cycles, it can be concluded that this material

has a fast adsorption rate. This means that this adsorbent is ideal for rapid PSA processes where a fast adsorption rate is required. Due to system limitation however, the kinetic limit was unfortunately not found.

Secondly, the recoveries seen for the cycles operated in this thesis showed high recoveries for an X-type zeolite. This is true even at lower pressure ratios of 2.5 and 3.5, which is not true of many other zeolites. This allows the zeolite to generate a high product flow rate and lower the BSF even at a lower pressure ratio, which lessens the power requirements for the pump and reduces operating costs.

Third, the effect of adsorption pressure was also shown and it was clear that a higher adsorption pressure will lower the recovery of the cycle while increasing the BSF. This is mainly due to the curvature of the nitrogen isotherm. Last, all of these experiments together provide a range of operating conditions for this specific type of adsorbent and show how the material can be used differently depending what the process requirements are. These results would be very useful to a designer of PSA process looking to use this zeolite for the development of larger scale PSA process for oxygen generation.

6.2 Considerations for Future Work

The nature of a PSA process allow for numerous ways of studying and optimizing a PSA process. So there are many directions future work could go in to further study this adsorbent in a PSA process. One major area of study that would be useful would be to optimize cycles utilizing product pressurization instead of an equalization step. This was attempted for this thesis, but the performance of the cycles was not good due to the dead

volume occupied by the filters at the entrances to the columns. In order to better study product pressurization, the effects of dead volume would need to be minimized by having larger columns.

Additionally, more work on finding the kinetic limit of the zeolite is needed in order to find what the maximum feed gas velocity is. This will require some modifications to the test system used for this thesis. Specifically, this would require new flow meters for the feed and waste streams that can measure larger flow rates. It may also require replacing the pneumatic valves if it is found that their C_v is not high enough to permit short cycles.

Lastly, all the cycles conducted were of the PSA/VSA hybrid kind. Future work could include a more in depth look at changing the adsorption pressure including operating the cycle as a pure VSA cycle or PSA cycle. Operating at higher adsorption pressures would require larger columns as the effects of the dead volume in the system are magnified at the higher adsorption pressures. Operating under VSA conditions would require another pump to pressurize the product gas in order to analyze it.

REFERENCES

- [1] 26 January 2007. [Online]. Available: <http://www.gasworld.com/oxygen-global-market-report/1277.article>. [Accessed 30 August 2013].
- [2] A. Chica, "Zeolites: Promised Materials for the Sustainable Production of Hydrogen," *ISRN Chemical Engineering*, no. 2013, p. Article ID 907425, 2013.
- [3] A. F. Masters and T. Maschmeyer, "Zeolites - From curiosity to cornerstone," *Microporous and Mesoporous Materials*, no. 142, pp. 423-438, 2011.
- [4] A. M. Mendes, C. A. Costa and A. E. Rodrigues, "Analysis of Nonisobaric Steps in Nonlinear Bicomponent Pressure," *Industrial Engineering and Chemistry Research*, vol. 39, pp. 138-145, 2000.
- [5] B. Crittenden and W. J. Thomas, *Adsorption Technology & Design*, Massachusetts: Reed Education and Professional Publishing Ltd 1998, 1998.
- [6] C. A. Grande, "Advances in Pressure Swing Adsorption for Gas Separation," vol. 2012.
- [7] C. C. Chao and S. J. Pontonio, "Advanced Adsorbent for PSA". United States Patent 6,425,940, 30 July 2002.
- [8] C. C. Chao, "Process for Separating Nitrogen From Mixtures Therof with Less Polar Substances". Patent 4,859,217, 22 August 1989.
- [9] C. C. Chao, J. D. Sherman, J. T. Mullhaupt and C. M. Bolinger, "Mixed Ion-Exchanged Zeolites and Processes for the Use Thereof in Gas Separations". United States Patent 5,174,979, 29 December 1992.
- [10] C. G. Coe, R. Pierantozzi, T. R. White and J. F. Kirner, "Nitrogen Adsorption with a CA and/or SR Exchanged Lithium X-Zeolite". United States Patent 5,152,813, 6 October 1992.
- [11] C. W. Skarstrom. US Patent 2,944,627, 1960.
- [12] D. M. Ruthven, *Principles of Adsorption and Adsorption Processes*, John Wiley & Sonce, Inc., 1984.
- [13] D. M. Ruthven, S. Farooq and K. Knaebel, *Pressure Swing Adsorption*, John Wiley & Sons, Inc., 1994.

- [14] D. W. Mckee, "Separation of an Oxygen-Nitrogen Mixture". United States Patent 3,140,933, 14 July 1964.
- [15] G. Reib, "Status and development of oxygen generation processes on molecular seive zeolites," vol. 8, no. 2, pp. 95-99, 1994.
- [16] H.-S. Shin, D.-H. Kim, K.-K. Koo and T.-S. Lee, "Performance of a Two-Bed Pressure Swing Adsorption Process," *Adsorption*, vol. 6, pp. 233-240, 2000.
- [17] I. PaPai, A. Goursot, F. Fajula, D. Plee and J. Weber, "Modeling of N₂ and O₂ Adsorption in Zeolites," vol. 99, no. 34, pp. 12925-12932, 1995.
- [18] J. C. Kayser and K. S. Knaebel, "Pressure Swing Adsorption: Development of an Equilibrium Theory for Binary Gas Mixtures with Nonlinear Isotherms.," *Chemical Engineering Science*, vol. 44, pp. 1-8, 1989.
- [19] J. D. Sherman, "Synthetic zeolites and other microporous oxide molecular sieves," *Proceedings of the National Academy of Sciences of the USA*, vol. 96, pp. 3471-3478, March 1999.
- [20] J. Kärger and D. M. Ruthven, *Diffusion in Zeolites and Other Microporous Solids*, Wiley, 1992.
- [21] J. M. Prausnitz, R. N. Lichtenthaler and E. Gomes de Azevedo, *Molecular Thermodynamics of Fluid-Phase Equilibria*, Third Edition ed., Upper Saddle River, New Jersey: Prentice-Hall, Inc., 1999.
- [22] J. Wietkamp, "Zeolites and catalysis," *Solid State Ionics*, pp. 175-188, 2000.
- [23] J. Zheng, S. J. Pontonio, N. A. Stephenson and P. A. Barrett, "High Rate and High Crush-Strength Adsorbents". United States Patent 8,123,835 B2, 28 February 2012.
- [24] K. Langmuir, vol. 40, no. 9, p. 1361, 1918.
- [25] K. Weston, D. Jaussaud and R. L. Chiang, "Lithium Exchanged Zeolite X Adsorbent Blends". United States Patent 7,300,899, 27 November 2007.
- [26] M. D. Koretsky, *Engineering and Chemical Thermodynamics*, Hoboken, New Jersey: John Wiley & Sons, Inc., 2004.
- [27] M. Suzuki, *Adsorption Engineering*, New York, New York: Elsevier Science Publishing Company, Inc., 1990.

- [28] M. W. Ackley and F. W. Leavitt, "Rate-Enhanced Gas Separation". United States Patent 6,500,234, 31 December 2002.
- [29] M. W. Ackley and J. Smolarek, "Enhanced Rate PSA Process". United States Patent 6,790,260 B2, 14 September 2004.
- [30] M. W. Ackley, J. Smolarek and F. W. Leavitt, "Pressure Swing Adsorption Gas Separation Method, Using Adsorbents with High Intrinsic Diffusivity and Low Pressure Ratios". United States Patent 6,506,234, 14 January 2003.
- [31] O. Talu, "Needs, status, techniques and problems with binary gas adsorption experiments," *Advances in Colloid and Interface Science*, vol. 1998, no. 76-77, pp. 227-269, 1998.
- [32] P. d. M. a. D. Domine. U.S. Patent 3,155,468, 1964.
- [33] P. M. Mathias, R. Kumar, J. J. D. Moyer, J. M. Schork, S. R. Srinivasan, S. R. Auvil and O. Talu, "Correlation of Multicomponent Gas Adsorption by the Dual-Site Langmuir Model. Application to Nitrogen/Oxygen Adsorption on 5A-Zeolite," *Industrial Engineering Chemistry Research*, vol. 35, no. 7, pp. 2477-2483, 1996.
- [34] P. Sampson, D. Parker and D. Ruff, "Purified Attapulgite Clay". United States Patent 6,130,179, 10 October 2000.
- [35] R. L. Chatburn and T. J. Williams, "Performance Comparison of 4 Portable Oxygen Concentrators," vol. 55, no. 4, 2010.
- [36] R. T. Yang, *Gas Separation By Adsorption Processes*, Stoneham, Massachusetts: Butterworth Publishers, 1987.
- [37] S. Sircar, "Pressure Swing Adsorption," *Industrial & Engineering Chemistry Research*, vol. 41, no. 6, 2002.
- [38] S. U. Rege and R. T. Yang, "Limits for Air Separation by Adsorption with LiX Zeolite," *Industrial Engineering Chemistry Research*, vol. 36, no. 36, p. 5358, 1997.
- [39] S. W. Chai, M. V. Kothare and S. Shivaji, "Rapid Pressure Swing Adsorption for Reduction of Bed Size Factor of a Medical Oxygen Concentrator," *Industrial & Engineering Chemistry Research*, vol. 50, pp. 8703-8710, 2011.
- [40] U. Müller and B. Yilmaz, "Catalytic Applications of Zeolites in Chemical Industry," *Topics in Catalysis*, vol. 52, no. 6-7, pp. 888-895, 2009.

- [41] W. D. Marsh, F. S. Pramuk, R. C. Hoke and C. W. Skarstrom. US Patent 3,142,547, 1964.
- [42] W. J. Weber Jr., P. M. McGinley and L. E. Katz, "Sorption Phenomena in Subsurface Systems: Concepts, Models and Effects on Contaminant Fate and Transport," vol. 25, no. 5, pp. 499-528, 1991.
- [43] W. Pengfei, L. Y. Chen and Z. Yongxian, "Lithium-containing modified low silicon-aluminum X type molecular sieve adsorbent and preparation method thereof". China Patent CN101766987 B, 26 December 2012.
- [44] Z. Fang and S. Ji, "Ion exchange method for preparing lithium type low silicon aluminum X-shape zeolite molecular sieve". China Patent CN100556808 C, 9 November 2009.

APPENDIX

APPENDIX A: Isotherm Data

A.1 Bucket Buoyancy

Table A.1. Bucket Buoyancy (Nitrogen).

P(torr)	T(C)	W(mg)
0.0	24.65	42.2
51.6	24.35	42.1
150.5	24.35	41.9
250.2	24.35	41.7
349.5	24.3	41.5
448.7	24.2	41.3
549.3	24	41.1
747.8	24.15	40.7

A.2 Cahn Balance Isotherm Data

Starting from room temperature, environmental temperature was increased inside the balance 50°C every thirty minutes until 317°C was reached under vacuum pressure of 10×10^{-4} torr.

Hot vacuum mass: 951.71 mg

Room temperature (23.2°C) vacuum mass: 951.85 mg

Table A.2. N₂ Isotherm data at 296.8 K (Avg. Temp).

Pressure (kPa)	Temperature (K)	N ₂ Adsorbed (mol/kg adsorbent)
0		0
6.906099	296.85	0.153417
20.25167	296.8	0.385869
33.42392	296.95	0.568425
46.30286	296.45	0.731244
73.20731	296.9	0.976439
99.91178	296.7	1.178885

APPENDIX B: Column Packing

B.1 Zeolite Activation

Table B.1. Activation in Cahn Balance.

	Mass(mg)
Empty bucket in air	40.38
Bucket with sample(pre activation)	963.62
Zeolite weight	923.24
After activation (Hot)	728.52
After activation (Room Temp)	728.64
Water lost	234.98

Ratio: Water adsorbed (mg)/zeolite mass (mg) = 0.25452

B.2 Column Dimensions and Packing Details

Table B.2. Column Dimensions.

Outer Diameter	0.5 in
Wall thickness	0.036 in
Length	19.6 cm

Table B.3. Column Packing Details.

	Column A mass(g)	Column B mass(g)
Empty Column	148.3952	149.1076
Pouring Beaker (Before Pour)	69.1822	54.0587
Beaker (After Pour)	55.0039	39.7294
Column Packed	162.5568	163.4278
Column Difference	14.1616	14.3202
Beaker Difference	14.1783	14.3293
Sample Lost	0.0167	0.0091
Activated Zeolite	10.5572	10.6755

APPENDIX C: Flow Calibrations and Pressure Drop Data

C.1 Calibration of Flow Meters

An industrial gas Meter was used to calibrate the flow meter per method described in the Materials and Methods section. This data was used to generate flow calibration factors used for all the experiments to determine what the actual flow was. All flows are in standard cc/min.

Table C.1. Flow Meter Calibration Data.

FC1	FC2	FC4	Gas Meter
100	103	105	107.5664
400	412	419	424.4513
797	816	822	839.1823
1400	1419	1423	1456.065
1975	1986	1998	2054.82

C.2 Relevant Pressure Drop Data

Table C.2. Pressure Drop Between P1 and P3.

Pressure(atm)	Flow(std. cc/min)	P1(torr)	P3(torr)	ΔP (torr)
1	502	890	885	5
1	998	1208	1199	9
1	1498	1683	1671	12
1	1898	2141	2126	15
2	500	1523	1520	3
2	1007	1527	1519	8
2	1499	1681	1668	13
2	1906	2146	2131	15
4	500	3040	3039	1
4	1006	3047	3044	3
4	1504	3048	3041	7
4	1902	3053	3044	9

Table C.3. Pressure Drop Between P1 and P6.

Pressure(atm)	Flow(std. cc/min)	P1(torr)	P6(torr)	ΔP (torr)
1	503	890	890	0
1	1001	1200	1195	5
1	1501	1657	1652	5
1	1923	2097	2091	6
2	503	1523	1522	1
2	1002	1521	1521	0
2	1503	1663	1657	6
4	503	3041	3042	0
4	1003	3043	3041	2
4	1505	3047	3044	3
4	1920	3044	3044	0
0.526	500	404	401	3
0.526	1000	406	399	7
0.526	1500	412	399	13
0.526	1918	418	401	17
0.263	503	204	201	3
0.263	1002	212	198	14
0.263	1500	288	271	17
0.263	1918	355	335	20

Table C.4. Pressure Drop Between P3 and P1.

Pressure(atm)	Flow(std. cc/min)	P3(torr)	P1(torr)	ΔP (torr)
1	503	943	890	53
1	1001	1308	1200	108
1	1501	1814	1657	157
1	1923	2286	2097	189
2	503	155	1523	31
2	1002	1612	1521	91
2	1503	1818	1663	155
4	503	3058	3041	17
4	1003	3085	3043	42
4	1505	3131	3047	84
4	1920	3189	3044	139
0.526	500	519	404	115
0.526	1000	729	406	323
0.526	1500	999	412	587
0.526	1918	1247	418	829
0.263	503	411	204	207
0.263	1002	699	212	487
0.263	1500	993	288	705
0.263	1918	1246	355	891

APPENDIX D: Experimental Data and Calculations

Table D.1. Cycle file names and step times

Run #	Date	File Name	Step times (s)					Cycle
			Feed	Blow	Purge	Equil.		
1	3/5/14	FPEQVSAP2.5F700	9.7	7.7	2	0.3	20	
2	3/5/14	FPEQVSAP3.5F860	9.7	7.7	2	0.3	20	
3	3/5/14	FPQVSAP4.5F877	9.5	7.5	2	0.5	20	
4	3/5/14		9.8	7.8	2	0.2	20	
5	3/5/14	FPQVSAP4.5F950-1	9.7	7.7	2	0.3	20	
6	3/5/14	FPQVSAP4.5F950-3	9.6	7.6	2	0.4	20	
7	3/6/14	FPweqVSAP5.4F973	9.4	7.4	2	0.6	20	
8	3/6/14	FPweqVSAP6.5F1008	9.3	7.3	2	0.7	20	
9	3/6/14	FPweqVSAP81008	9.3	7.3	2	0.7	20	
10	3/6/14	FPweqVSAP10F1175	9.3	7.3	2	0.7	20	
11	3/7/14	FPEQVSAP2.5F855	7.2	5.2	2	0.3	15	
12	3/7/14	FPEQVSAP3.5F1120	7.1	5.1	2	0.4	15	
13	3/7/14	FPEQVSAP4.3F1120	7	5	2	0.5	15	
14	3/7/14	FPEQVSAP5.4F1130	6.9	5	1.9	0.6	15	
15	3/7/14	FPEQVSAP6.5F1393	6.8	5	1.8	0.7	15	
16	3/7/14	FPEQVSAP8.0F1393	6.8	5	1.8	0.7	15	
17	3/10/14	FPEQF1300P2.5	4.7	3.5	1.2	0.3	10	
18	3/10/14	FPEQF1300P3.5	4.6	3.5	1.1	0.4	10	
19	3/10/14	FPEQF1790P4.5	4.5	3.5	1	0.5	10	
20	3/10/14	FPEQ1790P4.5-3	4.4	3.4	1	0.6	10	
21	3/10/14	FPEQF1650P6.5	5.3	4.3	1	0.7	12	
22	3/10/14	FPEQF1630P8	5.3	4.9	0.4	0.7	12	
23	3/11/14	FPEQVSAP3.5F815	9.6	7.6	2	0.4	20	
24	3/11/14	FPEQVSAP4.3F1190	7	5	2	0.5	15	
25	3/14/14	FPEQVSAP4.5F1150	7	5	2	0.5	15	
26	3/14/14	FPEQVSAP5.5F1180	6.9	5	1.9	0.6	15	
27	3/17/14	FPEQVSAP6.5F1250	6.8	5	1.8	0.7	15	
28	3/17/14	FPEQVSAP7.5F1262	6.8	6	0.8	0.7	15	
29	3/17/14	FPEQVSA3.5F1015	7.1	5.1	2	0.4	15	
30	3/18/14	FPEQVSA3.5F830	7.2	5.2	2	0.3	15	
31	5/16/14	FPEQVSAP4.5F1209	7	5	2	0.5	15	
32	5/16/14	FPEQVSAP4.5F1320	7	5	2	0.5	15	

Table D.2. Cycle Flow Settings

Run #	FC1		FC2		Product (A)	Act	Avg. Comp %	FC4		Avg. Comp %
	Avg	Act	Ave	Act				Blow (D)	Act	
1	702	722	83	85	60	61	97	670	684	13.9
2	860	885	68	70	84	86	98	807	824	12.1
3	877	903	53	54	102	104	98	810	827	10.5
4	1018	1048	53	54	103	105	98	948	968	12
5	953	981	53	54	104	106	98	882	901	11
6	905	931	52	53	103	105	98	838	856	10.8
7	973	1001	43	44	124	127	98	882	901	9.4
8	1008	1037	31	32	136	139	97	896	915	8.4
9	1105	1137	22	23	154	157	98	974	995	7.8
10	1174	1208	11	11	175	179	98	1026	1048	6.9
11	854	879	70	72	71	72	98	820	837	13.7
12	1120	1153	90	92	111	113	98	1040	1062	11.8
13	1193	1228	71	73	125	128	99	1097	1120	10.9
14	1325	1364	57	58	165	168	98	1185	1210	9.3
15	1393	1434	44	45	185	189	98	1236	1262	8.4
16	1471	1514	32	33	203	207	98	1304	1332	8
17	1293	1331	82	84	101	103	98	1230	1256	14
18	1649	1697	132	135	171	175	98	1512	1544	11.7
19	1785	1837	106	109	203	207	98	1610	1644	10.6
20	1916	1972	89	91	251	256	98	1780	1818	9.4
21	1652	1700	52	53	232	237	98	1512	1544	8.6
22	1620	1667	64	66	222	227	98	1480	1511	8.8
23	817	841	70	72	82	84	98	780	796	12.1
24	1197	1232	70	72	130	133	98	1110	1133	11.2
25	1150	1184	68	70	130	133	98	1066	1088	10.8
26	1182	1217	22	23	154	157	98	1072	1095	9.3
27	1251	1288	15	15	162	165	98	1136	1160	8.7
28	1260	1297	18	18	164	167	98	144	1144	8.7
29	1014	1044	55	56	96	98	98	967	966	11.8
30	830	854	67	69	65	66	98	806	823	13.6
31	1209	1244	92	94	113	115	98	1150	1174	12.4
32	1320	1359	115	118	104	106	98	1260	1287	13.7

Table D.3. Cycle volumes per cycle and material balances.

Run #	Scc per cycle				%	% O2	% N2
	Feed	Waste	Purge in	Product	error MB	MB error	MB error
1	241	228	28	20	-3.2	-1.8	-3.5
2	295	275	23	29	-2.8	1.1	-3.8
3	301	276	18	35	-3.2	0.3	-4.1
4	349	323	18	35	-2.4	0.4	-3.2
5	327	300	18	35	-2.6	1.4	-3.7
6	310	285	18	35	-3.2	0.1	-4.0
7	334	300	15	42	-2.6	0.7	-3.5
8	346	305	11	46	-1.6	2.9	-2.8
9	379	332	8	52	-1.3	3.0	-2.4
10	403	349	4	60	-1.5	2.5	-2.6
11	220	209	18	18	-3.5	-0.6	-4.3
12	288	265	23	28	-2.0	2.3	-3.1
13	307	280	18	32	-1.6	3.6	-3.0
14	341	303	15	42	-1.1	3.0	-2.2
15	358	316	11	47	-1.2	3.3	-2.4
16	378	333	8	52	-1.6	2.6	-2.8
17	222	209	14	17	-2.1	0.9	-2.9
18	283	257	23	29	-1.3	1.3	-1.9
19	306	274	18	35	-0.8	2.2	-1.6
20	329	303	15	43	-5.2	-1.9	-6.0
21	340	309	11	47	-4.7	-2.2	-5.4
22	333	302	13	45	-4.2	-1.4	-5.0
23	280	265	24	28	-4.7	-1.0	-5.6
24	308	283	18	33	-2.8	0.6	-3.7
25	296	272	17	33	-3.2	0.4	-4.1
26	304	274	6	39	-2.9	-0.2	-3.6
27	322	290	4	41	-2.9	2.7	-4.4
28	324	286	5	42	-1.1	3.2	-2.3
29	261	242	14	25	-2.0	4.2	-3.6
30	214	206	17	17	-4.1	1.3	-5.6
31	311	294	24	29	-3.6	1.0	-4.9
32	340	322	29	27	-2.5	1.7	-3.7

Table D.4. Cycle Pressures

Run #	Pressure Col B		Pressure P3		Pratio
	High	Low	High	Low	
1	1442	566	1400	1060	2.5
2	1430	406	1407	1000	3.5
3	1440	336	1420	960	4.3
4	1442	332	1420	960	4.3
5	1442	332	1420	960	4.3
6	1440	336	1420	960	4.3
7	1439	267			5.4
8	1431	227			6.3
9	1440	186	1415	1115	7.7
10	1438	153	1413	971	9.4
11	1424	561	1401	1080	2.5
12	1438	408	1415	1080	3.5
13	1445	336	1423	1080	4.3
14	1432	267	1409	997	5.4
15	1442	234	1418	983	6.2
16	1448	196	1426	990	7.4
17	1443	559	1425	1120	2.6
18	1436	410	1415	1080	3.5
19	1439	341	1410	1080	4.2
20	1443	270	1423	1080	5.3
21	1424	220	1404	1050	6.5
22	1427	197	1407	1050	7.2
23	1441	406	1427	1080	3.5
24	1441	331	1424	1024	4.4
25	1200	270	1181	850	4.4
26	1202	220	1183	830	5.5
27	1211	191	1188	790	6.3
28	1200	163	1178	760	7.4
29	1204	341	1183	880	3.5
30	1202	477	1182	890	2.5
31	1697	399	1650	1190	4.3
32	2002	452	1973	1430	4.4

Table D.5. Cycle Performance

Run #	P/F ratio	% Purity	% Recovery	% rec (W)	BSF (lb solid/tpd O ₂)
1	0.54	97	39.2	37.3	385
2	0.37	98	45.2	46.4	272
3	0.28	98	53.8	54.2	224
4	0.24	98	46.8	47.2	222
5	0.26	98	50.5	51.9	220
6	0.27	98	52.7	52.8	222
7	0.21	98	59.0	59.7	185
8	0.14	97	61.8	64.7	170
9	0.09	98	64.5	67.5	149
10	0.04	98	69.0	71.5	131
11	0.38	98	38.5	37.9	322
12	0.37	98	45.9	48.2	206
13	0.28	99	49.0	52.6	181
14	0.20	98	57.7	60.7	139
15	0.15	98	61.5	64.8	124
16	0.10	98	63.9	66.5	113
17	0.29	98	36.2	37.1	227
18	0.37	98	48.0	49.3	134
19	0.28	98	52.7	54.8	113
20	0.22	98	60.7	58.7	91
21	0.15	98	65.0	62.8	99
22	0.18	98	63.4	62.0	103
23	0.40	98	46.5	45.4	279
24	0.27	98	50.3	50.9	176
25	0.27	98	52.3	52.7	176
26	0.09	98	60.3	60.2	149
27	0.06	98	60.0	62.7	141
28	0.07	98	60.3	63.5	140
29	0.25	98	43.8	48.0	238
30	0.37	98	36.3	37.6	352
31	0.35	98	43.3	44.3	203
32	0.40	98	36.5	38.2	220